Hindbrain Glucocorticoid Action Regulates Hepatic Lipid Metabolism

by

Boyan Vasilev

A thesis submitted in partial fulfillment of the requirements for the degree of

Master of Science

Department of Physiology

University of Alberta

© Boyan Vasilev, 2024

Abstract

Background: Dyslipidemia is a common characteristic in both diabetes and obesity, due in part to elevated triglyceride (TG)-rich very-low density lipoprotein (VLDL-TG) secretion from the liver. Excessive levels and/or action of glucocorticoids (GCs) is also observed in these metabolic diseases and can contribute to dyslipidemia via both peripheral and central mechanisms. While mechanisms of peripheral GC action to regulate lipid metabolism and VLDL-TG secretion are well known, less is understood about its central mechanisms to regulate metabolism. The brain can sense hormones and nutrients to coordinate whole-body homeostasis, including lipid metabolism. In particular, the nucleus of the solitary tract (NTS) is a hindbrain region known to regulate metabolism. However, whether GCs act in the NTS to regulate VLDL-TG secretion remains unknown. There has also been evidence that central GC action may regulate peripheral metabolism by activating the sympathetic nervous system (SNS). Furthermore, it was recently discovered that the action of GCs are mediated by both their canonical cytosolic GC receptors (cGRs) and also via novel membrane-associated GRs (mGRs). In this study, we aimed to explore if GCs acting in the NTS could regulate hepatic VLDL-TG release through sympathetic outflow, and whether mGRs in the NTS may be involved as well to better understand the mechanisms by which elevated GCs may contribute to dyslipidemia. I hypothesize that: 1) NTS GC infusion increases VLDL-TG secretion via the SNS; 2) infusing a mGR agonist into the NTS increases VLDL-TG secretion.

Methods: Male Sprague-Dawley rats underwent stereotaxic NTS cannulation and vascular catheterizations to enable direct NTS infusions, intravenous injections, and arterial blood sampling. Following a 10-hour fast, rats were subjected to a direct, and continuous NTS infusion of a specific brain treatment or vehicle paired with an intravenous poloxamer injection to evaluate VLDL-TG secretion. Plasma was collected throughout the experiment, before euthanizing the rats and collecting tissues for further analysis.

Results: NTS GC infusion increased VLDL-TG secretion compared to NTS vehicle, and this effect was negated with NTS GR or heat shock protein 90 (Hsp90) inhibition. Next, peripheral pharmacological denervation of the SNS blocked the lipostimulatory effects of NTS GCs. The increase in VLDL-TG secretion was not associated with changes in hepatic lipid metabolism-related gene or protein expression. However, elevated plasma free fatty acids (FFAs) were observed in NTS GC rats, alongside increased pHSL:HSL levels in white adipose tissue (WAT), and notably, these increases were negated with SNS inhibition.

NTS infusion of a membrane-impermeant GC to target mGRs also stimulated VLDL-TG secretion. Interestingly, Hsp90 inhibition or NTS GR knockdown were not able to reverse the hyperlipidemic effects of NTS mGR agonism. However, antagonizing protein kinase C or mitogen-activated protein kinase specifically in the NTS blocked the lipostimulatory actions of NTS mGR activation. The changes in VLDL-TG secretion were associated with reduced hepatic expression of sterol regulatory element-binding protein

1c and peroxisome proliferator-activated receptor alpha. We also discovered an upregulation in WAT adipose TG lipase levels, as well as increased plasma FFAs.

Conclusion: We report that hindbrain GC action stimulates hepatic TG secretion via the SNS. Our data also indicates that novel mGRs in the NTS participate in the lipostimulatory actions of GCs. The findings in this thesis expand the knowledge of how excessive GC levels and/or actions can result in hypertriglyceridemia.

Preface

This thesis is an original work by Boyan Vasilev. The research project, of which this thesis is a part, received research ethics approval from the University of Alberta Research Ethics Board, Project Name “CNS regulation of metabolic homeostasis”, #1604. This project was funded by the Canadian Institute of Health Research (CIHR) grant to Dr. Yue. Boyan was funded by Faculty of Graduate Studies and Research (FGSR) Graduate Recruitment Award during the first year of the project. During the second year, Boyan was funded by the CIHR Canada Graduate Scholarships-Master’s (CGSM). Boyan was also award the FGSR, Graduate Student's Association (GSA), Alberta Diabetes Institute (ADI), and CIHR Institute of Circulatory and Respiratory Health (CIHR-ICRH) travel awards for conference travel.

In contribution to this project, data collection from *in vivo* experiments was done in part by Eyram Asem and Mantash Grewal. Robin Hou and Jacques Zhang also helped with some of the western blots presented in this thesis. All qPCR work shown was conducted with the guidance of Mr. Randal Nelson and utilizing the PCR machine in Dr. Richard Lehner’s laboratory at the University of Alberta. Lastly, vascular surgeries for *in vivo* experiments were performed by both Dr. Yue and our laboratory manager, Bryan Lum.

Acknowledgment

I would like to start off by first thanking my supervisor, Dr. Jessica Yue, for giving me a chance to be part of her laboratory. Thank you for the continuous guidance and genuine care you have provided to me for the past 4 years. The amazing life-long memories I have made from all the learning, travel, and lab get-togethers would not have been possible without you. Next, I want to thank Bryan Lum, our lab manager, for performing all the NTS cannulations and all the vascular catheterization surgeries along with Dr. Yue, which allowed my experiments to go smoothly. I would also like to specifically express my gratitude to Eyram Asem and Mantash Grewal for the contributions they have put into this thesis project. Next, I want to thank all the past and present students in the Yue lab. All of you made coming into the lab an unforgettable experience every day with the nonstop jokes we shared. I first joined the Yue lab as a volunteer in 2020, before beginning this project in the summer of 2021. Without the help and tutelage from Mantash Grewal and Miguel Cardoso, I would not have been able to do any of this, let alone a Master's degree. Furthermore, I want to thank Dr. Robin Clugston and his laboratory for always sharing their expertise, allowing me to use their equipment, and answering to my naive emails. A special thank you to Mr. Randal Nelson and Dr. Richard Lehner and his lab for teaching me to do PCR and letting me use their machine. Additionally, I would also like to my committee members Dr. René Jacobs and Dr. Paul LaPointe for their time, knowledge, expertise, and guidance for this thesis. Finally, a big thank you to my family for the love and support they have provided me not just during this Master's degree, but my whole life as well. Thank you from the bottom of my heart.

Table of Contents

List of Tables

List of Figures

List of Abbreviations

11β-HSD 1/2 - 11β-hydroxysteroid dehydrogenase 1/2

ACC - acetyl-CoA carboxylase

ACL - ATP-citrate lyase

ACS - acyl-CoA synthetase

ACTH - adrenocorticotropic hormone

AGPAT - acylglycerolphosphate acyltransferase

AgRP - Agouti-related protein

AMPK - AMP-activate protein kinase

ApoB100 - apolipoprotein B100

ApoB48 - apolipoprotein B48

ARC - arcuate nucleus

Arf1 - ADP-ribosylation factor 1

ATGL - adipose TG lipase

BIMI - Bisindolylmaleimide; PKC inhibitor

BMI - body mass index

BSA - bovine serum albumin

BSA-DEX - bovine serum albumin-conjugated dexamethasone

CGI58 - comparative gene identification-58

cGR - cytosolic glucocorticoid receptor

ChREBP - carbohydrate-response element-binding protein

cideB - cell death-inducing DFF45-like effector B

CM - chylomicron

CNS - central nervous system

CORT - corticosterone

CPT1α - carnitine palmitoyltransfrase 1α

CRH - corticotropin-releasing hormone

CVD - cardiovascular disease

DEX - dexamethasone

DG - diglyceride

DGAT - diacylglycerol acyltransferase

DMSO - dimethylsulfoxide

DNL - *de novo* lipogenesis

DVC - dorsal vagal complex

ER - endoplasmic reticulum

Erk - extracellular signal regulated kinase

FATP - fatty acid transport protein

FAS - fatty acid synthase

FFA - free fatty acid

FKBP51 - FK506 binding protein 51

GC - glucocorticoid

GLUT - glucose transporter

GPAT - glycerol phosphate acyltransferase

GPCR - G-protein coupled receptor

GR - glucocorticoid receptor

HFD - high fat diet

HGP - hepatic glucose production

HPA - hypothalamic-pituitary-adrenal axis

HSL - hormone-sensitive lipase

Hsp90 - heat shock protein 90

Hsp90i - heat shock protein 90 inhibitor

ICV - intracerebroventricular

IDF - International Diabetes Federation

i.v. - intravenous

LD - lipid droplet

LDL - low-density lipoprotein

LPA - lysophosphatidate

LPL - lipoprotein lipase

MAPK - mitogen-activate protein kinase

MBH - mediobasal hypothalamus

MG - monoglyceride

MGAT - monoacylglycerol acyltransferase

MGL - MG lipase

mGR - membrane-associated glucocorticoid receptor

MIF - mifepristone

MM - mismatch

MR - mineralocorticoid receptor

MTP - microsomal TG transfer protein

NMR - nuclear magnetic resonance

NPY - neuropeptide Y

NTS - nucleus of solitary tract

pACC - phosphorylated-acetyl-CoA carboxylase

PD - MEK inhibitor

pERK - phosphorylated-extracellular signal regulated kinase

pHSL - phosphorylated-hormone-sensitive lipase

PKA - protein kinase A

PKC - protein kinase C

POMC - pro-opiomelanocortin

PPARα - peroxisome proliferator-activated receptor α

PVN - paraventricular nucleus

RC - regular chow

RIA - radioimmunoassay

Rp - Rp-CAMPs; PKA inhibitor

SCD1 - stearoyl-CoA desaturase 1

SD - Sprague Dawley

shRNA - short-hairpin RNA

SNS - sympathetic nervous system

SNSi - sympathetic nervous system inhibitor

SREBP1c - sterol regulatory element-binding protein 1c

T2D - type 2 diabetes

TG - triglyceride

VLDL-TG - TG-rich very-low density lipoprotein

WAT - white adipose tissue

WHO - World Health Organization

Chapter 1: Introduction

1.1 Obesity and Diabetes

Two of the most prevalent metabolic diseases in the world are obesity and diabetes[1–6]. Both of these diseases increase the risk of other comorbidities, such as cardiovascular disease (CVD), liver steatosis, stroke, and chronic kidney disease[1–3,7,8]. The World Health Organization (WHO) defines obesity as an inappropriate amount of fat deposition that can compromise health and uses a clinical definition of a body mass index (BMI) of 30kg/m^2 or greater[1]. Due to its prevalence increasing over the past few decades, the WHO has labeled obesity as an epidemic[1]. For instance, in 2022, 1 in 8 people worldwide were diagnosed as obese[1]. Obesity in adults has also doubled since 1990, and quadrupled for adolescents[1]. In Canada, obesity has been increasing in the last 20 years, and according to Statistics Canada, 30% of Canadians live with obesity, which is higher than the worldwide share[9].

Diabetes is a chronic disease that is often characterized by sustained elevated sugar levels in the blood[2,10]. According to the International Diabetes Federation (IDF), this disease affected 537 million adults (10% of adults in the world population) globally in 2021[11]. For contrast, there were only about 108 million people that were diagnosed with diabetes in 1980 (4.5% of adults in the world population)[2]. In Canada alone, about 5.9 million individuals (15% of the population) were said to be afflicted by diabetes in 2023[3]. For about 95% of individuals with diabetes, it is said to be type 2 diabetes (T2D) and it is often also associated with obese individuals[2,3,7]. T2D is characterized by a dysregulation of glucose metabolism which results in hyperglycemia, due in part to insulin resistance[2,3,5]. T2D can increase the risk of developing CVD, as well as liver and kidney problems[2,3,7,8]. As a result of their increasing rates of prevalence, both obesity and diabetes are becoming massive health and economic burdens on health-care systems around the world, and research to better understand how to prevent or treat these metabolic disorders and its comorbidities is warranted[12].

1.1.1 Physiological and metabolic phenotypes in obesity

In an obese state, the body often has to deal with excess nutrients, which predominantly get stored as neutral triglycerides (TG)[13–15]. The adipose tissue is the major organ that is involved in storing these lipids within lipid droplets, but other organs

can also store them to a smaller extent (e.g. liver)[13–16]. In obesity, higher lipid storage in the liver and extensive expansion of adipose tissue leads to chronic low-grade systemic inflammation[13–15]. As a result, adipocytes, hepatocytes, and resident immune cells are triggered to secrete pro-inflammatory cytokines, such as interleukin 6 (IL-6) and tumor necrosis factor α (TNFα), leading to a local and systemic inflammatory response[13–17]. Sustained inflammation can induce insulin resistance in various tissues by disrupting the function of insulin receptors and its downstream signaling[17–19]. Some of the physiological roles insulin has on metabolism includes stimulating cellular glucose uptake and glycogen synthesis, inhibiting glycogenolysis, promoting storage of TG, and inhibiting lipolysis[13,16,20,21]. Therefore, one of the consequences of insulin resistance includes an inability of insulin to suppress lipolytic activity in adipose tissue resulting in increased plasma free fatty acids (FFAs)[13,16,21]. In fact, it was observed that individuals with T2D, which is associated with insulin resistance, exhibit almost 3-fold greater circulating plasma FFA levels compared to healthy controls[22]. Elevated levels of FFAs consequently have detrimental metabolic consequences on various tissues, such as the liver and muscle[23–25]. In the muscles, excessive FFAs can promote ectopic fat accumulation and impair local insulin signaling[23–25]. When FFAs are delivered to the liver, they can be re-esterified into a triglycerides (TGs) and subsequently incorporated into TG-rich very-low density lipoproteins (VLDL-TG), which can lead to hypertriglyceridemia, or the TGs can be stored in lipid droplets within the hepatocyte instead, contributing to the development of steatosis[20,23,24,26].

As insulin also has a huge role on glucose metabolism, insulin resistance can negatively impact the maintenance of blood sugar levels[13,20,21]. One thing that occurs is glucose uptake is reduced from both muscle and adipose tissue, resulting in elevated glycemia[20,21]. On top of this, one of insulin's actions when acting on hepatocytes is to inhibit gluconeogenesis and glycogenolysis, but under an insulin-resistant state, this does not occur, and the liver produces more glucose, exacerbating the hyperglycemia[20,21,27,28]. Pancreatic insulin-producing β-cells try to overcome this higher level of blood glucose by secreting more insulin, causing hyperinsulinemia and eventual β-cell failure in a vicious cycle [20,21,25]. To link this back to elevated plasma TGs, the increased circulating glucose can activate carbohydrate response element binding

protein (ChREBP) in adipose tissue and the liver, whereas the higher insulin levels can stimulate sterol regulatory element binding protein 1C (SREBP-1c) in the same tissues, which both are transcription factors involved in mediating lipogenesis and thus, can exacerbate hypertriglyceridemia[21,28–31]. Overall, even though obesity and insulin resistance are two separate conditions, they are inherently related, and dyslipidemia is often observed in both.

1.2 Lipid Metabolism

1.2.1 Intestinal breakdown of dietary lipids

Dietary fats we consume are mainly in the form of TGs, although a smaller portion includes cholesterol (typically in the form of cholesterol esters), phospholipids, and fat-soluble vitamins[32–36]. Digestion of TGs begins in the oral cavity through mastication and the release of lingual lipases from secretory glands within the tongue[32,34,35]. As the food bolus passes through to the stomach alongside the lingual lipases, digestion continues with the addition of gastric lipases[32,34,35]. Specifically, gastric lipases are responsible for the breakdown of TGs to diglycerides (DGs) via hydrolysis[32,34]. Next, the resulting chyme with crudely emulsified lipids from the stomach's churning passes into the small intestines where the majority of lipid digestion takes place[32–35]. In the duodenum, the first part of the small intestines, chyme triggers the release of cholecystokinin (CCK) from enteroendocrine cells[33,37]. This hormone acts on the gallbladder to stimulate bile release, and on the pancreas to secrete pancreatic lipases[32–36]. Bile acids emulsify the TGs completely to enable the pancreatic lipases to perform their hydrolytic tasks[33,34].The main products of these reactions are 2-monoglyceride (2-MG) and fatty acids, which subsequently form micelles with bile salts to be absorbed by the intestinal lumen[32,33,35,36]. Importantly, FFAs are taken up by the enterocytes directly, as enterocytes express fatty acid transport protein 4 (FATP4) and CD36[33,38–40]. At the same time, cholesterol esters in chyme also get digested by cholesterol esterase, releasing cholesterol and a fatty acid, with the former being taken up by Niemann-Pick C1-Like 1 protein[34].

Inside the enterocytes, fatty acids have one of two fates: beta-oxidized in the mitochondria, or transported to the endoplasmic reticulum (ER) for resynthesis into TGs[32,34,35]. To get to their location, these substrates must be carried around the cell via fatty acid binding proteins (FABPs)[32,34]. In the ER lumen, fatty acids are re-esterified into TGs with the 2-MG that was absorbed, mainly via the monoglyceride (MG) pathway, and to a smaller extent, the glycerol-3-phosphate pathway[32,34]. Alongside the resynthesized TGs, cholesterol, and phospholipids can either be stored in the enterocytes within lipid droplets, or get packaged into chylomicrons and exocytosed into the lymphatic system before reaching the circulation[41,42]. Subsequently, these intestinal-derived lipoproteins carry dietary lipids throughout the body to tissues such as the liver, adipose, and muscles[41,42]. To release their TG content, chylomicrons interact with lipoprotein lipase (LPL) on the capillary walls, where the TGs will be broken down to FFAs and glycerol which the nearby cells can uptake[41,42]. As chylomicrons hydrolyze TGs, they begin to shrink and lose other components until they become chylomicron remnants that can be removed from the blood by the liver's low-density lipoprotein (LDL) receptors via a process called receptor-mediated endocytosis[41,42].

1.2.2 *De novo* lipogenesis

The liver and adipose can synthesize fatty acids *de novo* from excess non-lipid substrates, such as carbohydrates and some amino acids via *de novo* lipogenesis (DNL) (Figure 1.1, pathway 1)[43–47]. Upon feeding, plasma glucose levels are high, and glucose is taken up into cells via glucose transporters (GLUTs)[44,48]. Glucose enters the glycolytic pathway to get converted to pyruvate, which is transported into the mitochondria via pyruvate translocase[49,50]. There, pyruvate is converted to acetyl-CoA which enters the citric acid cycle by reacting with oxaloacetate to generate citrate[44,45]. Citrate is transported back into the cytosol and converted back into acetyl-CoA via the actions of ATP-citrate lyase (ACL)[44,45]. Next, the DNL rate-limiting enzyme, acetyl-CoA carboxylase (ACC), takes acetyl-CoA and carboxylates it into malonyl-CoA[44,45]. Fatty acid synthase (FAS) is the next enzyme involved in DNL which utilizes acetyl-CoA and malonyl-CoAs as substrates to generate palmitate, a 16-carbon long saturated fatty acid[44,45]. To make a variety of different and more complex fatty acids, enzymes, such as elongases and desaturases, can elongate palmitate and/or introduce double-bonds to

desaturate the product, respectively[44,51,52]. For example, the generation of stearate, an 18-carbon long saturated fatty acid, is made from elongases interacting with palmitate[46,53]. Stearate is then desaturated by stearoyl-CoA desaturase 1 (SCD1), which generates oleate[46,47,53]. This monounsaturated fatty acid is the most abundant fatty acid found in membrane phospholipids, TGs and cholesterol esters[46,53]. Finally, the newly synthesized fatty acids from DNL need to be activated by being converted to their acyl-CoA counterpart with the actions of acyl-CoA synthetase (ACS) before being used as substrates for TG, phospholipid, or cholesterol ester synthesis[54,55].

Importantly, DNL is a highly regulated metabolic pathway, utilizing both hormones and nutrient status as signals. As mentioned, DNL occurs when there are excess nutrients present in the system which occurs predominantly in the postprandial state[44,45,56,57]. Importantly, in this state, insulin levels should be elevated[44]. Insulin receptor activation on adipocytes and hepatocytes can lead to the upregulation and activation of SREBP-1c[44–46]. This transcription factor is involved in upregulating the expression of genes coding for the DNL enzymes described above (e.g. ACL, ACC, FAS, SCD1)[45–47,58]. Similarly, due to the higher levels of glucose from the food consumed, this molecule does not just act as a substrate for DNL, but also stimulates ChREBP, another transcription factor which promotes DNL by increasing the expression of similar DNL genes as SREBP-1c[44–46,53,58]. Conversely, in the fasting state, DNL is suppressed due to the lack of substrates available and reduced insulin levels[44]. During this time, both ChREBP and SREBP-1c both get inhibited through phosphorylation by protein kinase A (PKA) and AMP-activated protein kinase (AMPK), which get activated by low energy states and hormones such as glucagon and norepinephrine[44].

1.2.3 TG synthesis pathways

Triglycerides can be synthesized from two pathways, the MG pathway or the glycerol phosphate pathway[59–61]. Both pathways require acyl-CoAs to donate their acyl group to a glycerol molecule and form ester bonds[59–63]. To start, the MG pathway is mainly utilized by the small intestines to generate TGs from the dietary MGs and fatty acids[59,61]. In the smooth endoplasmic reticulum of the cells, MGs are acted upon monoacylglycerol acyltransferases (MGATs) which esterifies an acyl group from a acyl-

CoA substrate to generate DGs[59–61]. The final step requires diacylglycerol acyltransferase (DGAT) to convert DGs into TGs by utilizing another acyl-CoA[59,61].

The glycerol phosphate pathway, is the major pathway utilized by the liver and adipose tissue to generate TGs (Figure 1.1, pathway 2)[59,61]. Glycerol-3-phosphate, the starting substrate in this pathway, can be generated from an intermediate in glycolysis, or from the phosphorylation of glycerol by glycerol kinase[64,65]. The first step of the glycerol phosphate pathway involves converting glycerol-3-phosphate into lysophosphatidate (LPA) with glycerol phosphate acyltransferase (GPAT)[59,61,62]. LPA is then acted upon acylglycerolphosphate acyltransferase (AGPAT) to generate phosphatidate (PA)[59,61]. In the following step, PA needs to be dephosphorylated into DG, and this is done through the enzymatic action from phosphatidate phosphatase (PAP) (also called lipin 2)[59,61]. Just like in the MG pathway, another acyl-CoA gets esterified onto the DG molecule to make a TG via DGAT[59,61].

As both TG synthesis pathways converge onto DG, DGAT enzymes become important which may explain why there are two different isoforms (DGAT1, DGAT2) at varying expression levels based on the tissue[66,67]. In humans, the DGAT1 isoform is highly expressed in the intestines, and less so in the liver and adipose[66,68]. DGAT2 on the other hand is the main isoform expressed in the liver[66,68,69]. Adipose tissue seems to express DGAT2 to a high degree as well[68–71]. This differential expression pattern likely indicates DGAT1 may mostly be involved in the monoacylglycerol pathway in the small intestines, whereas DGAT2 may be more important for the glycerol phosphate pathway for TG synthesis in the liver and adipose tissue.

1.2.4 Lipid storage and lipolysis

Synthesized TGs in the liver or adipose tissue that are meant for storage are stored in the cytosol within dynamic organelles called lipid droplets[72–75]. These lipid droplets are made up of a phospholipid monolayer, with a hydrophobic lipid core[76]. Other lipids (e.g. cholesterol esters) can also be stored in these organelles[73–76]. Importantly, many proteins coat the exterior of the lipid droplets which are involved in maintaining the structure of the organelle and regulate its functions[73–75,77,78]. Perilipins are one of the predominant proteins located on the surface of the lipid droplets with their

main role being to prevent catabolism of the stored neutral lipids[74,77,78]. They do this role by acting as a barrier to lipolytic enzymes, such as hormone-sensitive lipase (HSL), and by sequestering comparative gene identification 58 (CGI58), the co-activating lipase of adipose TG lipase (ATGL)[73,74,77,78].

In conditions that require the mobilization of these stored lipids, lipolysis of the TGs in the lipid droplets occurs in both liver and adipose tissue (Figure 1.1, pathway 3)[73,78]. Hormones like norepinephrine and glucagon can activate PKA signaling, which then phosphorylates perilipin and HSL[73]. Phosphorylated perilipin loses its ability to act as a barrier to lipolysis and it releases CGI58 to activate ATGL as well[73]. Phosphorylation of HSL (pHSL) activates its lipolytic activity and promotes its translocation from the cytosol towards the lipid droplets[77,78]. Next, lipolysis occurs with the first step involving the breakdown of TGs to DGs and a fatty acid, catalyzed predominantly by ATGL, however HSL may also enable this hydrolysis reaction[77]. The second step of lipolysis is the further breakdown of DG to MG and a fatty acid, which can only be done through the actions of HSL[72,74,77]. Finally, MGs are completely broken down to glycerol and a fatty acid via MG lipase (MGL)[79]. Conversely, the liver also highly expresses triacylglycerol hydrolase (TGH)[77,78]. This lipase is located in the endoplasmic reticulum of hepatocytes and hydrolyzes TGs from hepatic lipid droplets[77,78]. The resulting fatty acids released can be subsequently utilized for different pathways, such as re-esterification into TG for lipoprotein production by the liver, β-oxidation for ketone body or ATP production.

1.2.5 Liver β-oxidation

In fasting conditions where the energy levels are low (low cellular ATP, high AMP), AMPK gets activated[80–82]. AMPK signaling helps promote β-oxidation of fatty acids in the liver and muscle for ATP production[81,82]. One mechanism is through the phosphorylation of ACC to inhibit this enzyme's activity, diverting cellular activities away from anabolism, and redirecting them towards catabolic pathways[81,82]. As ACC produces malonyl-CoA, its phosphorylation by AMPK leads to a drop in cellular concentration of malonyl-CoA. This is important as malonyl-CoA is a potent inhibitor of carnitine palmitoyltransfrase 1α (CPT1α), which is a crucial protein for β-oxidation[80–82].

Another way AMPK promotes fatty acid oxidation is through stimulating the increase in translocation of CD36 to the plasma membrane to increase fatty acid uptake into the cells[83–85]. Once fatty acids enter, they get activated to acyl-CoAs by ACS[81]. Also, some fatty acids that enter are used to activate the nuclear receptor peroxisome proliferator-activated receptor α (PPARα), involved in upregulating β-oxidation gene expression[80–82]. The acyl-CoAs are transported towards the mitochondria to get converted to acylcarnitine by CPT1α prior to entering the mitochondrial matrix via carnitine-acylcarnitine translocase[81,82]. Inside the mitochondrial matrix, acylcarnitine is reconverted back to its acyl-CoA via carnitine palmitoyltransferase 2 (CPT2)[81,82]. From there, acyl-CoAs enter the β-oxidation pathways where they will be broken down to acetyl-CoA that can be used for either ATP production via the citric acid cycle and the electron transport chain or ketone body production (Figure 1.1, pathway 4)[80–82].

1.2.6 Very-low density lipoprotein assembly and secretion

During the postabsorptive state, the liver secretes lipid-filled particles called TG-rich very-low density lipoproteins (VLDL-TGs) into the circulation to provide an energy source to other tissues (Figure 1.1, pathway 5)[86–90]. In contrast, the intestines release similar lipoprotein particles called chylomicrons containing dietary lipids during the postprandial state[42,86–91]. Briefly, lipoproteins are particles made up of a phospholipid monolayer with free cholesterol molecules and apolipoproteins on the surface, with a hydrophobic core filled with TGs and cholesterol esters[87,90]. In humans, the main apolipoprotein on VLDL particles is apolipoprotein B-100 (ApoB100), whereas intestinal-derived chylomicrons contain the truncated form of ApoB100, apolipoprotein B-48 (ApoB48), which is obtained from posttranscriptional modification of ApoB100 mRNA[42,87,88]. However, in rats and mice, their hepatocyte-derived VLDL can be made with either ApoB100 or ApoB48, with the latter being the more prevalent form secreted[88]. Additionally, it is important to note that each VLDL or chylomicron particle is made with one ApoB protein[86]. Chylomicrons and VLDLs also possess other apolipoproteins, such as apolipoprotein E, apolipoprotein C, with the former also having apolipoprotein A, with each protein providing specific functions in the metabolism and roles of these particles[92–97].

VLDL assembly in the liver begins at the rough ER membrane, where the translation of ApoB100 protein takes place[86,88,90]. As the protein is translated into the ER, it is also partially lipidated at the same time through the actions of microsomal TG transfer protein (MTP) to generate a poorly-lipidated pre-VLDL particle[90,98]. MTP is also involved in the formation of ER luminal TG-rich lipid droplets[89,98]. The following step in VLDL assembly involves the core lipidation of the pre-VLDL. In this step, a transport vesicle from the ER fuses with the ER-Golgi intermediate compartment (ERGIC) organelle to carry the pre-VLDL and MTP-derived ER lipid droplet towards the Golgi apparatus and it is where the pre-VLDL gets further lipidated using the TGs from the lipid droplet to generate a bulky VLDL-TG[98–100]. One protein that has recently been described to potentially be important in the core lipidation of the pre-VLDL is cell death-inducing DFF45-like effector B (cideB)[98,100,101]. This protein is associated with lipid droplets and its deficiency has been shown to reduce VLDL-TG secretion, but not VLDL-ApoB, suggesting it has a role in the lipidation of these lipoproteins[102]. Another factor that has been linked with VLDL assembly and secretion is ADP-ribosylation factor 1 (Arf1). This protein is involved in the activation of phospholipase D (PLD), where this enzyme catalyzes the production of phosphatidic acid which is: one, required for VLDL assembly[89,90,103]; and two, needed for the recruitment of coat protein complex I (COPI) proteins that promote ERGIC movement towards the Golgi[89,90,101,104]. As the VLDL particle passes through to the Golgi apparatus, it matures further before it is secreted into the circulation via exocytosis[98,99].

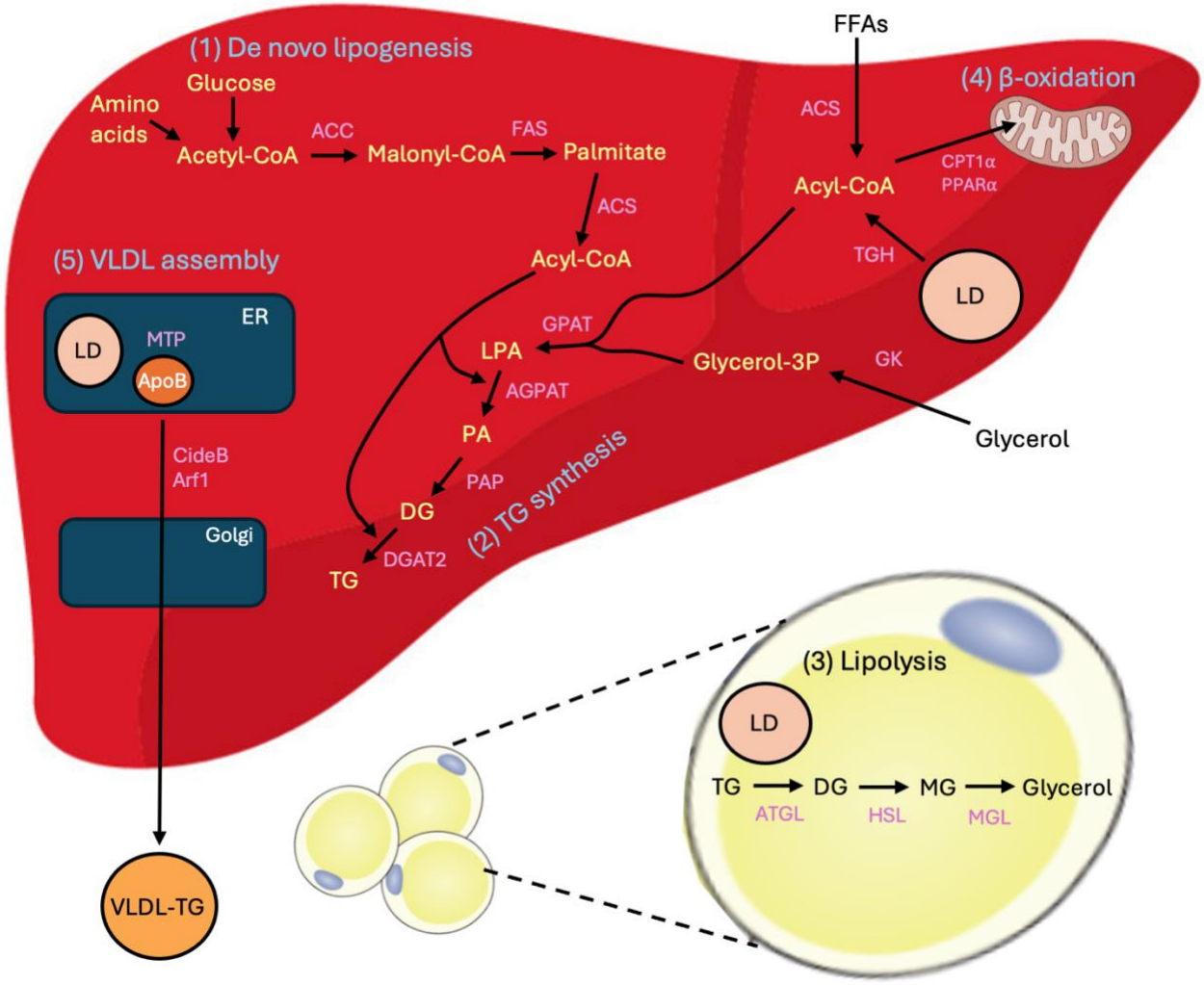

Figure 1.1: Lipid Metabolism Pathways. Pathway 1: *De novo lipogenesis*. Non-lipid substrates get converted to acetyl-CoA. Acetyl-CoA carboxylase (ACC) acts to produce malonyl-CoA to supply fatty acid synthase (FAS) with substrates for fatty acid production, namely palmitate. Activation of the fatty acid is done by the addition of coenzyme A by acyl-CoA synthetase (ACS) is required for these molecules to enter various metabolic pathways. Pathway 2: *Triglyceride synthesis*. The liver predominantly uses the glycerol pathway to synthesize TGs. Glycerol-3-phosphate (glycerol-3P) is made from the phosphorylation of glycerol by hepatic glycerol kinase (GK). Glycerol can be obtained from the plasma or lipolysis directly in liver lipid droplets (LDs). Two acylation reactions ensue on glycerol-3P. The acyl-CoAs substrates can come from DNL, free fatty acids (FFAs) in circulation, or lipolysis of hepatic LDs by triacylglycerol hydrolase (TGH). The first acylation reaction of glycerol-3P is catalyzed by glycerol

phosphate acyltransferase (GPAT), generating lysophosphatidate (LPA). Further acylation of LPA to produce phosphatidic acid (PA) is achieved by the enzyme acylglycerolphosphate acyltransferase (AGPAT). PA undergoes a dephosphorylation reaction catalyzed by phosphatidate phosphatase (PAP) (also called lipin2) to get a diglyceride (DG) molecule. DGAT2 is the main isoform of DGAT found in the liver and it esterifies an acyl-CoA substrate to the DG, thereby making a triglyceride (TG). TGs can be stored into lipid droplets or used for very-low density lipoprotein (VLDL) synthesis. Pathway 3: *Lipolysis*. In the adipose, TG within LDs get broken down to DG by adipose TG lipase (ATGL). DGs get metabolized to MGs through the actions of hormone-sensitive lipase (HSL). Finally, MGs get broken down completely to glycerol via MG lipase (MGL). Fatty acids get released after each reaction as well. In the liver, TG stores in LD can be broken down by triacylglycerol hydrolase (TGH). Pathway 4: *β-oxidation*. Oxidation of fatty acids requires activation by ACS. Acyl-CoAs travel to the mitochondria and enter with the help of carnitine palmitoyltransfrase 1α (CPT1α). Inside, acyl-CoAs undergo fatty acid oxidation for energy production or ketone body synthesis. Genes involved in β-oxidation get upregulated by peroxisome proliferator-activated receptor α (PPARα) signaling. Pathway 5: *VLDL assembly*. TGs get packaged into VLDL-TG particles to be secreted into the bloodstream. The first step involves the initial lipidation of apolipoprotein B100 during its translation into the endoplasmic reticulum lumen to produce a pre-VLDL particle. Microsomal TG transfer protein is crucial in this step, as well as for the production of luminal lipid droplets (LD). The second step of VLDL assembly involves the core lipidation of pre-VLDLs, which is facilitated by cell death-inducing DFF4-like effector B (CideB). VLDL-TGs pass through the Golgi apparatus prior to release into the blood and ADP-ribosylation factor 1 (Arf1) is involved in this. Image adapted from Saporano et al., Nutrients[105].

1.3 Glucocorticoids

Glucocorticoids (GCs) are steroid hormones that have a role in many physiological processes and the maintenance of homeostasis[106,107]. Given their involvement in a multitude of processes, synthetic analogs of GCs, such as dexamethasone (DEX), hydrocortisone, and prednisolone, are often used clinically, particularly for their strong anti-inflammatory and immunosuppressive effects[108,109]. However, it is worth mentioning that long-term therapy with GCs or conditions that chronically elevate physiological GC concentrations, such as Cushing's disease, is associated with adverse effects, such as insulin resistance, hyperglycemia, weight gain, dyslipidemia, CVD, osteoporosis etc.[107,110–114]. In relation to this, excessive GC levels and/or action coupled with increased expression of GC receptors have been linked to obesity and diabetes[110,111,114–118].

1.3.1 Hypothalamic-pituitary-adrenal axis

GCs are secreted in response to the hypothalamic-pituitary-adrenal (HPA) axis activation (Figure 1.2)[107,108]. When environmental stressors are perceived by sensory pathways in the central nervous system (CNS), they get transmitted to the amygdala, the fear center of the brain[119,120]. The amygdala then sends projections towards the hypothalamic paraventricular nucleus (PVN), to stimulate the release of corticotropin releasing hormone (CRH) into the hypophyseal portal vein[107,120,121]. CRH then reaches the anterior pituitary to trigger the synthesis and secretion of adrenocorticotropic hormone (ACTH) into the systemic circulation[107,120]. PVN-derived vasopressin (AVP) is often also required to synergistically increase the effects of CRH on the pituitary[107,120,121]. In circulation, ACTH reaches the adrenal cortex to stimulate GC secretion[107,121,122]. Subsequently, these hormones reach their target tissues and cells by being carried through the bloodstream bound to corticosteroid-binding globulin[115]. In humans, the main GC is cortisol, whereas in most rodents it is corticosterone (CORT)[122]. Importantly, the bioavailability of GCs is not based on how much is released in the blood, as they are initially secreted as an inactive precursor (humans: cortisone; rodents: 11-dehydrocorticosterone)[123,124]. Bioavailability is instead determined by local regulation where GCs are converted into their active forms (humans: cortisol; rodents: CORT) by 11β-hydroxysteroid dehydrogenase 1 (11β-HSD1)[123,124]. Conversely, if

intracellular GCs are too high, 11β-hydroxysteroid dehydrogenase 2 (11β-HSD2) can inactivate the GCs[123,125]. From there, GCs can mediate their physiological actions to fight off the perceived stressor and bring the body back to homeostasis. Once that is complete, circulating GC levels would be high which will be important for the negative feedback of the HPA axis[107,122]. To terminate this axis, the elevated GCs act on their receptors in the PVN and pituitary to bring a close to the neuroendocrine feedback loop[122].

Moreover, the HPA axis is not just activated during times of stress. In fact, it is also under the rhythmic control of the hypothalamic suprachiasmatic nucleus (SCN), the biological clock center[122,126]. The SCN aids the circadian and ultradian rhythm release of cortisol via pulsatile release of CRH[107,122]. This regulation keeps GC levels at a basal state, allowing GCs to constantly bind high-affinity mineralocorticoid receptors (MRs) keeping the GC concentration low[107,122,127]. Only when GC levels are high, such as during a stress response or in circadian peaks, do GCs bind to GC receptors (GR)[107,121,122].

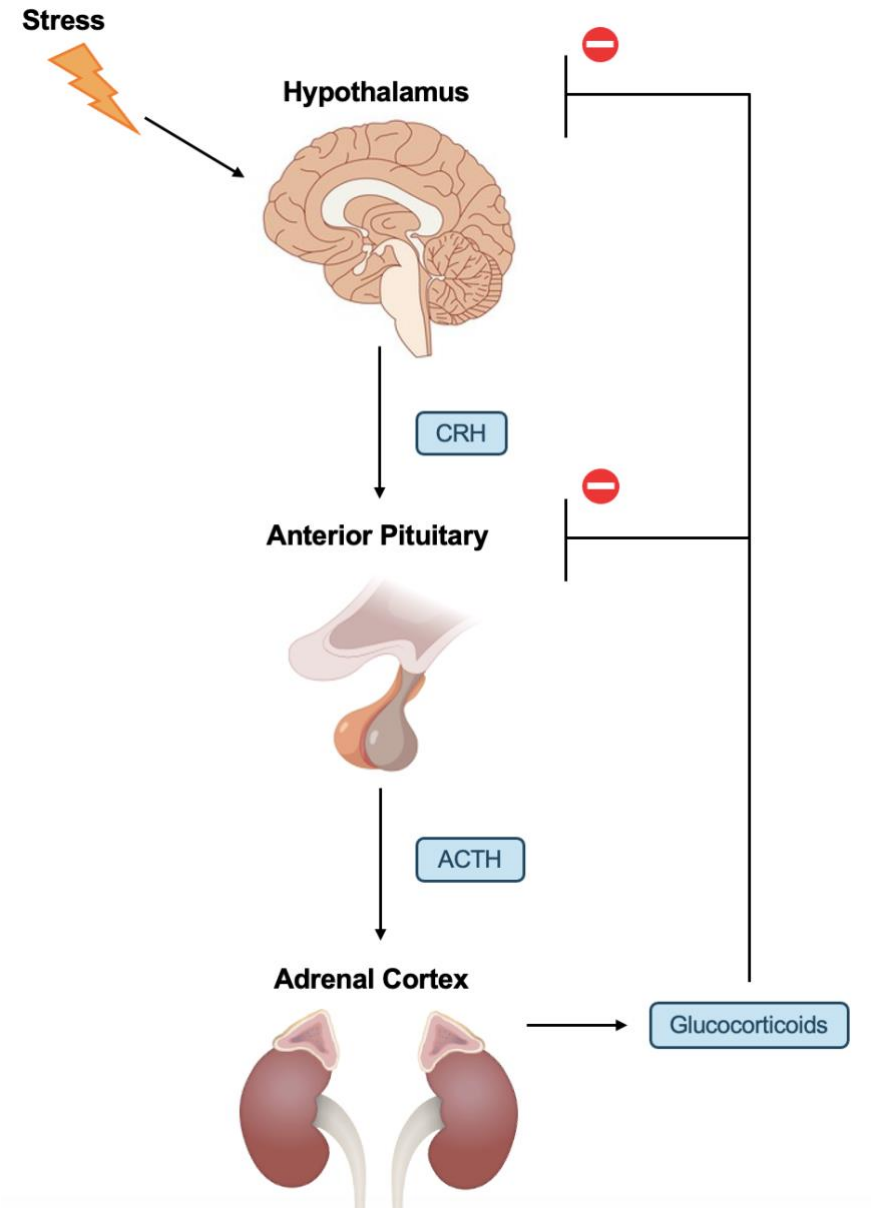

Figure 1.2: The Hypothalamic-Pituitary-Adrenal Axis. When an individual is challenged with a stressor, neuronal projections signal to the paraventricular nucleus of the hypothalamus to secrete corticotropin-releasing hormone (CRH). CRH acts on the anterior pituitary to trigger the release of adrenocorticotropic hormone (ACTH) into the circulation. The adrenal cortex is activated by ACTH to release glucocorticoids. At the end of the stress response, glucocorticoids negatively feedback onto the hypothalamus and pituitary gland to bring an end to the axis.

1.3.2 Glucocorticoid synthesis

GC production commences when ACTH activates its G-protein coupled receptors (GPCR), the melanocortin type-2 receptor (MC2R), on steroidogenic cells within the zona fasciculata of the adrenal cortex[115,127–130]. MC2Rs are linked to the $G_{\alpha s}$ pathway leading to PKA activation, with this kinase involved in activating steroidogenic acute regulatory protein (StAR) whose role is to facilitate the import of cholesterol into the mitochondria[107,127,129–131]. There are two sources of cholesterol which steroidogenic cells can use: the first is the storage of cholesterol esters within their lipid droplets, and the second is an increased uptake of cholesterol-rich low-density lipoproteins[127,130]. In the mitochondria, cholesterol is converted to pregnenolone by cytochrome P450 (CYP) 11A enzyme before moving back into the cytoplasm[130]. Following, pregnenolone undergoes a series of biochemical reactions catalyzed by various CYP enzymes with intermediates moving between the ER and mitochondria before finally being converted into cortisone[130].

1.3.3 Glucocorticoid receptors

1.3.3.1 Canonical glucocorticoid receptor

Once GCs reach their target cell, they can passively diffuse across the plasma membrane due to their hydrophobic properties[132–134]. The classical cytosolic glucocorticoid receptor (cGR) is a nuclear receptor located in the cytosol in complex with other regulatory proteins when unbound by GCs (Figure 1.3)[115,128,132–135]. When GCs bind to the cGR, the GC-cGR complex undergoes a conformational change such that the accessory proteins dissociate from the GR and promote its dimerization and translocation into the nucleus[133–136]. cGRs induce their genomic effects by interacting with their target genes at glucocorticoid response elements (GREs) on DNA to mediate gene transcription[133,135,136]. Afterwards, mRNAs get synthesized before being translated into functional proteins to mediate the GC effects[133,134].

Two important accessory proteins for the cGR are heat shock protein 90 (Hsp90) and FK506 binding protein 51 (FKBP51)[108,132,133,136,137]. To start, Hsp90 is a major chaperone protein described to keep the cGRs stable and in their primed conformation in the absence of GCs[135,138,139]. Studies have shown that blocking the actions of Hsp90 leads to the ubiquitination and degradation of the cGR[138,139]. In contrast, FKBP51 has a

different role for the cGR function. When GC levels are low, cGRs are unbound and kept in the cytosol[135]. This is due to the actions of FKBP51 which represses the cGRs from entering the nucleus[140–142]. In fact, studies have reported that knocking out FKBP51 increases the GR sensitivity[143,144] Upon GC binding, cGRs unbind FKBP51, and recruit FKBP52 which promotes translocation into the nucleus[140–142]. Interestingly, when activated cGRs are exerting their genomic effects, they also upregulate the *Fkbp5* gene which codes for FKBP51[141,145,146]. The increased levels of FKBP51 then inhibit the cGR again, allowing for an ultra-short negative feedback loop[145,146]. As such, measuring the expression levels of the *Fkbp5* gene or measuring FKBP51 protein levels has been used as a marker of cGR activity in research[146–149].

1.3.3.2 Membrane-associated glucocorticoid receptor

Emerging evidence has suggested that GCs can mediate a part of their functions through nongenomic, intracellular signaling mechanisms via membrane-associated GRs (mGRs) (Figure 1.3)[108,132,133,136]. These receptors have been proposed to participate in the inhibition of the HPA axis at the level of the hypothalamus, as well as induce some anti-inflammatory effects on immune cells[133,150–152]. Of note, since increased expression of glucocorticoid receptors has been observed in individuals with metabolic diseases (e.g. diabetes)[117,118], potentially mGRs may also be upregulated and involved in the disease pathogenesis, although no research on this has been done yet.

Unfortunately, the genetic origin or structural identity of these receptors remains unknown. Some studies have provided evidence to suggest that the mGR is a GPCR[150,153–158]; however, other studies have indicated that the mGRs may simply be the cGRs migrating to the plasma membrane to regulate nongenomic signaling cascades[159–164]. Nonetheless, there is a consensus that mGRs mediate their effects by triggering cellular signaling pathways[132,165–167]. Multiple studies have tried to elucidate the downstream effectors and second messengers associated with the mGRs[154,157,168,169]. Investigations on various cell types (e.g. neuron, immune, muscle, and epidermal cells) have previously described different effectors for the mGR signaling cascade which include: PKA, PKC, Akt, and MAPK[154,157,159,168–171]. Of interest, GCs are not the only steroid hormones with a membrane receptor counterpart. In fact, estrogen membrane receptors have been extensively studied as well[172–174].

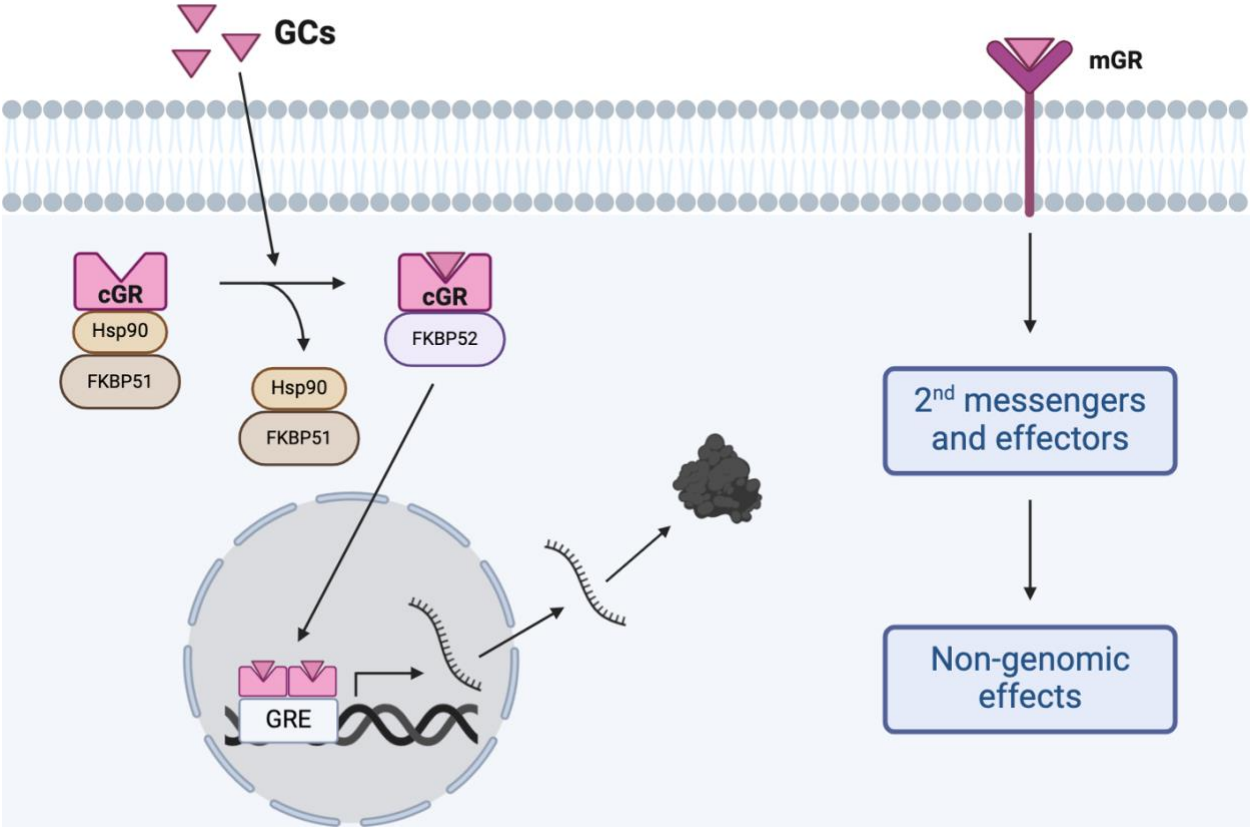

Figure 1.3: Glucocorticoid Receptor Signaling. The canonical genomic mechanisms of glucocorticoids (GC) begin when these hormones diffuse across the plasma membrane and activate their cytosolic glucocorticoid receptors (cGR). This induces the unbinding of accessory proteins such as heat shock protein 90 (Hsp90) and FK506 binding protein 51 (FKBP51), whilst promoting the recruitment of FK506 binding protein 52 (FKBP52) and translocation into the nucleus. As dimers, cGRs interact with genes that possess GC response elements (GRE) to mediate gene transcription. Subsequently, transcribed mRNAs get translated into functional proteins. GCs can also exert some of their effects via membrane-bound GC receptors (mGR). These receptors initiate signaling cascades intracellularly to mediate nongenomic effects. Of note, since the identity of the mGR is currently unknown, the structure of the receptor depicted here may not be accurate. Figure made with Biorender.com.

1.3.4 Glucocorticoid effects

GCs have a role in regulating a vast number of physiological processes, such as metabolism, immune function, bone remodeling, cardiovascular, and many more[115,128,133,175–177]. GCs manage this due to their receptors being ubiquitously expressed throughout the body[178,179].

1.3.4.1 Non-metabolic glucocorticoid effects

One of the most commonly prescribed drugs are synthetic GCs due to their potent immunosuppressive effects[108,175]. There are a couple mechanisms by which GCs achieve their inhibitory actions on the immune system. For instance, GRs can repress the expression of transcription factors involved in inflammation, such as NF-κB[175,180]. Additionally, GCs reduce the expression of pro-inflammatory cytokines (e.g. IL-6 and TNFα), whilst increasing anti-inflammatory cytokine synthesis (e.g. IL-10)[175,180].

The cardiovascular system is also regulated by GC signaling. Firstly, GCs can induce contraction from vascular smooth muscle cells[181]. These hormones also reduce endothelial nitric oxide production, which is a potent vasodilator[182]. Each of these effects can lead to increased blood pressure[181,182]. In fact, individuals on synthetic GC therapy have an increased risk of developing hypertension[183,184].

GC action can also regulate bone remodeling. Bone cells are constantly breaking down old bone tissue and replacing it with new bone[185]. GCs upregulate the levels of osteoclasts (bone resorption cells), while downregulating osteoblasts (bone-forming cells)[176,186]. An important component of bone structure is calcium, and GCs can lower calcium levels by reducing intestinal calcium absorption and increase calcium excretion by the kidneys [187,188]. As a result, the development of osteoporosis with chronic-GC treatment remains a huge healthcare problem[176,186]. Overall, these represent some of the non-metabolic physiological processes of GCs.

1.3.4.2 Metabolic glucocorticoid effects

An important role of GCs is on metabolism, particularly during a stress response to mobilize fuel sources. Accordingly, GCs have been documented to extensively regulate glucose and lipid metabolism via its direct actions on the liver, adipose tissue, and muscle[115,177,189].

In the liver, GCs can stimulate gluconeogenesis, lipogenesis, and VLDL-TG secretion[177,189]. GCs increase hepatic glucose production by activating the transcription of phosphoenolpyruvate carboxykinase and glucose-6-phosphatase, which are the rate-limiting enzymes for gluconeogenesis[115,177,189]. Hepatic insulin sensitivity is also hampered when GCs act on hepatocytes by impairing the liver insulin receptors directly[177,190], or their signaling cascade (e.g. reduced Akt phosphorylation) indirectly[189]. Taken together, the net effect results in increased blood glucose levels. GCs can also participate in liver lipid metabolism. Enzymes such as ACC and FAS are upregulated with GC treatment which increases DNL[189,191,192]. TG synthesis pathways are also potentiated, with enzymes like DGAT2 upregulated, whereas TG catabolic pathways become suppressed[192]. GCs also inhibit PPARα activity, which coupled with the higher levels of malonyl-CoA from increased ACC levels, leads to reduced β-oxidation[191,192]. As a result, liver TG accumulation occurs, which can exacerbate hepatic insulin resistance[189]. GCs can also increase the release of VLDL-TG, contributing to dyslipidemia[115,189,192,193].

At the level of the adipose tissue, GCs can also coordinate glucose and lipid metabolism. GCs reduce glucose uptake by adipocytes by decreasing GLUT4 translocation to the plasma membrane[189,194,195]. GC also reduce phosphorylation of downstream factors (e.g. IRS1 and Akt) of insulin receptor signaling, therefore promoting insulin resistance[189]. Further, GCs can stimulate both lipogenesis and adipocyte expansion in visceral fat depots, but TG breakdown by lipolysis in subcutaneous fat stores[115,189]. This phenomenon is believed to occur due to differences in 11β-HSD1 between fat depots, where greater activity of this enzyme, and thus higher levels of active GCs, is found in visceral fat tissue[196]. In fact, studies in 11β-HSD1 knockout mice fed with a high fat diet revealed significantly lower visceral fat deposition in mice devoid of 11β-HSD1 compared with their wildtype counterparts[197]. To add to this, GCs increase LPL action preferentially in visceral fat, suggesting increased lipid uptake from circulating lipoproteins compared to subcutaneous fat[198]. As mentioned, GCs also increase circulating FFAs by inducing lipolysis in the adipose which is mediated through the upregulation of ATGL and HSL[189,199]. Finally, GCs can also alter the release of

various adipokines (e.g. leptin) from adipose tissue, indirectly affecting lipid and glucose homeostasis[200].

GCs can also interact with muscle. Similar to their effects on hepatocytes and adipocytes, GCs also impair insulin action in the myocytes via reduced PI3K/Akt signaling and GLUT4 translocation[115,189,200]. Another mechanism employed by GCs to increase fuel mobilization is by stimulating the catabolic breakdown of muscle proteins into amino acids by induction of the ubiquitin-proteasome system[201–203]. As for lipid metabolism, GCs promote the accumulation of intra-myocellular lipids within muscles[189,191,200]. Finally, GC treatment in rat and chicken has shown to reduce AMPK activity in skeletal muscle, suggesting that β-oxidation may get suppressed, which could contribute to lipid build-up[204,205].

1.4 Brain Regulation of Metabolism

So far, several factors affecting peripheral regulation of lipid metabolism have been reviewed. This includes the direct effects of nutrients (e.g. glucose) and hormones (e.g. insulin) on liver and adipose TG metabolism. In addition to these effects, it has become apparent from recent research on the brain's ability to sense hormones and nutrients, that central regulation of metabolism is also critical for maintaining homeostasis. This next section will introduce two key brain regions that have been extensively studied in the regulation of peripheral metabolism, namely the medial basal hypothalamus (MBH) and the hindbrain dorsal vagal complex (DVC).

1.4.1 Hypothalamic control of metabolism

The hypothalamus is often referred to as the master regulator of homeostasis. It regulates functions including, but not limited to, feeding, digestion, energy expenditure, thermoregulation, and glucose metabolism[206,207]. Of particular importance to metabolic regulation is the mediobasal portion of the hypothalamus which is comprised of the entire arcuate nucleus (ARC), and part of the ventromedial hypothalamus, and this region is involved in various physiological neuroendocrine responses controlling metabolic processes (Figure 1.4)[206,208–210]. The ARC is adjacent to the third ventricle of the brain, as well as the circumventricular organ, median eminence, which possesses a leaky blood-brain barrier with fenestrated capillaries[206–209]. These characteristics permit

the ARC to sense a myriad of nutrient and hormone fluctuations reflected by the peripheral circulation, and to respond accordingly by regulating peripheral glucose and lipid metabolism, food intake, or energy expenditure[207,208,210].

Circulating hormone levels provide information about the metabolic state of the body. The ARC is equipped with various receptors it expresses to sense these hormones and initiate regulatory responses. For instance, receptors for insulin, glucagon, leptin, ghrelin, glucagon-like peptide 1 (GLP-1) have all been described in the ARC[211–215]. As an illustration of the ARC's ability to regulate metabolism, a study done by Mighiu et al. investigated the effects of glucagon administration into the MBH[214]. The study revealed that activating glucagon receptors and/or downstream PKA in the MBH reduced hepatic glucose production (HGP) via the hepatic branch of the parasympathetic vagal nerve[214]. Another study also revealed that intact insulin signaling in specific cell types in the ARC is required to suppress HGP[216]. Moreover, the ARC is also involved in regulating food intake principally through the actions of its agouti-related peptide (AGRP)/neuropeptide Y (NPY)-expressing neurons and pro-opiomelanocortin (POMC)-expressing neurons, which stimulate and suppress appetite, respectively[217–219]. For example, Schwartz et al. revealed that giving rats insulin into the third ventricle of the brain to target the hypothalamus lowers food intake by decreasing ARC NPY expression[220]. Similar effects on energy intake were found with leptin administration into the ARC[221,222]. This region of the brain has also been implicated in lipid metabolism. Hackl et. al previously observed that leptin administered into the third ventricle can increase liver VLDL-TG secretion and diminish hepatic DNL[223]. Likewise, NPY acutely acting on its receptors in the hypothalamus also triggers hepatic TG secretion via sympathetic outflow to the liver[224,225]. The MBH has also been reported to block white adipose tissue (WAT) lipogenesis and adipogenesis in response to central leptin signaling by decreasing WAT expression of SREBP-1c and PPARγ[215]. Whereas it was shown that MBH insulin action upregulates WAT lipogenesis and inhibits lipolysis in adipocytes[226].

Changes in nutrient levels such as glucose, fatty acids, and amino acids in the blood can also be sensed by the ARC. The hypothalamus has glucose sensing abilities which helps regulate glycemia by modulating HGP[227,228]. Previous work that examined

the effects of direct glucose infusion into the hypothalamus reported a lowering in HPG[227,228]. Additionally, the ARC can also sense lactate, a metabolite of anaerobic glycolysis, to regulate glucose homeostasis[229]. Another molecule that can be sensed is malonyl-CoA, which was linked to reduced energy intake[230]. Subsequent studies that artificially lowered hypothalamic malonyl-CoA levels *in vivo* observed a hyperphagic response[231,232]. Long-chain fatty acid sensing by the hypothalamus has also been reported in a study by Yue et al. where infusion of oleate directly into the MBH led to a reduction in liver lipid secretion[209]. Furthermore, the amino acid leucine can signal in the MBH to regulate both HGP and food intake[233,234]. Overall, the hypothalamus plays a critical role in regulating whole-body metabolism. However, it is worth mentioning that defects in hypothalamic sensing of nutrients or hormones leads to altered homeostasis, which can contribute to the development of metabolic diseases[209,214,226,235].

1.4.1.1 Hypothalamic glucocorticoid control of metabolism

As discussed above, elevated GC levels are associated with obesity and diabetes[110,115]. One mechanism by which GCs contribute to the pathophysiology of obesity and diabetes is through hypothalamic signaling. Mice given CORT in drinking water for 4 weeks showed increased food intake and body weight[236]. In particular, it was observed that GC-treated mice had higher levels of GCs and higher GR activity in their hypothalamus compared to control-treated mice[236]. Rats that received a 3-day infusion of CORT into the lateral ventricles of the brain to target the hypothalamus were seen to experience hyperphagia, increased body weight gain, hypertriglyceridemia, and elevated levels of plasma insulin[237]. Additionally, the Yue laboratory has also shown evidence that acute infusion of GCs into the MBH impairs hepatic insulin sensitivity resulting in increased HGP under hyperinsulinemic-euglycemic clamp conditions[238,239]. Further studies in the Yue laboratory revealed that central administration of dexamethasone (DEX), a synthetic GC, directly into the MBH stimulates hepatic VLDL-TG release[240]. One mechanism by which central GC action induce changes in the periphery could be through the sympathetic nervous system (SNS). The HPA axis and the SNS are inherently linked as both systems work in tandem to coordinate the stress response, and are known to activate one another[107,241,242]. Evidence from a study by Yi et al. backs the claim that acute, central GC administration mediates peripheral effects

via the SNS[243]. This paper revealed that infusing GCs into the ARC resulted in lower hepatic insulin sensitivity; however, this was negated with sympathetic denervation of the liver[243].

Interestingly, in many of the studies on central GC action in the regulation of metabolism, the expression of hypothalamic NPY was also increased with hypothalamic exposure to GCs[236,237,240,244]. The importance of this rise in NPY seems to be more than just this peptide's orexigenic properties. To elaborate, intracerebroventricular (ICV) injections of DEX caused hyperinsulinemia and a reduction in brown adipose tissue thermogenesis in mice, but these effects were negated with ICV PYX-2, a NPY receptor antagonist[245]. Similarly, acute DEX treatment in the ARC induced insulin resistance, but concomitant antagonism of the NPY Y1 receptors in the ARC blocked this effect[243]. Another study observed that hypothalamic NPY expression increases under a fasted state, but this upregulation is blocked in adrenalectomized animals, and exogenous CORT supplementation is required to rescue the phenotype[244]. Interestingly, another group also reported that direct administration of ICV NPY was unable to stimulate food intake in adrenalectomized rats, although food intake did increase with ICV NPY plus DEX in the adrenalectomized animals[246], suggesting that in the hypothalamus, increases in both GCs and NPY are required to stimulate feeding. Finally, it was discovered that ICV NPY signals via the SNS to stimulate hepatic VLDL secretion by increasing hepatic Arf1 and reducing CPT1α expression[225]. Although this study did not investigate the requirement of GCs on the effects of ICV NPY to modulate liver TG secretion, one could speculate that hypothalamic GC action may also increase central NPY to yield a similar effect. Thus, literature evidence suggest that hypothalamic effects of either GCs or NPY are indeed co-dependent.

1.4.2 Brainstem control of metabolism

Beyond the hypothalamus, another brain region involved in metabolic regulation is the brainstem. One of the earliest findings of this was done by Claude Bernard[247]. He found that lesioning the floor of the fourth ventricle of the brainstem caused hyperglycemia and impairments in glucose homeostasis[247]. More specifically, this region is now known as the dorsal vagal complex (DVC), which is a group of three nuclei located in the brainstem which contribute to homeostatic maintenance (Figure

1.4)[210,248]. The DVC encapsulates the circumventricular organ area postrema, the nucleus of the solitary tract (NTS), and the dorsal motor nucleus of the vagus[248]. Similar to the ARC, the NTS is located next to a brain ventricle (the fourth ventricle) and a circumventricular organ (area postrema) which possesses permeable capillaries. Both of these characteristics make the NTS a perfect candidate for regulating whole-body metabolism independently, in similar fashion to the ARC[210]. Indeed, the DVC is a major region that relays signals between the periphery and the brain, important for regulating energy and nutrient homeostasis[249].

The NTS has been heavily implicated in controlling glucose and lipid metabolism. To start, insulin's inhibitory role on HGP requires signaling in the NTS via the ERK pathway[250]. Importantly, insulin acting in the MBH also suppresses HGP; however, this is mediated via the PI3K/Akt pathway[251]. These studies illustrate how, despite a common effect between the MBH and NTS mediated by the same hormone, the underlying mechanisms may differ which could be important considerations for future therapeutic designs. Continuing, glucagon infusion directly into the DVC was observed to reduce HGP under pancreatic clamp studies[252]. At the same time, VLDL secretion experiments in the Yue laboratory has elucidated a role of NTS glucagon infusion to lower hepatic VLDL-TG release[253]. In contrast, DVC leptin action triggers VLDL secretion from the liver via vagal innervation[223]. In addition to hormone detection, the NTS can also directly sense nutrients. Oleate sensing in the DVC decreases VLDL-TG secretion, similar to its signaling in the MBH[209,249]. This lowering effect also required oleate's conversion to acyl-CoA through the enzymatic functions of long chain acyl-CoA synthetase[249]. Glycine action in the DVC to regulate glucose production has also been reported[254,255]. Whether the extracellular levels of glycine in the DVC were increased by direct infusion, or by pharmacological blockade or genetic knockdown of glycine transporters, HGP and food intake were both lowered[254,255]. Moreover, DVC glycine was also shown to lower VLDL-TG secretion by reducing hepatic expression of SCD1, which is an enzyme involved in generating monounsaturated fatty acids, particularly important for VLDL assembly[256]. Thus, there is clear evidence that implicates the DVC in regulating glucose metabolism through its sensing abilities, and specifically VLDL-TG secretion.

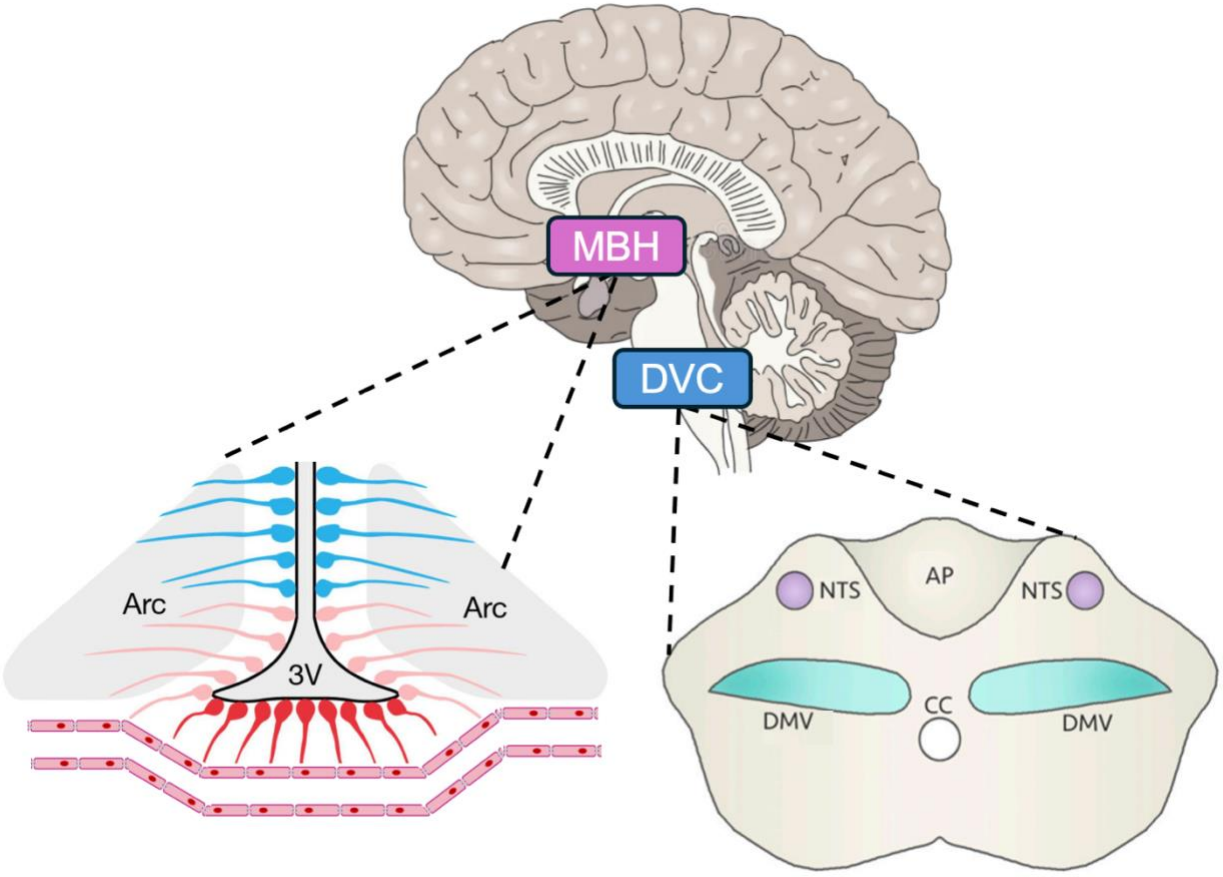

Figure 1.4: Schematic Representation of the Mediobasal Hypothalamus (MBH) and Dorsal Vagal Complex (DVC). The MBH within the hypothalamus contains the arcuate nucleus (ARC) located adjacent to the 3rd ventricle (3V) of the brain. The ARC is also in close proximity to fenestrated capillaries (image adapted from Fong and Kurrasch Front. Neurosci., 2023)[257]. The DVC is part of the brainstem and comprised of the nucleus of the solitary tract (NTS), area postrema (AP), and the dorsal motor nucleus of the vagus (DMV) (image adapted from Freeman et al. Neurosci, 2021)[258].

1.5 Aim, Hypothesis, and Objectives

1.5.1 Aims

Central GC action via the hypothalamus has previously been described to regulate lipid metabolism[237,240], and it is known that GRs (both cGRs and mGRs) are present throughout the brain[150,154,157,237,238,240,259]. Recent findings have also indicated that the brainstem region, the DVC, can independently sense nutrients and hormones to regulate hepatic VLDL-TG metabolism[223,249,253,256]. Therefore, in the present thesis, we sought to examine the effects of GC action in the NTS on hepatic VLDL-TG secretion.

1.5.1.1 Aim 1: To assess GC action and GR requirement in the NTS, and delineate downstream neuronal mediators for the modulation of hepatic TG secretion

Knowing that: 1) the brainstem, namely the NTS, controls metabolism[249,253,254], 2) GCs can regulate hepatic VLDL release through central mechanisms[240], and 3) central GC effects may be mediated via sympathetic innervation to the periphery[243], we aimed to elucidate if GCs acting in the NTS would alter hepatic lipid secretion. *We hypothesize that NTS GC infusion activates NTS GRs to stimulate liver VLDL-TG secretion via the sympathetic nervous system* (Figure 1.5).

1.5.1.2 Aim 2: To assess whether NTS mGRs affect liver VLDL-TG release

With the knowledge that Aim 1 revealed that GC action in the NTS modulates liver lipid metabolism, and that mGRs are expressed in neural tissue[150,157,166,260,261], our second aim was to test whether a membrane-impermeant DEX, which is able to activate mGRs[156,157,262,263], modulates hepatic lipid homeostasis. *We hypothesize that using membrane-impermeant DEX will activate mGRs, and require downstream intracellular signaling mediators, in the NTS to stimulate hepatic VLDL-TG secretion* (Figure 1.6).

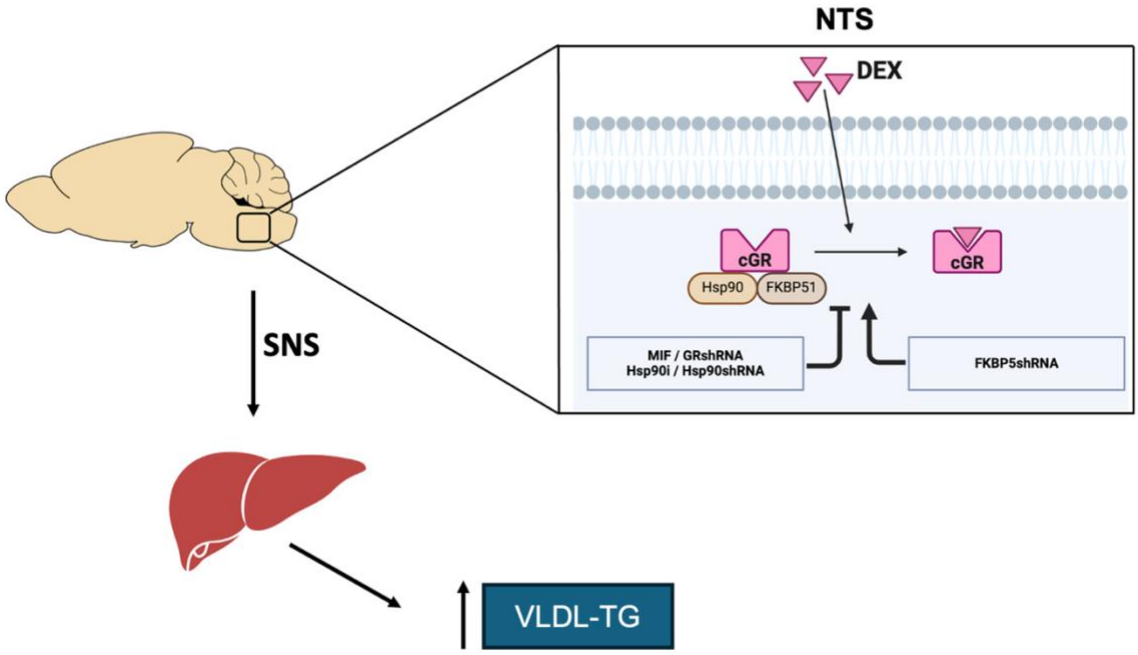

Figure 1.5: Schematic Representation of Aim 1 Working Hypothesis. Infusion of dexamethasone (DEX), a synthetic glucocorticoid into the nucleus of the solitary tract (NTS), a region within the dorsal vagal complex (DVC), act on cytosolic glucocorticoid receptors (cGRs) to stimulate lipid secretion from the liver via the sympathetic nervous system (SNS). The requirement of the cGR was tested through multiple ways. First, cGRs were antagonized directly with a pharmacological inhibitor of the cGR, mifepristone (MIF), or genetically knocked down using GR shRNA. cGR involvement was also indirectly assessed via Hsp90 inhibition with Hsp90i. Finally, FKBP51 knockdown in the NTS was also tested to activate the cGR. Figure made with Biorender.com.

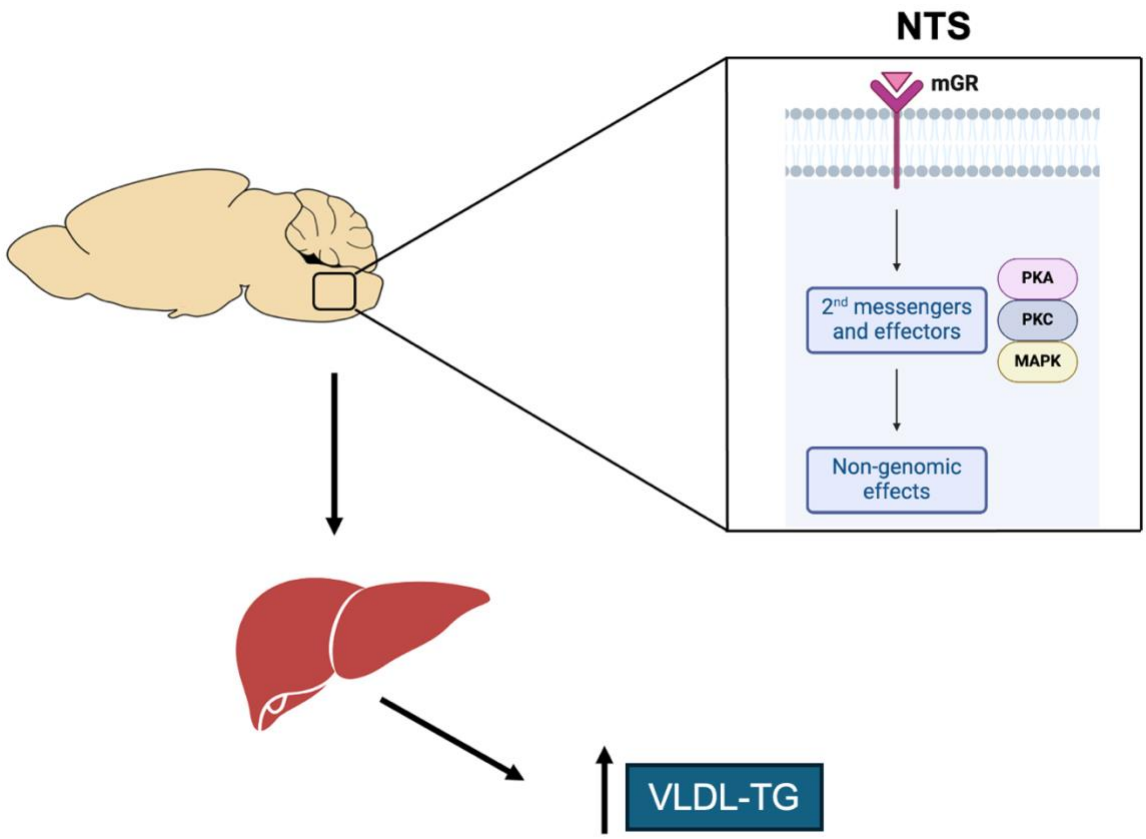

Figure 1.6: Schematic Representation of Aim 2 Working Hypothesis. Administration of a membrane-impermeant glucocorticoid into the nucleus of the solitary tract (NTS), acts on membrane glucocorticoid receptors (mGRs) to stimulate VLDL secretion from the liver. Downstream signaling effectors in the NTS were assessed, namely protein kinase A (PKA), protein kinase C (PKC), and mitogen-activated protein kinase (MAPK), to delineate the signaling cascade for NTS mGRs. Pharmacological inhibitors for the aforementioned kinases were used to test their necessity. Figure made with Biorender.com.

Chapter 2: Methods

2.1 Animal Care, Maintenance, and Surgical Procedures

All procedures and protocols for animal care and experiments were in accordance with AUP #1604 and approved by ACUC-2 at the University of Alberta Animal Care and Use Committee in accordance with regulations set forth by the Canadian Council for Animal Care.

Male Sprague Dawley (SD) rats, obtained from Charles River Laboratories (Stone Ridge, NY, USA), were used for *in vivo* experimentation for this study. Animals were housed in the Health Sciences Laboratory Animal Services building at the University of Alberta. Eight-week-old rats arrived weighing 220 - 240g and were placed with one other littermate for one week to acclimatize, before being housed in individual cages following stereotaxic cannulation surgery (see below) and kept on a standard 12h light-dark cycle with *ad libitum* access to water and standard regular chow (RC) (LabDiet PicoLab® Laboratory Rodent Diet, 5LOD; 57.491% cal. from carbohydrate, 28.903% cal. from protein, and 13.606% cal. from fat; 2.86kcal/g of total metabolized energy).

2.2 Surgeries

2.2.1 Stereotaxic Cannulation Surgery

Following the acclimatization period and reaching a body weight of 300 ± 20g, animals underwent bilateral stereotaxic cannulation surgery targeting the nucleus of solitary tract (NTS) under anesthesia (intraperitoneal administration of 60mg/kg ketamine (Ketalean, Bimeda-MTC) and 8mg/kg xylazine (Rompun, Bayer) (Figure 2.1). A 26-gauge, stainless steel, bilateral cannula (C235G, Plastics One Inc.) was implanted into the NTS following the coordinates on the occipital crest, 0.4 mm lateral to midline, 7.9 mm below the cranial surface[209,254,256]. Stereotaxic cannulation enabled direct NTS infusions (rate of 0.0055 µL/min) of 0.9% saline (vehicle) (Baxter #533-JB1323); 1.7% ethanol dissolved in 0.9% saline (another vehicle group) (Commercial Alcohols, Greenfield Global, P016EAAN), dexamethasone (DEX) (Sigma, D1756; 100ng/µl (255µM)), a synthetic glucocorticoid (GC) and potent GC receptor (GR) agonist; mifepristone (MIF) (Tocris #1479; 25nM), a GR antagonist; 17-allylamino-17-demethoxygeldanamycin (17-AAG) (HSP90i) (Tocris #1515; 0.606nmol/µl), a heat-shock protein 90 inhibitor; DEX conjugated to bovine serum albumin (BSA-DEX)

(Steraloids, P0516; 2.35µg/µL (28µM), a membrane-associated GR (mGR) agonist; Rp-cAMPs (Rp) (Tocris #1337/1; 40 µM), a PKA inhibitor; Bisindolylmaleimide I (BIMI) (Tocris #0741; 120µM), a selective PKC inhibitor; and PD98059 (PD) (Sigma Aldrich #19-143; 40 µM), a MEK inhibitor (used to prevent MAPK activation). Immediately after cannulation surgery, a subset of the animals received a bilateral 3 µL injection of a lentivirus (LV) that expresses a GR shRNA (Santa Cruz Biotechnology, sc-35506-V), Hsp90 shRNA (Santa Cruz Biotechnology, sc-156099-V), FKBP51 shRNA (Santa Cruz Biotechnology, sc-35381-V), or a control mismatch shRNA (MM) sequence (Santa Cruz Biotechnology, sc-108080). Verification of NTS cannulation placement and localization of brain infusions for the NTS was done by injecting 3µL of bromophenol blue dye following the end of the *in vivo* experiments.

2.2.2 Vascular Catheterization Surgery

Eight days post-NTS cannulation surgery, animals were subjected to vascular catheterization surgery on their left carotid artery and right jugular vein (Figure 2.1). This allowed conscious, unrestrained rats to undergo intravenous (i.v.) injections and repeated arterial blood sampling during *in vivo* experimentations. Animals were put under anesthesia (intraperitoneal administration of 90mg/kg ketamine (Ketalean, Bimeda-MTC), 10mg/kg xylazine (Rompun, Bayer) and underwent catheterization using catheters made up of polyethylene (PE-50) (ID: 0.58mm, OD: 0.965mm; Becton, Dickinson and Company) and silastic tubing (*Jugular:* ID: 0.64mm, OD: 1.19mm; *Carotid*: ID: 0.51mm, OD: 0.94mm; Dow Corning Corporation). The catheters were then filled with 10% heparinized saline to maintain patency and sealed with a metal pin.

For the first two days post-catheterization surgery, rats were administered 2mg/kg of Metacam for analgesia. Body weight and food intake was assessed daily following both surgeries to ensure animal welfare and recovery of all animals. Rats were only used for *in vivo* studies if they attained a minimum of 90% of their pre-catheterization surgery body weight.

2.3 *In vivo* VLDL Secretion Studies

Approximately five days post-vascular catheterization, rats that regained 90% of their body weight were fasted for ten hours the night before the experiment (Figure 2.1). Freely moving and conscious rats were subjected to a continuous NTS infusion of specific brain treatments (saline, DEX, MIF, MIF+DEX, HSP90i, HSP90i+DEX, BSA-DEX, Rp, Rp + BSA-DEX, BIMI, BIMI + BSA-DEX, PD, PD + BSA-DEX, HSP90i + BSA-DEX) (0.0055µL/min infusion rate) after a basal blood sample was taken. A subset of SD rats used to assess pharmacological sympathetic denervation were also administered an i.v. injection of a vehicle control solution of 15% dimethyl sulfoxide (DMSO) dissolved in 0.9% saline (Sigma Aldrich, D8418; 1mg/kg) or a cocktail comprising alpha- (phentolamine) (Sigma Aldrich, PHR1403-1; 1mg/kg) and beta- (propranolol) (Sigma Aldrich, P0884-1G; 1mg/kg) adrenergic antagonists (SNSi) ten minutes prior to the start of the brain treatment infusions. At the end of the pre-infusion period, another blood sample was obtained before starting the experiment by administering an i.v. injection of Poloxamer 407 (Sigma, #16758; 600mg/kg, dissolved in saline) at time 0 minutes. Poloxamer 407 inhibits lipoprotein lipase (LPL), thereby preventing the clearance of TG-rich lipoprotein particles such as chylomicrons and/or VLDL and in turn, elicit an accumulation of TG in the plasma. The rate of appearance of plasma TG over time is the rate of TG-rich lipoprotein secretion[209,256]. Given that the rats were fasted for 10-hours, the newly TG-rich lipoproteins being secreted are likely VLDL-TG being released from hepatocytes, and not from enterocyte-derived chylomicron-TGs. It has previously been discovered that chylomicron-TGs coming from the gut become negligible following a 4-hour fast, suggesting that gut-derived TG-rich lipoproteins will not have impacted the changes in plasma TG in our study[224]. Following the beginning of the experiment, arterial blood samples were taken at half-hour increments for 180 minutes, before a final sample was withdrawn at the end of the experiment at time 240 minutes. Blood samples were added to heparinized tubes and subjected to centrifugation to separate the plasma from the red blood cells. Glucose concentration of the plasma samples was measured using a glucose analyzer (GM9, Analox Instruments). This analyzer works through the glucose oxidase method, whereby the reagent solution used by the apparatus contains glucose oxidase, which

catalyzes the oxidation of glucose in the plasma sample to gluconic acid and hydrogen peroxide. The rate of oxygen consumption by the sample is directly proportional to glucose concentration. The Clark-type amperometric oxygen electrode inside the analyzer measures oxygen levels in the sample. Plasma samples were then aliquoted and stored at -20°C for later analysis of TGs and FFAs. Plasma used for ApoB48/100, or insulin analyses, was also treated with protease inhibitor (Sigma Aldrich, P8340) prior to storing. The leftover plasma and red blood cells were resuspended in 0.2% heparinized saline and reinfused into the rat to prevent hypovolemia and anemia. Following the end of the experiment at time 240 minutes, a 50µl i.v. injection of ketamine was administered to the rats to anesthetize animals before euthanasia via decapitation. A DVC (containing the NTS) wedge, liver, and WAT tissue samples were obtained immediately, and flash frozen in liquid nitrogen. Tissues were stored at -80°C for subsequent analysis.

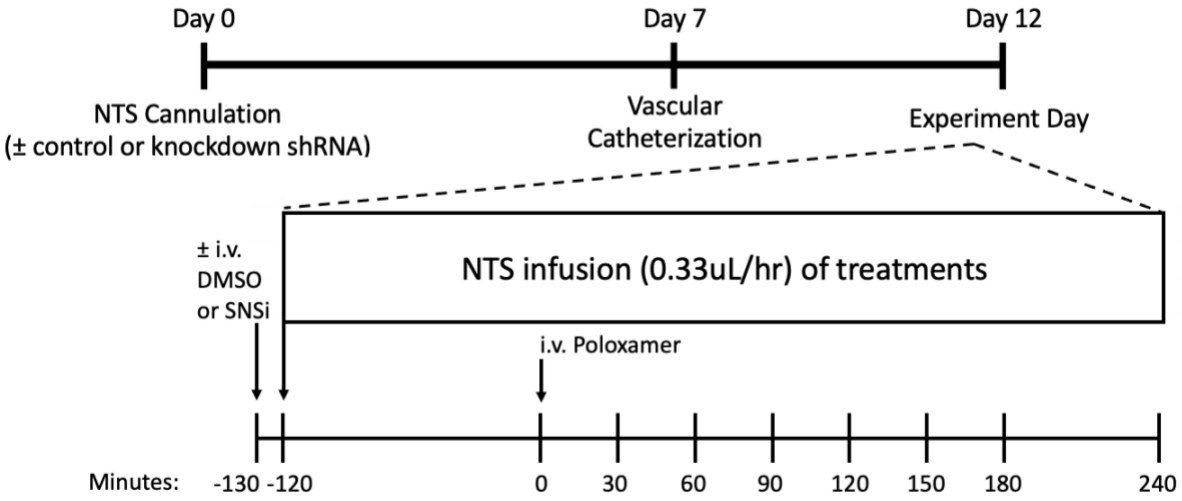

Figure 2.1: Experimental Design Protocol. Male Sprague Dawley rats underwent stereotaxic cannulation of the nucleus of the solitary tract (NTS). During NTS cannulation, a subset of animals received a lentivirus encapsulating a mismatch (MM) control shRNA or shRNA targeting the knockdown of a protein of interest. Eight days later, rats underwent vascular catheterization surgery. On day 12, *in vivo* experimentation took place where all rats were given a pre-infusion of brain treatments, followed by an i.v. injection of poloxamer, a lipoprotein lipase inhibitor. Blood samples were obtained for the duration of the experiment (240 minutes). At the end of the experiment, rats were euthanized via decapitation and tissues were collected for analyses.

2.4 Plasma TG Assay

Plasma triglycerides (TGs) were assayed using a commercially available enzymatic colorimetric assay kit (Fujifilm Wako Chemicals lab (Cat# 994-02891, Cat# 990-02991, Cat# 464-01601). Importantly, this Wako kit assesses plasma TGs, and not total lipids. This two-step assay first entails the elimination of free glycerol present in the sample, before subsequently hydrolyzing plasma TGs to glycerol. This glycerol is then oxidized and generated into a product that reacts with a peroxidase producing a blue pigment that can be detected using a microplate spectrophotometer at an absorbance wavelength of 600nm. TG concentrations are obtained by interpolating the absorbance value of each plasma sample to a standard curve of known concentration values.

Frozen plasma samples were thawed on ice, vortexed, and centrifuged at 2500rpm at 4°C for 30 seconds. Glycerol standards (Fujifilm Wako #464-01601, reconstituted with distilled water) were pipetted onto a standard 96-well plate to generate a standard curve, alongside 4µL of undiluted plasma samples. Next, 90µL of reagent one (R1) was added to each well that contained standard or sample and incubated at 37°C for 5 minutes. R1's purpose is to decompose free glycerol to a product that will not interfere with the colorimetric reaction.

Following the R1 incubation step, the plate was placed in the spectrophotometer (Epoch, BioTek) where the absorbances were measured at 600nm. Then, 30µL reagent two (R2) was added to each well and incubated at 37°C for 5 minutes. R2 contains lipases that hydrolyze the triglycerides in each sample to glycerol. Subsequent enzymatic reactions utilize this glycerol for the overall production of hydrogen peroxide, which contributes to the oxidative condensation of 4-aminoantipyrine and HMMPS (chemicals also present in R2), leading to the generation of a blue pigment.

Following the R2 incubation step, the plate was placed in the spectrophotometer where the absorbances of the samples were read at 600nm. The data was quantified by subtracting sample background (data after R1 added) from absorbance values of blue pigment (data after R2 added). The corrected absorbance values were plotted against the reference curve from known standards to determine concentration of TGs (mM).

2.5 Plasma FFA Assay

Plasma free fatty acids (FFAs) were assayed with a commercially available enzymatic colorimetric analysis kit (Fujifilm Wako Chemicals Lab #999-34691, 995-34791, 991-34891, 993-35191, and 276-76491). This two-step assay first generates acyl-CoAs from the FFAs present in the plasma samples by using acyl-CoA synthetase. Acyl-CoAs are then oxidized to produce hydrogen peroxide, which then interacts with a peroxidase enzyme allowing for various oxidative condensation reactions to form a colour that is measurable with a microplate spectrophotometer at 550nm. The FFA concentration is determined by comparing the absorbance of each sample to a standard curve of known concentration values.

The protocol followed for this assay kit was as follows, and samples were assayed in duplicate. Plasma samples were thawed, vortexed, and centrifuged at 2500rpm a 4°C for 30 seconds, then kept on ice. Reagent 1 (R1) and reagent 2 (R2) were made by reconstituting their corresponding solute with their applicable solvent. The standard curve was made using the non-esterified fatty acid, oleic acid, at varying concentrations, as provided by the kit. In a standard 96-well assay plate, 5µl of each standard or sample was pipetted, followed by 200µl of R1 and an incubation for 5 minutes at 37°C. R1 contains acyl-CoA synthetase (ACS), adenosine triphosphate (ATP), and CoA, which are needed to produce acyl-CoAs. After the incubation period, 100µl of R2 was added before another incubation step at 37°C for 5 minutes. R2 contains the enzymes (acyl-CoA oxidase and peroxidase) that catalyze the enzymatic colorimetric reactions, leading to a colour change that can be analyzed at a wavelength of 550nm.

2.6 Plasma Insulin

Plasma insulin levels were assessed using a commercially available radioimmunoassay (RIA) kit (EMD Millipore Corporation, RI-13K) with 100% specificity for rat insulin. The RIA assay is a two-day protocol and a very sensitive technique that measures antigen (insulin) concentrations by determining how much of it binds to its antibody. The assay works by adding a fixed concentration of labelled tracer antigen (^{125}I-labeled insulin) and incubating it with a known amount of antibody resulting in the binding of the two. When adding plasma samples, the unlabeled plasma insulin

competes with the labelled insulin for the binding sites of the antibody. The higher the concentration of unlabeled insulin from plasma samples, the less amount of labeled insulin binds to the antibody, resulting in more free labeled insulin. Precipitation and centrifugation are used to separate the bound and unbound antigen. The supernatant that is aspirated from the sample contains unbound labeled antigen, and the radioactivity of the remaining precipitate is measured using a gamma counter. The concentration of plasma insulin can be quantified by interpolation of a standard curve that is generated with known concentrations of unlabeled antigen standard provided by the kit.

The protocol was as follows. The entire assay was done using borosilicate 12x75mm glass tubes (Fisher Scientific, 14-961-26). On day one, the insulin standard curve was prepared using 10ng/ml of unlabeled antigen standard which was also diluted further down. The standards, quality controls, and each experimental plasma sample (treated with protease inhibitor) were pipetted (50µl) into their respective tubes. Assay buffer was added to non-specific binding (NSB = blank) tubes (100µl) and in reference (B_0=100% binding) tubes (50µl). ^{125}I-labeled insulin (50µl) was added to every tube followed by 50µl of insulin antibody (guinea pig anti-rat insulin serum). However, total count (TC) and NSB tubes did not receive any insulin antibody. Tubes were vortexed, covered with parafilm, and incubated overnight (20-24h) at 4°C. On day two, 500µl of cold precipitating reagent was added to every tube except the TC tubes. All tubes were vortexed, before a 20-minute incubation at 4°C. Next, all tubes barring TCs were centrifuged at 2000xG for 20 minutes at 4°C to form an insulin-bound pellet. The resulting supernatant in each tube was aspirated to generate a liquid-free pellet. Radioactivity of the pellet was measured for 5 minutes with a gamma counter (Packard, Cobra II Series). The sample and standard counts (B) were expressed as a percentage of the mean counts of the total binding (B_0) tubes. The percentage of total binding (%B/B_0) for all standards and plasma samples was plotted against the reference curve of known standards to interpolate the insulin concentrations.

2.7 Plasma Lipoprotein Fractionation

Lipoprotein (VLDL, LDL, and HDL) fractionation was conducted by Audric Moses from the Lipidomics Core Facility at the University of Alberta. Plasma lipoproteins were separated via fast protein liquid chromatography (FPLC). Briefly, 100µL of heparinized plasma (collected from *in vivo* experimentation) was injected by an autosampler into an Agilent 1200 HPLC instrument equipped with a Superose 6 Increase 10/300 GL gel-filtration FPLC column which separates intact lipoproteins by size and detecting them at an absorbance of 280nm. Total run time was 60 minutes with a flow rate of 500µL/min. Twenty fraction samples were collected at 2-minute intervals starting at 15 minutes into the run lasting until the 55^{th} minute mark.

TG levels were next assayed in the VLDL-containing fraction (note: although fractions #1-3 all eluted within the VLDL range, fraction #2 was chosen to be assayed as it eluted during the highest point of the VLDL-absorbance peak) through a modified protocol of the TG assay described above. These were the steps followed: a series of glycerol standards (Fujifilm Wako #464-01601, reconstituted with distilled water) were added onto a standard 96-well plate, followed by 100µL of fraction #2. Next, 30µL of R1 was added to each well and incubated at 37°C for 5 minutes. After the incubation step, the plate was placed in the spectrophotometer (Epoch, BioTek) and absorbances were measured at 600nm. R2 was next added (10µL), and the plate was incubated once more at 37°C for 5 minutes. A final absorbance reading at 600nm was recorded with the spectrophotometer. Data analysis of TG quantification was the same as described above.

It is also worth mentioning that this technique is not without limitations. Although intestinal chylomicrons are generally larger than VLDL particles, their size ranges do overlap. Due to this, the VLDL fraction obtained from FPLC may contain some chylomicron-TGs. Thus, this technique is a semi-quantitative measurement of VLDL-TG.

2.8 Hepatic TG Content

Hepatic TG quantification was done by using a modified form of the Folch method[264], in collaboration with Dr. Robin Clugston. The step-by-step protocol followed was as follows. On day one, approximately 50mg of frozen liver tissue (exact weights were recorded and used for subsequent calculations) was homogenized in 12x75mm glass tubes (Fisher Scientific, 14-961-26) using 5mL of 2:1 chloroform:methanol solution. Glass tubes were sealed with parafilm and incubated overnight at 4°C. On day two, the homogenized solution was filtered through #1 Whatman® paper (4.25cm, #1001-042) into 13x100mm glass tubes (Fisher Scientific, 14-961-27). Next, another 2mL of 2:1 chloroform:methanol solution was added into original 12x75mm glass tubes to extract any leftover liver TGs and filtered into the 13x100mm glass tube. Then, 1.25mL of acidified saline solution (100mL 0.9% saline solution and 1mL of 1N HCl (Fisher Scientific, SA48B-1)) was added to the filtrate and vortexed. Samples were left for 5 minutes at room temperature before being centrifuged at 1000 rpm for 15 minutes. The upper phase of the solution was removed with a Pasteur pipette (Fisher Scientific, 13-678-20C) and discarded. The steps above of adding acidified saline, centrifugation, and removal of the upper layer were repeated a second time. After, 1.25mL of an upper phase solution containing methanol (480mL/L), chloroform (30mL/L), water (470mL/L), and calcium chloride dehydrated (400mL/L) (Fisher Scientific, BP5100500) was added to the liquid phase. Samples were vortexed, centrifuged, and their top layer was discarded as described above. These steps were performed two times over. The leftover solution was dried under nitrogen gas, and the remaining pellet was resuspended in 100µl of 100% ethanol (Commercial Alcohols, Greenfield Global, P016EAAN). Samples were diluted in a 1:5 ratio and TGs were quantified with the Fujifilm WAKO TG assay kit (described above). TG concentrations (mM) obtained were next corrected for the mass of tissue used. Using the mM concentration of TGs, the units were converted to µg of TGs. Then we divided this value by the weight of liver that was recorded, and final results of liver TG content were reported as µg/mg.

2.9 Western Blotting

Western blotting was used for protein analysis on tissue (liver, WAT, and DVC) and plasma samples.

2.9.1 Tissue Western Blotting

Frozen tissue of liver (~20mg), WAT (~50mg), and DVC (~10mg) was homogenized in 1% NP- 40 lysis buffer (20mM Tris-HCl (pH 7.4), 5mM EDTA, 1% (w/v) Nonidet P-40, 2mM sodium orthovanadate, 5mM sodium pyrophosphate tetrabasic, 100mM sodium fluoride, phosphatase inhibitor, and protease inhibitor at a dilution factor of 1:10 (tissue (mg) to homogenizing buffer (µL)). Samples were then placed on ice for 30 minutes, followed by centrifugation at 1200xG for 30 minutes at 4°C. The supernatant (or lysate) was preserved and transferred into a new tube. Lysates were then assayed to determine their protein concentration, which is needed for subsequent loading sample preparation. Protein concentrations were assessed using a Pierce™ BCA Protein Assay Kit (Thermo Scientific, 23225). Lysates were diluted with double distilled water at 1:20 for liver and DVC tissue, and 1:10 ratio for WAT. This colorimetric assay uses a microplate spectrophotometer and uses a 540nm wavelength for optimal absorbance. Tissue loading samples were prepped at a final concentration of 1.67µg/µl (25µg of protein/lane and 15µl of volume loaded per lane). Final loading samples were loaded onto a polyacrylamide gel (5%, 8%, 12%, or 15%) and subjected to gel electrophoresis (Mini-PROTEAN® Tetra Vertical Electrophoresis Cell, Bio-Rad) at 130V until the proteins were sufficiently separated. The proteins were next transferred from the gel onto a nitrocellulose membrane (0.45µm, Bio-Rad, #1620115) for 2.5 hours at 90V at 4°C. To confirm that the proteins were successfully transferred, nitrocellulose membranes were stained with Ponceau S Solution (Abcam, ab270042). Following this, membranes were incubated in blocking buffer (5% milk in Tris-buffered saline containing 0.2% Tween-20 (TBST) (Sigma, P1379)) for 1 hour at room temperature and rinsed with 1xTBST, prior to primary antibody incubation overnight at 4°C (Table 2.1). The next day, membranes were washed three times with 1xTBST for 5 minutes each, before incubating in horseradish peroxidase-linked secondary antibody (diluted 1:1000 in blocking buffer) for 1 hour at room temperature (Table 2.2). Following incubation, membranes were washed again three times with 1x TBST for 5 minutes each and

protein expression was enhanced using a chemiluminescence reagent (Pierce™ ECL Western Blotting Substrate, Thermo Scientific, 32106). A chemiluminescent imaging system (Bio-Rad,ChemiDoc) was used to image the immunoblots, which were then quantified by densitometry with ImageJ image analysis software.

2.9.2 Plasma ApoB Western Blotting

Protease inhibitor-treated plasma was diluted to 1:50 by mixing 2µl of plasma in 98µl of double distilled water. Next, 100µl of 2x Laemmli Sample Buffer (BioRad, 1610737) was then added to each sample. Plasma samples were then boiled for 5 minutes. The diluted plasma samples were then pipetted (10µl) onto a 4-15% gradient gel (4-15% Mini-PROTEAN® TGXTM Precast Protein Gels, Bio-Rad, #4561086) and subjected to gel electrophoresis at 130V for approximately 3 hours. Separated proteins in the gel were then transferred at 90V for 2.5 hours onto a nitrocellulose membrane (0.45 µm, Bio-Rad, #1620115). Again, membranes were stained with Ponceau S to verify the transfer step. The remaining steps were the same as tissue western blotting described above.

Primary Antibody	Company and Catalogue Number	Dilution	Secondary Antibody
Fatty-Acid Synthase (FAS)	Santa Cruz #sc-55580	1:1000	GAM
phospho Acetyl-CoA Carboxylase (pACC)	Cell Signaling #3661	1:1000	GAR
Acetyl-CoA Carboxylase (ACC)	Cell Signaling #3662	1:1000	GAR
Microsomal Triglyceride Transfer Protein (MTP)	BD Transduction Laboratories #612022	1:1000	GAM
ADP-ribosylation factor 1 (Arf1)	Santa Cruz #sc-53168	1:1000	GAM
Apolipoprotein B (ApoB)	Santa Cruz #sc-393636	1: 500	GAM
CD36	Novus Biologicals #NB400-144	1:1000	GAR
Fatty Acid Transport Protein 2 (FATP2)	Thermo Fisher #PA5-42429	1:1000	GAR
Fatty Acid Transport Protein 5 (FATP5)	Thermo Fisher #PA5-42028	1:1000	GAR
phospho Hormone-Sensitive Lipase (pHSL)	Cell Signaling #45804	1:1000	GAR
Hormone-Sensitive Lipase (HSL)	Cell Signaling #4107	1:1000	GAR
Adipose Triglyceride Lipase (ATGL)	Cell Signaling #2138	1:1000	GAR
Comparative Gene Identification 58 (CGI-58)	Santa Cruz #sc-376931	1:500	GAM
Perilipin	Abcam #ab3526	1:1000	GAR
Glucocorticoid Receptor (GR)	Cell Signaling #3660	1:1000	GAR
FK506 Binding Protein 5 (FKBP51)	Santa Cruz #sc-271547	1:1000	GAM
β-Actin	Santa Cruz #sc-47778	1:1000	GAM
Vinculin	Santa Cruz #sc-25336	1:1000	GAM

Table 2.1: List of all Primary Antibodies used for western blotting in this study

Secondary Antibody	Company and Catalogue Number	Dilution
Anti-Mouse IgG, HRP-Linked Antibody (GAM)	Cell Signaling #7076	1:1000
Anti-Rabbit IgG, HRP-Linked Antibody (GAR)	Cell Signaling #7074	1:1000

Table 2.2: List of Secondary Antibodies used for western blotting in this study

2.10 Quantitative PCR (qPCR)

2.10.1 RNA extraction

Approximately 35mg of liver and 10mg of DVC tissue were homogenized using 1000µL and 330µL of Trizol (Ambion, 15596026), respectively, to break down the biological material and proteins without affecting the RNA. Homogenized samples were centrifuged at 8700 rpm for 10 minutes at 4°C, and the resulting supernatant was kept. Chloroform (200µL for liver samples; 67µL for DVC samples) was added to the supernatants, causing a phase separation where the denatured proteins get extracted into the organic phase, leaving just the RNA in the aqueous phase. The solution rested at room temperature for 3 minutes, and then centrifuged at 8700 rpm for 15 minutes at 4°C. The upper (aqueous) phase was stored into a new sterile microtube, where isopropanol (Sigma-Aldrich, 439207) (500µL for liver samples; 167µL for DVC samples) was added and mixed in. RNA extracts were incubated overnight at -20°C. On day two, samples were centrifuged at 12,000xG for 10 minutes at 4°C, causing the RNA to settle at the bottom as a pellet. The supernatant was discarded and then 1000µL (for liver) or 330µL (for DVC) of 75% ethanol was added to cleanse the RNA pellet from any contaminants. Next, samples were centrifuged at 7500xG for 5 minutes at 4°C. The supernatant was discarded, and steps from the ethanol wash process were repeated a second time for DVC samples or 3 times for liver samples. After, the samples were air dried in a fume hood at room temperature for 30 minutes to evaporate the ethanol. The RNA pellets were then resuspended in 100µL (for liver) or 20µL (for DVC) of

UltraPure™ DNAse/RNase-Free Distilled Water (Invitrogen, #10977-015). To quantify the concentration of the RNA samples, 1µL of sample was pipetted onto a NanoDrop 1000 spectrophotometer (Thermo Fisher) measuring at a 260nm wavelength absorbances. Samples with a 260nm/280nm ratio ranging between 1.8 and 2.0 (indicated little-to-no protein contamination in our RNA extracts) and a 260nm/230nm ratio between 2.0 and 2.2 (indicated little-to-no organic contamination in our RNA extracts) were deemed relatively pure RNA extracts and used for cDNA synthesis.

2.10.2 cDNA synthesis

Complementary DNA (cDNA) was synthesized using RNA extracted from liver or DVC tissue samples. The volume of sample containing 2µg of total RNA (determined with the concentration of RNA obtained with the NanoDrop) was added to RNase-free water (Invitrogen, #10977-015) to make a 9µl mixture. Next, 2µl of Random Hexamer Primers (1µg/µl) (Invitrogen, #48190011) was added to each sample, before being put through a PCR program (Eppendorf, Mastercycler gradient) to denature the RNA at 70°C for 10 minutes. Following this, a mixture containing: Superscript II IV VILO Master Mix kit (Invitrogen, #11756050), 1.25mM dNTP (Invitrogen, #10297-018), and 2U/µL RNaseOUT (Invitrogen, #10777-019) was added (9µL) to each sample, yielding a final volume of 20µL per sample. Samples were next run through a PCR program for cDNA transcription for 1 hour at 40°C to generate cDNA at a concentration of 100ng/µL. Prior to running the qRT-PCR, cDNA was diluted to 1ng/µL (1:100) using RNase-free water.

2.10.3 qRT-PCR

Quantitative real-time PCR (qRT-PCR) was performed using a StepOne™ Real-Time PCR Systems (Applied Biosystems™), in collaboration with Mr. Randal Nelson and Dr. Richard Lehner's laboratory. Gene assessment was done on MicroAmp™ 96-Well Reaction Plate with Barcode (Applied Biosystems, #4346906) with POWER SYBR Master Mix (Applied Biosystems, #4367659) and custom designed primers, developed by Integrated DNA Technologies (Table 2.3). Cyclophilin (gene name: *Ppia*) was used as the housekeeping gene and all expression values were normalized to its Ct value. Quantification was done using the $2^{-\Delta\Delta Ct}$ method.

Gene Name	Designed By	Forward Primer Sequence	Reverse Primer Sequence
Srebf1c	Integrated DNA Technologies	ACAAGATTGTGGAGCTCAAGG	TGCGCAAGACAGCAGATTTA
Dgat1	Integrated DNA Technologies	TACGGCGGGTTCTTGAGAT	CGTGAATAGTCCATGTCCTTGA
Dgat2	Integrated DNA Technologies	GTGTGGCGCTATTTTCGAG	GGTCAGCAGGTTGTGTGTCTT
Scd1	Integrated DNA Technologies	CATGTCTGACCTGAAAGCTGA	CAGGAGGCCAGGCTTGTAG
Lpin2	Integrated DNA Technologies	AAGATGCCGAAGAAATCTGG	CTTGGTCTCCGGCAACTG
Arf1	Integrated DNA Technologies	TGGCGCCACTACTTCCAG	TCGTTCACACGCTCTCTGTC
Chrebp	Integrated DNA Technologies	CAGATGCGGGACATGTTTGA	AATAAAGGTCGGATGAGGATGCT
Ampk	Integrated DNA Technologies	CCGTCTGATATTTTCATGGTCA	ACTCTCCTTTTCGTCCAACCT
Cpt1a	Integrated DNA Technologies	ACAATGGGACATTCCAGGAG	AAAGACTGGCGCTGCTCA
Ppara	Integrated DNA Technologies	TGCGGACTACCAGTACTTAGGG	GGAAGCTGGAGAGAGGGTGT
Fkbp5	Integrated DNA Technologies	GAACCCAATGCTGAGCTTATG	ATGTACTTGCCTCCCTTGAAG
Pdk4	Integrated DNA Technologies	GAACACCCCTTCCGTCCAGCT	TGTGCCATCGTAGGGACCACA
Npy	Integrated DNA Technologies	AGAGATCCAGCCCTGAGACA	ACCACATGGAAGGGTCTTCA

Table 2.3: All DNA custom primers used for PCR analyses conducted for this study.

2.11 Statistical Analysis

All data values are represented as the mean + standard error of the mean (SEM). Unpaired Student’s t-tests were done when statistical analysis compared two groups. For comparisons of three or more groups, analysis of variance (ANOVA) was used assuming unequal standard deviation, and if significant, was followed by Fisher's post-hoc tests. Two-way repeated measures ANOVA with unequal standard deviation was conducted on measurements collected over time as well as receiving different treatments, followed by a Fisher's post-hoc test if significance was achieved. The significance threshold for this study was set at a P-value < 0.05.

Chapter 3: Aim 1 Results

The first aim for this thesis was to test whether GCs acting in the NTS would trigger hepatic VLDL-TG secretion. We further assess the requirements of GRs in the NTS and the sympathetic nervous system. *We hypothesize that NTS GC infusion activates NTS GRs to stimulate liver VLDL-TG secretion via sympathetic outflow* (Figure 1.4).

3.1 Effects of Glucocorticoid Receptor Activation in the Nucleus of the Solitary Tract on Lipid Metabolism

3.1.1 Acute glucocorticoid infusion into the nucleus of the solitary tract triggers hepatic triglyceride-rich very-low density lipoprotein secretion.

To test if glucocorticoid (GC) action in the nucleus of the solitary tract (NTS) affects triglyceride (TG)-rich very-low density lipoprotein (VLDL-TG) secretion from the liver, we first directly infused dexamethasone (DEX), a synthetic GC, into the NTS of Sprague Dawley (SD) rats, and TG secretion rates were assessed via VLDL secretion experimentation (Figure 3.1.1A). All animals were 10-h fasted, conscious, and freely moving in their home cages during the *in vivo* studies.

Infusion of DEX into the NTS triggered a significant increase in plasma TG (Figure 3.1.1B) and VLDL-TG secretion rate (Figure 3.1.1C) compared to NTS Vehicle control. When infusing the GC receptor (GR) antagonist, mifepristone (MIF), alone into the NTS, plasma TG and VLDL-TG secretion rates were similar to the control group, indicating that acutely blocking NTS GRs does not impact plasma TG levels or hepatic VLDL-TG secretion (Figure 3.1.1B, C). Interestingly, when we co-infused MIF+DEX together into the NTS, the stimulatory effects of NTS DEX on plasma TG and the VLDL-TG secretion rate were negated (Figure 3.1.1B, C). This suggests that the effects on lipid metabolism of DEX acting in the NTS are mediated through NTS GRs. We next sought to confirm that it was indeed VLDL-TG that was increased in the NTS DEX treated animals by fractionating the plasma lipoproteins via FPLC (Figure 3.1.1D). Compared to the NTS Vehicle/NTS MIF combined group, NTS DEX showed higher TG levels in the VLDL-containing plasma fraction, and MIF was able to reverse this effect in the NTS MIF+DEX-infused SD rats (Figure 3.1.1D), supporting an increase in VLDL-TG levels in the NTS DEX group. Since we found that VLDL-TG levels were increased in the NTS DEX group, we next assessed plasma ApoB levels through western blotting (Figure

3.1.1E). As a VLDL particle contains one ApoB protein, the amount of ApoB found in the plasma can be directly related to the amount of VLDL particles secreted from the liver. Since rat hepatocytes secrete VLDLs containing either ApoB48 or ApoB100[85], we used western blot to measure plasma ApoB48 and ApoB100 levels in plasma taken at the beginning (T = 0) and end (T = 240. min) of the *in vivo* VLDL secretion experiments. As expected, plasma ApoB48 and ApoB100 levels significantly increased by time 240 min which was induced by the administration of poloxamer 407 (Figure 3.1.1E). However, there was no difference between groups at time 240 min for either ApoB48 or ApoB100, suggesting that the liver may not be releasing more VLDL particles, but rather more lipidated particles in response to NTS DEX infusion. Interestingly though, NTS DEX did not affect liver TG content levels (Figure 3.1.1F). Additionally, we found that plasma FFAs at the end of the experiment were significantly increased in the NTS DEX group (Figure 3.1.1G). Of note, increased FFAs could be contributing to the increased VLDL-TG with NTS DEX treatment since. FFAs are a substrate for TG synthesis and overall secretion by the liver[26]. Finally, the NTS DEX induced increase in plasma TG was independent of plasma glucose (Figure 3.1.1H), plasma insulin (Figure 3.1.1I) levels at the end of the experiment, or body weight at the start of the experiment (Figure 3.1.1J).

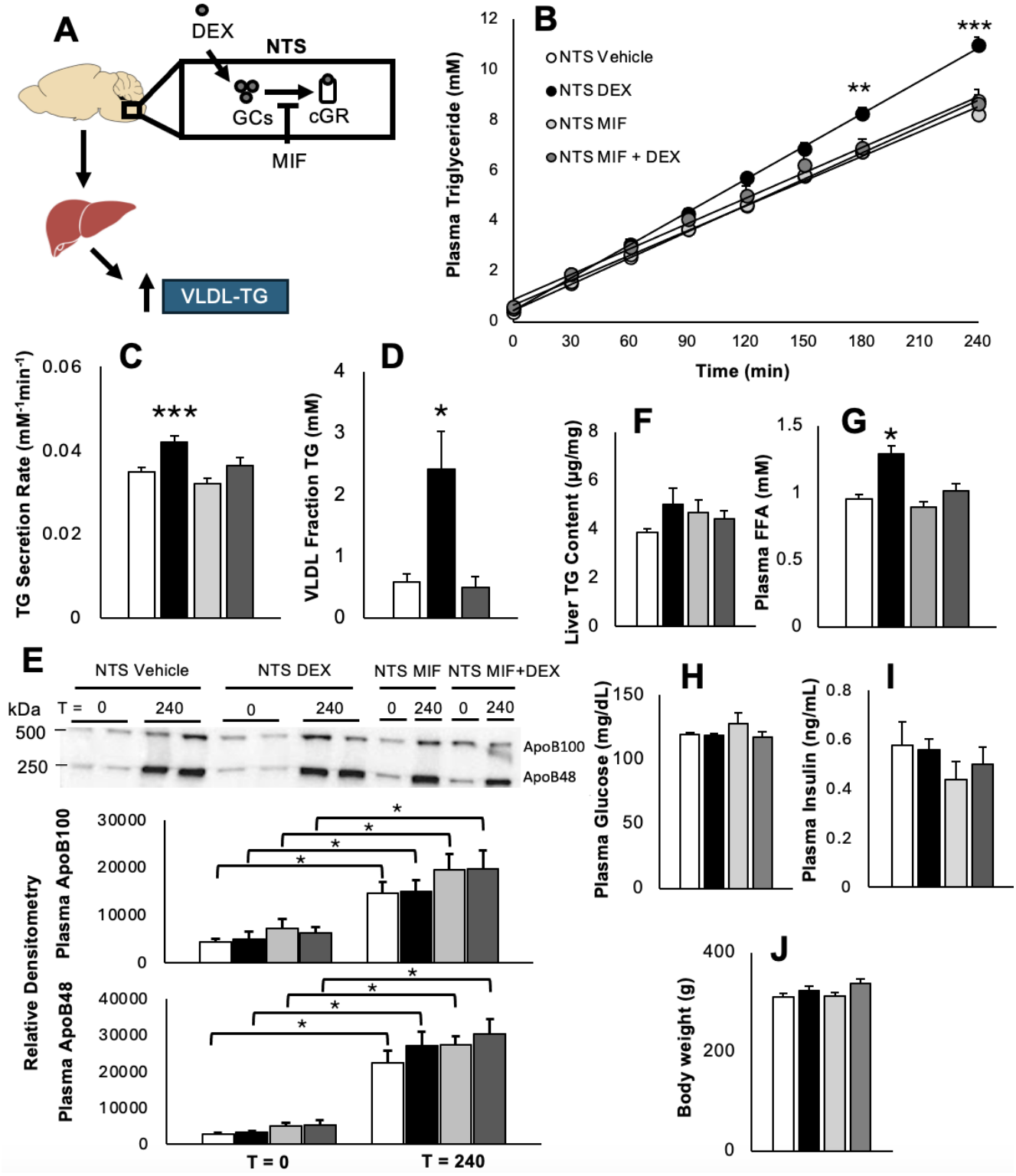
A
DEX
NTS
GCs
cGR
MIF
VLDL-TG
B
NTS Vehicle
NTS DEX
NTS MIF
NTS MIF + DEX
Plasma Triglyceride (mM)
Time (min)
C
TG Secretion Rate (mM-1min-1)
D
VLDL Fraction TG (mM)
E
NTS Vehicle
NTS DEX
NTS MIF
NTS MIF+DEX
kDa
T =
ApoB100
ApoB48
Relative Densitometry
Plasma ApoB100
Plasma ApoB48
T = 0
T = 240
F
Liver TG Content (µg/mg)
G
Plasma FFA (mM)
H
Plasma Glucose (mg/dL)
I
Plasma Insulin (ng/mL)
J
Body weight (g)

Figure 3.1.1. Acute NTS glucocorticoid infusion increases plasma triglycerides. **A)** Schematical representation of working hypothesis about NTS DEX's lipostimulatory effects. **B)** Plasma TG concentration for animals that received NTS Vehicle (white; n = 10), NTS DEX (black; n = 9), NTS mifepristone (MIF) (light gray; n = 10), and NTS MIF+DEX (dark gray; n = 7). **C)** Hepatic triglyceride secretion rate. **D)** Triglyceride levels in very-low density lipoprotein fraction. NTS Vehicle and NTS MIF combined (white; n = 4), NTS DEX (n = 5), and NTS MIF+DEX (dark gray; n = 3). **E)** Western blot for plasma ApoB100 and ApoB48 at beginning (t = 0 min) and end (t = 240 min) of experiment and quantification (NTS Vehicle n = 6; NTS DEX n = 6; NTS MIF n = 6; NTS MIF+DEX n = 5). **F)** Liver triglyceride levels. **G)** Plasma free fatty acids (FFAs), **H)** glucose, and **I)** insulin at end of experiment. **J)** Body weight at start of experiment. For **B)**, NTS DEX vs NTS Vehicle, NTS MIF, NTS MIF+DEX **P < 0.01 for effect of time, treatment, and interaction between time and treatment (two-way ANOVA). ***P < 0.001 and **P < 0.01 at t=240 and t=180min, respectively, using Fisher's posthoc test. For **C)**, **D)**, and **G)**, one-way ANOVA was used prior to conducting a Fisher's posthoc test (*P < 0.05, and ***P < 0.001 for NTS DEX vs NTS Vehicle, NTS MIF, NTS MIF+DEX). For **E)**, ApoB100 and ApoB48 graphs: *P < 0.05 for effect of time, treatment effect n.s., and interaction between time and treatment n.s. Data was measured as mean + SEM.

3.1.2 Assessement of changes in the nucleus of the solitary tract upon glucocorticoid administration.

To confirm that DEX infusions induced neural responses in the targeted region of infusion, we conducted qPCR on hindbrain DVC wedges (containing the NTS) analyzing for markers of GR activation (Figure 3.1.2). We measured the levels of two genes, *Fkbp5* and Pdk4, which show increased levels of expression upon GR activation[145,265]. NTS DEX was able to significantly increase the expression of both *Pdk4* (Figure 3.1.2A) and *Fkbp5* (Figure 3.1.2B) compared to NTS Vehicle and NTS MIF. However, in the NTS MIF + DEX co-infusion group, MIF was only able to block the up regulation of the *Pdk4* gene, and not *Fkbp5* (Figure 3.1.2A, B).

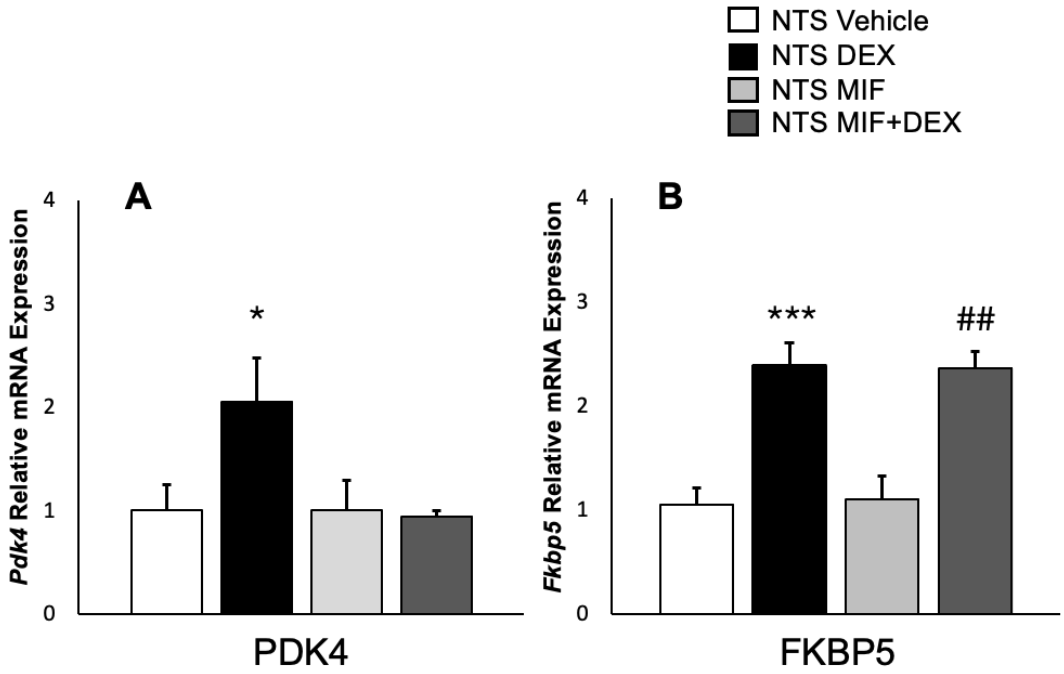

Figure 3.1.2. Assessment of glucocorticoid receptor activity markers. A) Relative expression of *Pdk4* in dorsal vagal complex (DVC) tissue between NTS Vehicle (white; n = 5), NTS DEX (black; n = 5), NTS MIF (light gray; n = 5), and NTS MIF+DEX (dark gray; n = 3). **B)** Relative expression of *Fkbp5* in DVC tissue between NTS Vehicle (white; n = 5), NTS DEX (black; n = 5), NTS MIF (light gray; n = 5), and NTS MIF+DEX (dark gray; n = 3). For **A)**, *P < 0.05 NTS DEX vs NTS Vehicle, NTS MIF, NTS MIF+DEX. For **B)**, ***P < 0.001 for NTS DEX vs NTS Vehicle and NTS MIF; ##P < 0.01 for NTS MIF+DEX vs NTS Vehicle and NTS MIF. Data was measured as mean + SEM.

3.1.3 Investigation of hepatic mechanisms involved in the NTS DEX mediated increase in hepatic triglyceride-rich very-low density lipoprotein secretion via western blotting.

To begin to delineate a peripheral mechanism by which NTS DEX stimulates an increase in plasma TG, we first investigated lipid metabolic pathways within the liver through western blotting and PCR. The proteins and genes analyzed were related to hepatic lipogenesis, VLDL assembly and secretion, and fatty acid transport and oxidation (Figure 3.1.3A).

We first found that NTS DEX's ability to regulate VLDL-TG secretion is independent to changes in levels of phosphorylated-acetyl-CoA carboxylase (pACC) to total acetyl-CoA carboxylase (ACC) and fatty acid synthase (FAS), indicating *de novo* lipogenesis (DNL) is unlikely to be involved in the change of plasma TGs (Figure 3.1.3B, C). This was expected since in the fasting state (e.g. animals were 10h fasted prior to VLDL secretion studies), DNL is suppressed. Next, we probed for the levels of liver ApoB48 and ApoB100, microsomal TG transfer protein (MTP), or ADP-ribosylation factor 1 (Arf1) all of which are proteins involved in either the structure (ApoB48/100), assembly (MTP), or secretion (Arf1) of rat VLDL particles, but no difference was found between groups (Figure 3.1.3D-G). Lastly, protein levels for fatty acid transport protein 2 and 5 (FATP2, FATP5) and CD36 were assessed to see if FFA uptake into the liver may have been enhanced with NTS DEX treatment since FFAs can be used as a substrate for TG synthesis (Figure 3.1.3H-J). Our results showed no significant change in the levels of any fatty acid transporters we looked at.

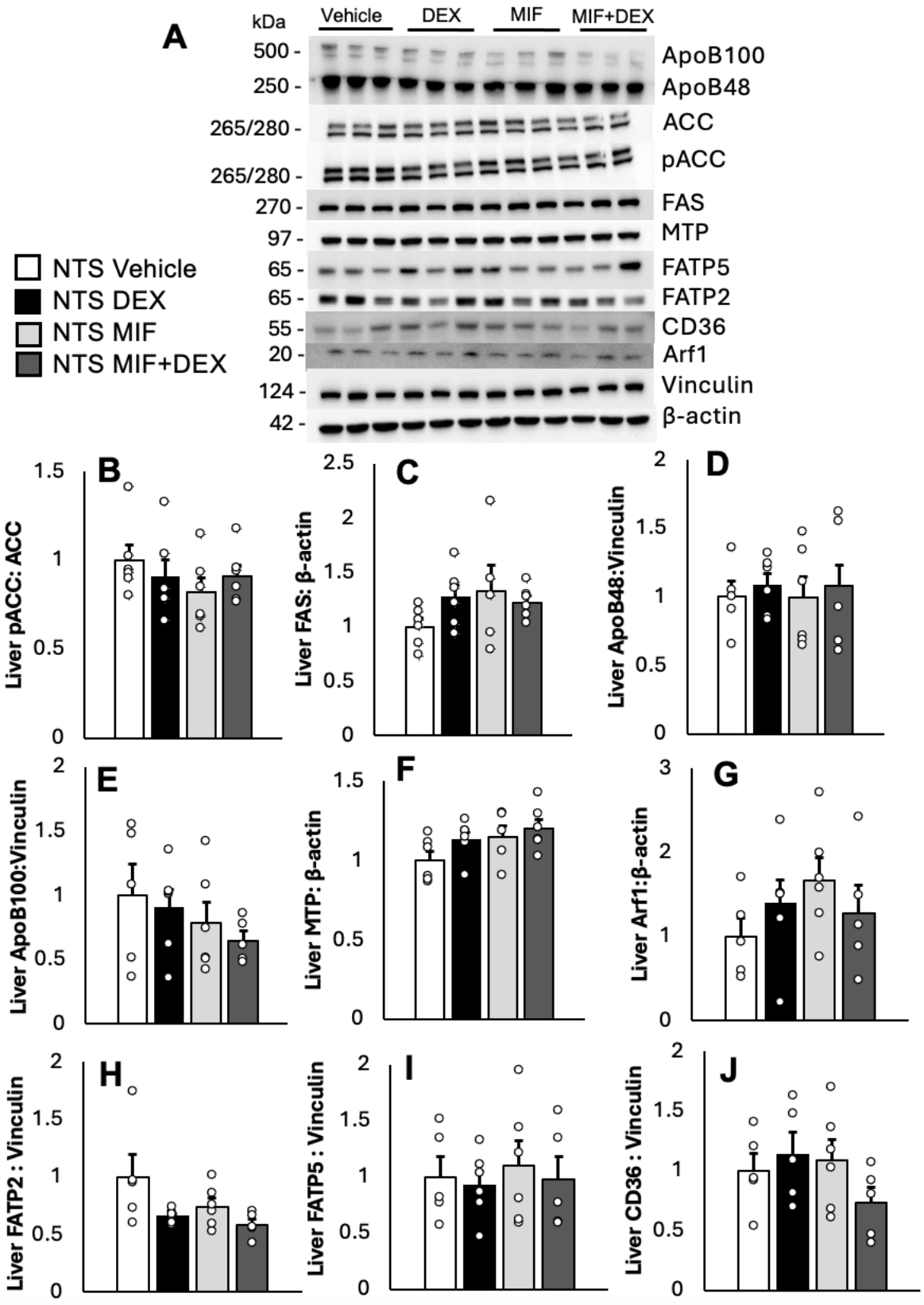
A
kDa
Vehicle
DEX
MIF
MIF+DEX
500 -
250 -
265/280 -
265/280 -
270 -
97 -
65 -
65 -
55 -
20 -
124 -
42 -
ApoB100
ApoB48
ACC
pACC
FAS
MTP
FATP5
FATP2
CD36
Arf1
Vinculin
β-actin
NTS Vehicle
NTS DEX
NTS MIF
NTS MIF+DEX
B
Liver pACC: ACC
C
Liver FAS: β-actin
D
Liver ApoB48:Vinculin
E
Liver ApoB100:Vinculin
F
Liver MTP: β-actin
G
Liver Arf1:β-actin
H
Liver FATP2 : Vinculin
I
Liver FATP5 : Vinculin
J
Liver CD36 : Vinculin

Figure 3.1.3. The increased VLDL-TG secretion induced by NTS glucocorticoid treatment was independent to hepatic lipid metabolism-related protein levels. **A)** Representative western blots from liver tissue. Levels of **B)** phosphorylated acetyl-CoA carboxylase: acetyl-CoA carboxylase (pACC:ACC), **C)** fatty acid synthase (FAS), **D)** apolipoprotein 48 (ApoB48), **E)** apolipoprotein 100 (ApoB100), **F)** microsomal triglyceride transfer protein (MTP), **G)** ADP-ribosylation factor 1 (Arf1), **H)** fatty acid transport protein-2 (FATP2), **I)** fatty acid transport protein-5 (FATP5), and **J)** CD36. Data was given as mean + SEM.

3.1.4 Investigation of hepatic mechanisms involved in the NTS DEX mediated increase in hepatic triglyceride-rich very-low density lipoprotein secretion via PCR.

Subsequently, we next conducted qPCR to measure if the expression of any hepatic genes were altered with NTS DEX infusion. Firstly, there were no changes in the mRNA expression of carbohydrate-responsive element-binding protein (ChREBP or *MLXIPL*) or hepatic sterol regulatory element-binding protein 1c (*Srebf1c*), which are considered master regulators of gene expression for genes involved in lipogenesis (Figure 3.1.4A, B). Additionally, the expression levels of stearoyl-CoA desaturase 1 (*Scd1*), lipin 2 (*Lpin2*), diacylglycerol acyltransferase 1 and 2 (*Dgat1*, *Dgat2*), and Arf1 (*Arf1*), which are genes involved in lipid synthesis and VLDL secretion, remained unchanged with NTS DEX treatment (Figure 3.1.4C-G). Finally, we also found no difference between treatment groups when analyzing genes involved in stimulating fatty acid oxidation, such as PPARα (*Ppara*), carnitine palmitoyltransferase 1α (*Cpt1a)*, and AMP-activated protein kinase (*Ampk*) (Figure 3.1.4H-J). Taken together, these results indicate that the hyperlipidemic effects following NTS DEX treatment were independent to changes in the liver lipogenic proteins and genes involved in TG synthesis, VLDL-TG assembly and secretion, and fatty acid oxidation which we assessed.

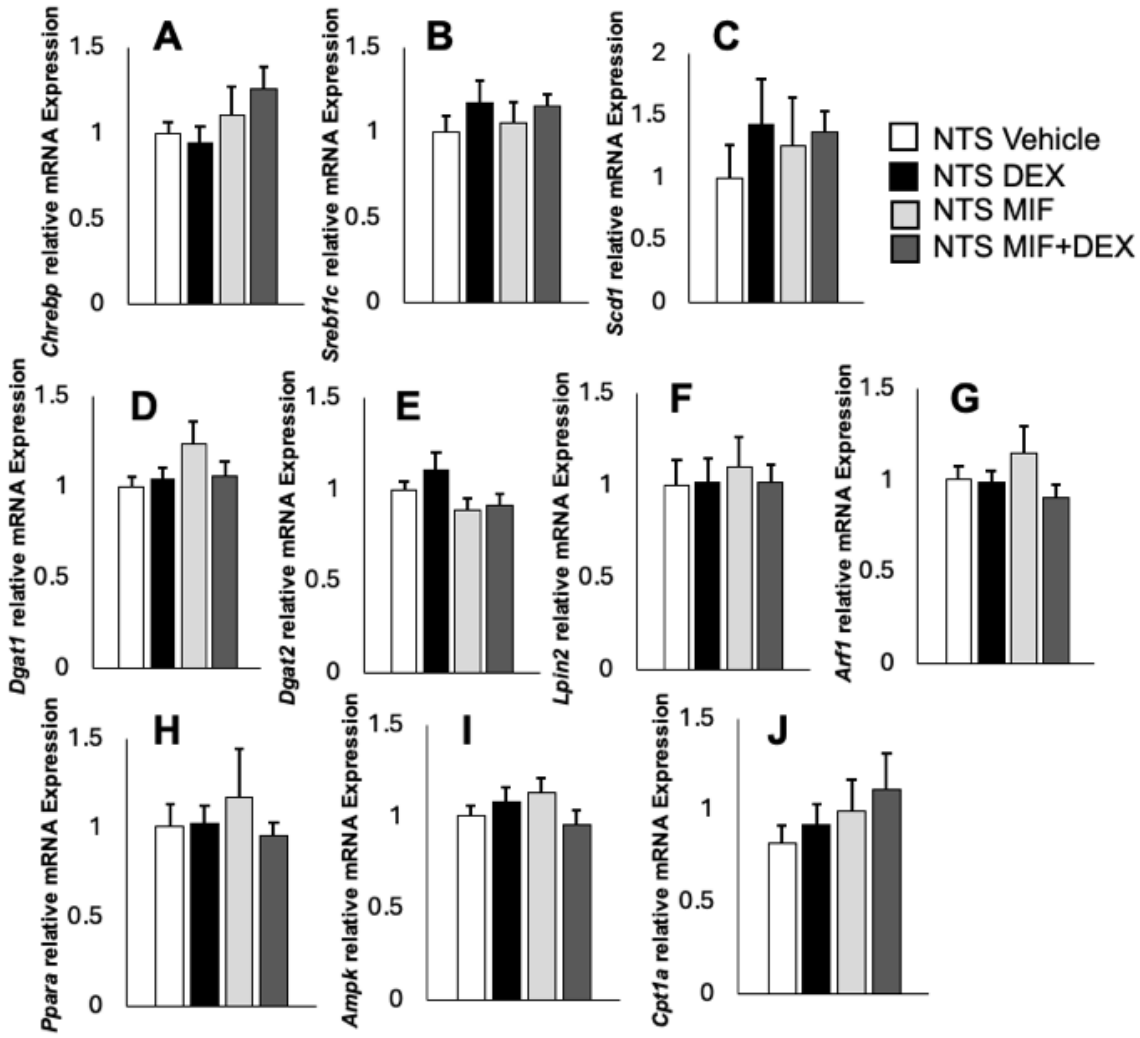

Figure 3.1.4. The increased VLDL-TG secretion induced by NTS glucocorticoid treatment was independent to hepatic lipid metabolism-related gene expression. Relative expression levels for **A)** carbohydrate response element binding protein (*ChREBP*), **B)** sterol regulatory element-binding transcription factor 1c (*Srebf1c*), **C)** stearoyl-CoA desaturase 1 (*Scd1*), **D)** diacylglycerol acyltransferase 1 (*Dgat1*), **E)** *Dgat2*, **F)** lipin 2 (*Lpin2*), **G)** ADP-ribosylation factor 1 (*Arf1*), **H)** peroxisome proliferator-activated receptor α (*Ppara*), **I)** AMP-activated kinase (*Ampk*), and **J)** carnitine palmitoyltransferase 1α (*Cpt1a*). Data measured as mean + SEM.

3.1.5 Investigation of white adipose tissue mechanisms involved in the NTS DEX mediated increase in hepatic triglyceride-rich very-low density lipoprotein secretion.

Since NTS GC treatment increased plasma FFAs, we next investigated the white adipose tissue (WAT) to better understand the underlying mechanisms of the changes in plasma TG. One major function WAT has in the fasted state is mobilizing its TG stores as FFAs into the circulation[73]. Thus, we probed for lipolytic enzymes in WAT which could have been upregulated in response to NTS DEX via western blotting (Figure 3.1.5A). The ratio of phosphorylated-hormone-sensitive lipase (pHSL) to total hormone-sensitive lipase (HSL) (Figure 3.1.5B) was significantly higher in the NTS DEX treated animals. Phosphorylation of this enzyme (pHSL) activates its lipolytic action which is consistent with increased lipolysis[73], which leads to increased FFAs in the circulation. We also looked at the levels of adipose TG lipase (ATGL) (Figure 3.1.5C), comparative gene-identification 58 (CGI-58) (Figure 3.1.5D), and perilipin (Figure 3.1.5E), but these remained unchanged. These results suggest that the changes in plasma FFAs observed with GC infusion into the NTS may be related to enhanced lipolysis in the WAT.

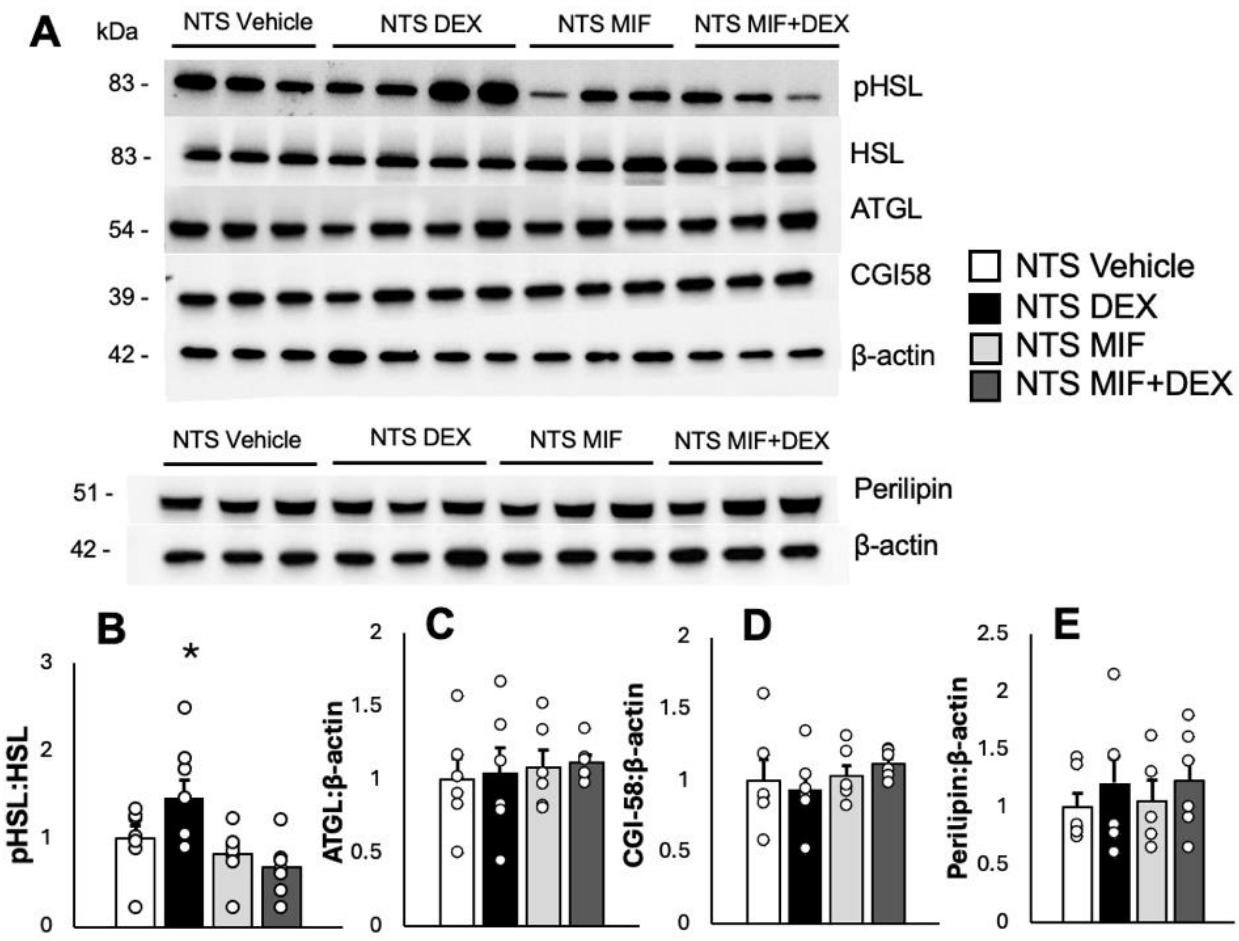

Figure 3.1.5. Changes in VLDL-TG secretion induced by NTS dexamethasone infusion altered lipolytic enzyme levels in white adipose tissue (WAT). A) Representative western blots from white adipose tissue. Levels of **B)** phosphorylated hormone sensitive lipase: total hormone sensitive lipase (pHSL:HSL), **C)** adipose triglyceride lipase (ATGL), **D)** comparative gene identification-58 (CGI-58), **E)** perilipin. For **B)**, one-way ANOVA was done, followed by a Fisher's posthoc test; *P < 0.05 NTS DEX vs NTS Vehicle, NTS MIF, NTS MIF+DEX. Data was given as mean + SEM.

3.2 Glucocorticoid Receptor Knockdown in the Nucleus of the Solitary Tract

3.2.1 Chronic glucocorticoid receptor knockdown in the nucleus of the solitary tract negates the ability of dexamethasone to stimulate hepatic triglyceride-rich very-low density lipoprotein secretion.

To alternatively test the requirement of NTS GRs to mediate DEX's ability to trigger hepatic VLDL-TG secretion, a subset of the SD rats received a lentivirus encapsulating a GR short-hairpin RNA sequence (GR shRNA) to genetically knockdown GRs selectively in DVC tissue two weeks prior to VLDL-TG experiments (Figure 3.2.1A). Control animals were injected with a lentivirus containing a mismatch control (MM) shRNA sequence. Knockdown confirmation was achieved via western blotting, where the rats that received the GR shRNA into the NTS displayed significantly lower levels of GRs in their DVC tissues (Figure 3.2.1B).

As expected, NTS DEX's hyperlipidemic effects on plasma TG (Figure 3.2.1C) and VLDL-TG secretion (Figure 3.2.1D) were preserved in the NTS MM treated rats. Interestingly, chronic GR knockdown in the NTS did not affect basal plasma TGs which suggests that basal GC signaling in the NTS does not participate in regulating hepatic lipid metabolism. However, NTS DEX was no longer able to trigger an increase in plasma TG or VLDL-TG secretion in animals that received GR shRNA, further supporting the necessity of NTS GRs to modulate hepatic TG release (Figure 3.2.1C, D). Furthermore, NTS DEX treatment stimulated an increase in plasma FFAs in the control-virus rats (Figure 3.2.1E), similar to the non-virus treated rats. Both NTS GR knockdown animal groups also displayed higher FFAs at the end of the experiment; importantly, however, NTS DEX was unable to further increase plasma FFAs following GR shRNA (Figure 3.2.1E). All these changes were independent of plasma glucose (Figure 3.2.1F) and plasma insulin (Figure 3.2.1G) levels at the end of the experiment, and body weight at the start of the experiment (Figure 3.2.1H). Taken together, this data further reinforces the requirement of NTS GRs for NTS DEX to regulate hepatic TG secretion.

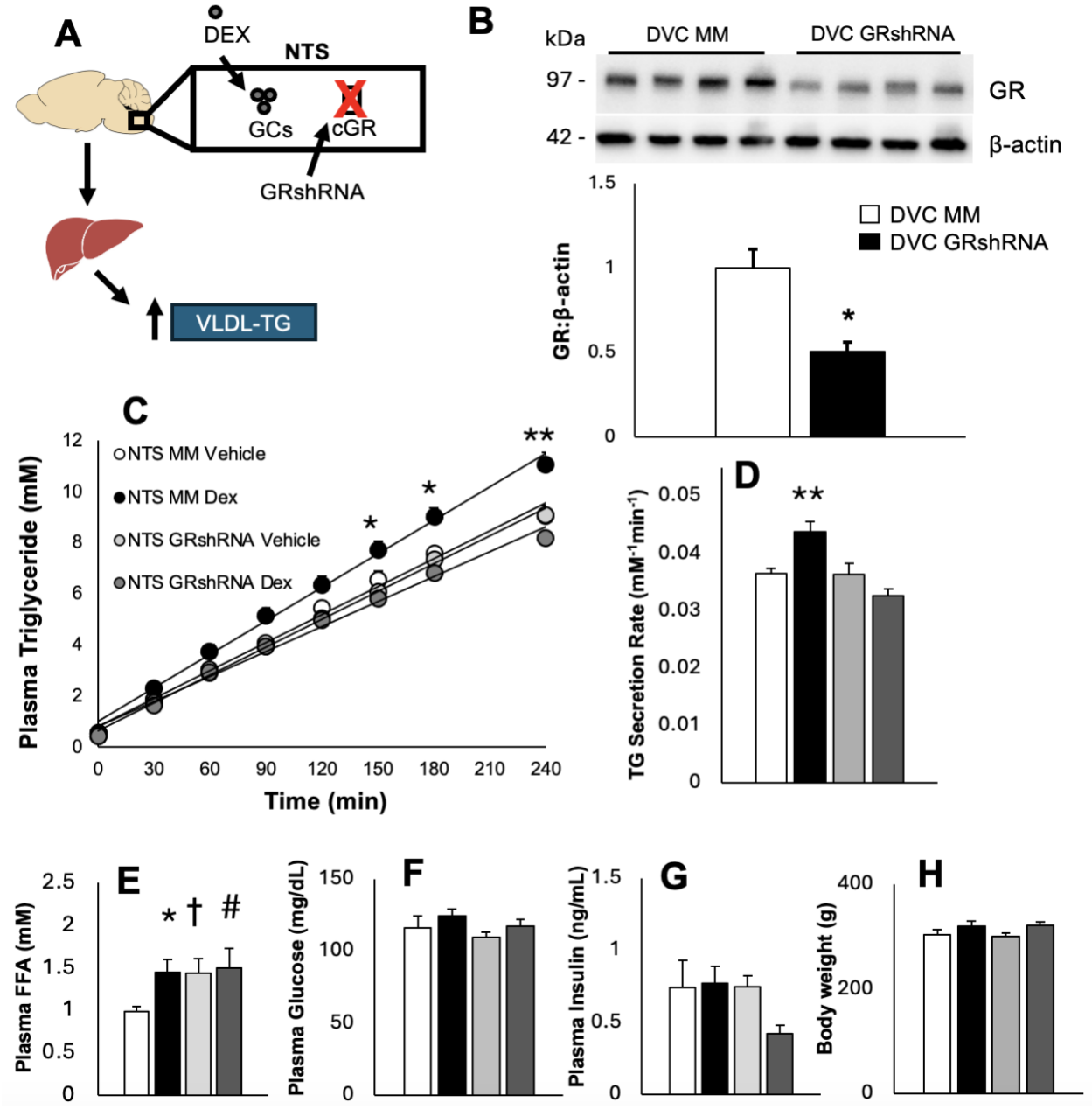

Figure 3.2.1. Chronic inhibition of NTS glucocorticoid receptors negates NTS glucocorticoid effects on plasma triglycerides. A) Schematical representation of working hypothesis for NTS GR knockdown assessment. **B)** Confirmation of glucocorticoid receptor knockdown in the dorsal vagal complex (DVC) via western blot analysis. NTS MM group (white bar; n= 4), and NTS GR shRNA group (black bar; n = 4). **C)** Plasma TG concentration and **D)** hepatic triglyceride secretion rate for animals that received NTS MM Vehicle (white; n = 7), NTS MM DEX (black; n = 13), NTS GR

shRNA Vehicle (light gray; n = 5), and NTS GR shRNA DEX (dark gray; n = 8). Plasma levels for **E)** free fatty acids (FFAs), **F)** glucose, and **G)** insulin at end of experiment. **H)** Body weight at start of experiment. For **B)**, *P < 0.05 for DVC MM vs DVC GR shRNA. For **C)**, NTS MM DEX vs NTS MM Vehicle, NTS GR shRNA Vehicle, NTS GR shRNA DEX **P < 0.01 for effect of time, treatment, and interaction between time and treatment (two-way ANOVA); **P < 0.01 at t=240 min, *P < 0.05 at t=180 and t=150min using Fisher's posthoc test. For **D)**, one-way ANOVA was done, followed by a Fisher's posthoc test; NTS MM DEX vs NTS MM Vehicle, NTS GR shRNA Vehicle, NTS GR shRNA DEX **P < 0.01. For **E)**, one-way ANOVA was done, followed by a Fisher's posthoc test; NTS MM DEX vs NTS MM Vehicle *P < 0.05, NTS GR shRNA Vehicle vs NTS MM Vehicle †P < 0.05, and NTS GR shRNA DEX vs NTS MM Vehicle #P < 0.05. Data was measured as mean + SEM.

3.3 Heat Shock Protein 90 Inhibition in the Nucleus of the Solitary Tract

3.3.1 Acute and chronic heat shock protein 90 antagonism in the nucleus of the solitary tract reverses glucocorticoids' hyperlipidemic effects.

To continue testing the necessity of NTS GRs to modulate hepatic VLDL-TG secretion, we then looked at heat shock protein 90 (Hsp90) (Figure 3.3.1A) This chaperone protein is required for the biological function and stability of the GR[138,139]; therefore, blocking its actions within the NTS would be expected to also block the lipostimulatory effects of NTS GCs.

To test whether acute inhibition of Hsp90 would alter NTS DEX's effects, we infused a pharmacological Hsp90 inhibitor,17-AAG (Hsp90i), which binds to the ATP-binding site of Hsp90 to block its activity, into the NTS of a subset of animals. NTS Hsp90i blockade alone had no effect on plasma TG (Figure 3.3.1B) or VLDL-TG secretion (Figure 3.3.1C) relative to control rats, suggesting acute NTS Hsp90 inhibition does not alter hepatic lipid metabolism. However, when co-infused with DEX, Hsp90i blocked the NTS DEX-mediated increase in plasma TG and VLDL-TG secretion. Again, these changes were independent to plasma glucose end of experiment (Figure 3.3.1D) or body weight at start of experiment (Figure 3.3.1E).

We next assessed if a chronic 2-week knockdown of Hsp90 in the NTS would impact NTS GC action on lipid metabolism. Rats injected with a lentiviral containing Hsp90 shRNA and given a control saline infusion (NTS Hsp90 shRNA Vehicle) during VLDL experimentation, showed similar plasma TG and VLDL-TG secretion rate compared to their NTS MM Vehicle counterparts (Figure 3.3.1F, G), suggesting chronic inhibition of Hsp90 in the NTS does not affect hepatic lipid secretion, similar to that which was observed with NTS Hsp90i. However, NTS knockdown of Hsp90 was capable of suppressing the stimulatory effects of DEX (Figure 3.3.1F, G), similar to acute co-infusion of Hsp90i and DEX into the NTS of non-virus rats and NTS GR knockdown animals. There was also no significant difference between groups for plasma glucose at end of experiment (Figure 3.3.1H) or body weight at start of experiment (Figure 3.3.1I). Together, this data further supports the requirement of functional NTS GRs to modulate VLDL-TG release.

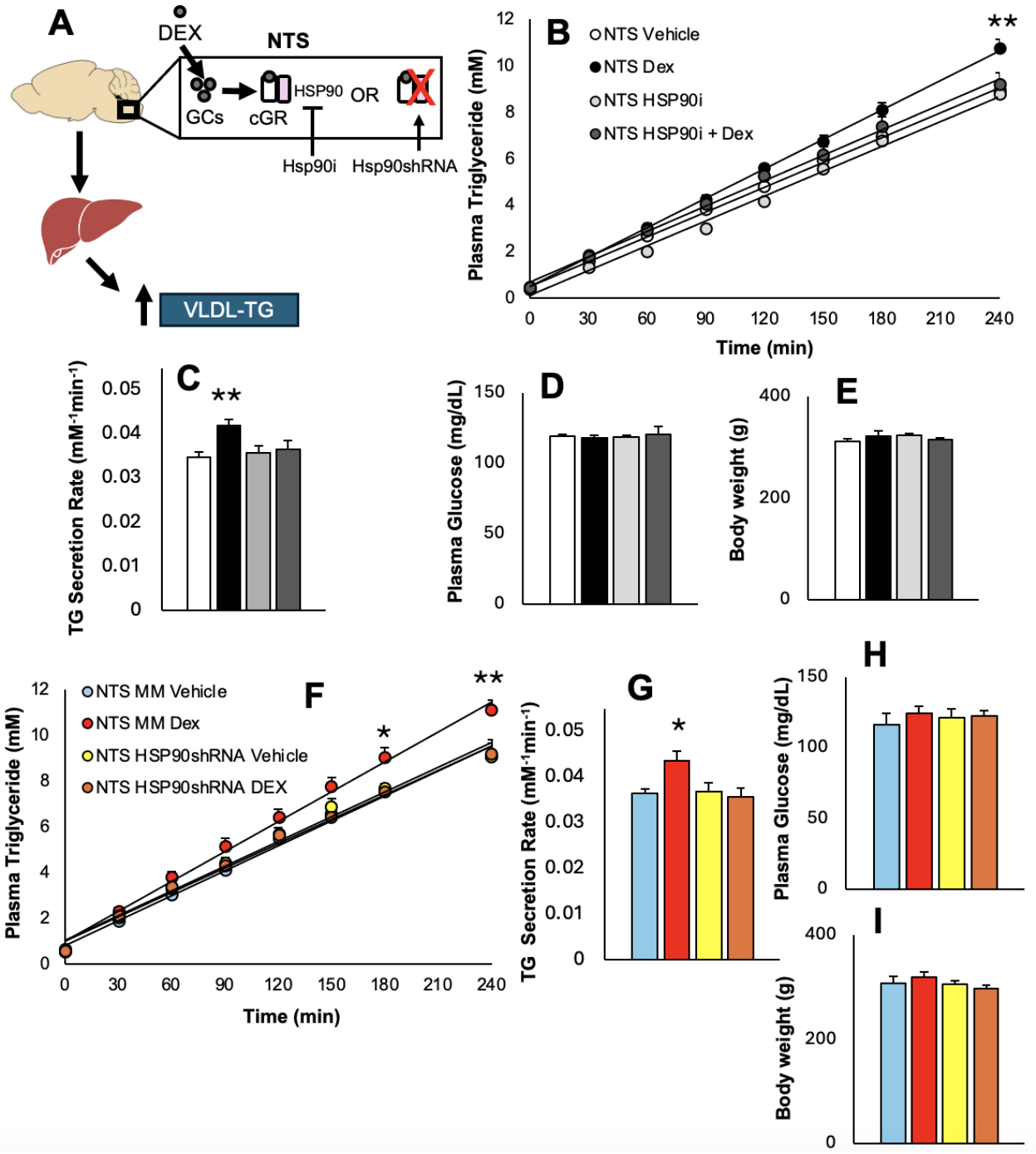

Figure 3.3.1. NTS glucocorticoid hyperlipidemic effects require functional NTS Hsp90. A) Schematical representation of working hypothesis on Hsp90 requirement for NTS GC hyperlipidemic effects. **B)** Plasma TG concentration and **C)** hepatic triglyceride secretion rate for animals that received NTS Vehicle (white; n = 10), NTS DEX (black; n = 9), NTS Hsp90i (light gray; n = 10), and NTS Hsp90i+DEX (dark gray; n = 10). **D)** End

of experiment plasma glucose, and **E)** start of experiment body weight for the aforementioned groups. **F)** Plasma TG concentration and **G)** hepatic triglyceride secretion rate for animals that received NTS MM Vehicle (light blue; n = 7), NTS MM DEX (red; n = 13), NTS Hsp90 shRNA Vehicle (yellow; n = 7), and NTS Hsp90 shRNA DEX (orange; n = 6). **H)** End of experiment plasma glucose and **I)** start of experiment body weight for the aforementioned groups. For **B)**, NTS DEX vs NTS Vehicle, NTS Hsp90i, and NTS Hsp90i+ DEX **P < 0.01 for effect of time, treatment, and interaction between time and treatment using two-way ANOVA; **P < 0.01 at t=240 min using Fisher's posthoc test. For **C)**, a one-way ANOVA test was conducted, followed by a Fisher's posthoc test; NTS DEX vs NTS Vehicle, NTS Hsp90i, and NTS Hsp90i + DEX **P < 0.01. For **F)**, NTS MM DEX vs NTS MM Vehicle, NTS Hsp90 shRNA Vehicle, and NTS Hsp90 shRNA DEX *P < 0.05 for effect of time, treatment, and interaction between time and treatment using two-way ANOVA; **P < 0.01 at t=240 min and *P < 0.05 at t=180 min using Fisher's posthoc test. For **G)**, a one-way ANOVA test was conducted, followed by a Fisher's posthoc test; NTS MM DEX vs NTS MM Vehicle, NTS Hsp90 shRNA Vehicle, and NTS Hsp90 shRNA DEX *P < 0.05. Data was measured as mean + SEM.

3.4 FK506 Binding Protein 51 Down Regulation in the Nucleus of the Solitary Tract

3.4.1 FK506 Binding Protein 51 (FKBP51) knockdown in the nucleus of the solitary tract induces a hyperlipidemic phenotype.

Another important protein involved in proper GR functioning is FKBP51[140–142]. This co-chaperone suppresses GR activity by stopping it from translocating into the nucleus in the absence of GCs[140–142]. FKBP51 therefore has an important role in the regulation of GR activity. Thus, we tested whether NTS GC effects on liver VLDL-TG secretion would be impacted by chronically knocking down FKBP51 selectively in the NTS (Figure 3.4.1A). To ascertain the knockdown, western blotting was performed on DVC tissues of rats infused with FKBP5 shRNA into the NTS. FKBP5 shRNA treated animals displayed a significant reduction in FKBP51 levels compared to MM control rats (Figure 3.4.1B).

Results from VLDL experiments indicate that knocking down FKBP51 specifically in the NTS (NTS FKBP5 shRNA Vehicle) resulted in significantly higher levels in plasma TG (Figure 3.4.1C) and VLDL-TG secretion rate (Figure 3.4.1D) compared to NTS MM controls. One explanation could be that due to the lack of FKBP51, basal NTS GR activity may be enhanced, and future studies will investigate the effects of chronic FKBP51 inhibition on GR activity. In support of this, previous studies have reported that: one, FKBP51 silencing leads to increased GR activation[143]; and two, that unliganded GRs also possess the ability to regulate gene transcription[266,267]. Importantly, infusing DEX in the FKBP5 shRNA-treated rats was no longer able to further increase plasma TG or VLDL-TG secretion (Figure 3.4.1C, D). This could potentially be explained by a higher basal NTS GR activation, where the liver's VLDL secretion rate is already at its maximum capacity. However, there was no difference in basal plasma TG levels between the FKBP51 knockdown and control virus groups (NTS MM Vehicle = 0.497 ± 0.096mM; NTS FKBP5 shRNA Vehicle = 0.407 ± 0.071mM). Again, all these effects were independent to plasma glucose at end of experiment (Figure 3.4.1E) and body weight (Figure 3.4.1F).

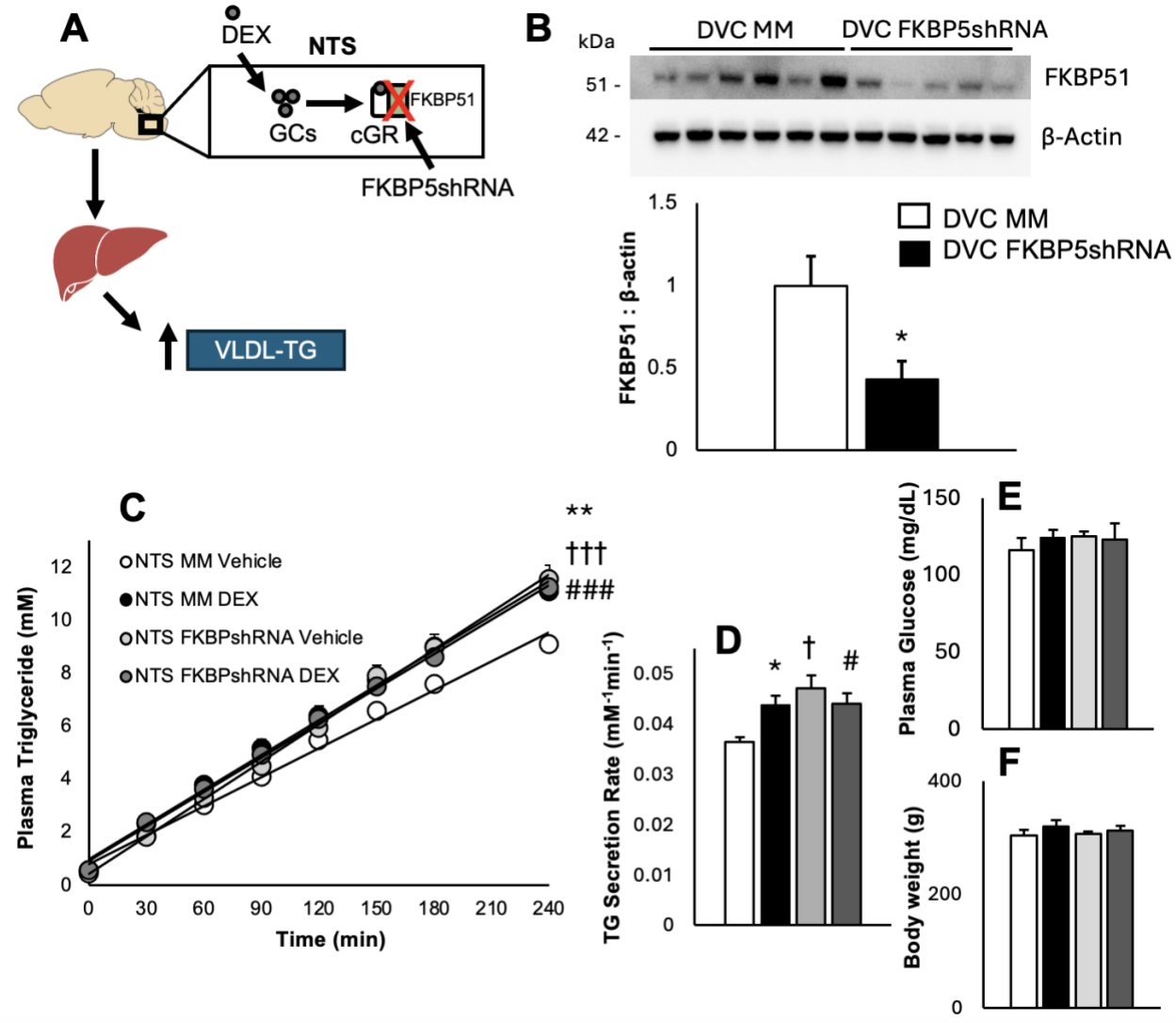

Figure 3.4.1. Knockdown of NTS FKBP51 augments plasma triglyceride levels. A) Schematical representation of working hypothesis for role of FKBP51 on NTS GC hyperlipidemic effects. **B)** Confirmation of NTS FKBP51 knockdown via western blot analysis between DVC MM (white; n = 6) and DVC FKBP5 shRNA (black; n = 5). **C)** Plasma TG concentration and **D)** hepatic triglyceride secretion rate for animals that received NTS MM Vehicle (white; n = 7), NTS MM DEX (black; n = 13), NTS FKBP5 shRNA Vehicle (light gray; n = 10), and NTS FKBP5 shRNA DEX (dark gray; n = 9). **E)** Plasma glucose at end of experiment. **F)** Body weight at start of experiment. For **B)**, P < 0.05 for DVC MM vs DVC FKBP5 shRNA using a Student's t test. For **C)**, NTS MM Vehicle vs NTS MM DEX, NTS FKBP5 shRNA Vehicle, and NTS FKBP5 shRNA DEX *P < 0.01 for effect of time, treatment, and interaction between time and treatment using

two-way ANOVA; **P < 0.01 at t=240 min using Fisher's posthoc test for NTS MM DEX vs NTS MM Vehicle, †††P < 0.001 at t=240 min for NTS FKBP5 shRNA Vehicle vs NTS MM Vehicle, and ###P < 0.001 at t=240 min for NTS FKBP5 shRNA DEX vs NTS MM Vehicle. For **D)**, a one-way ANOVA test was done, followed by a Fisher's posthoc test; *P < 0.05 for NTS MM DEX vs NTS MM Vehicle, †P < 0.05 for NTS FKBP5 shRNA Vehicle vs NTS MM Vehicle, and #P < 0.05 for NTS FKBP5 shRNA DEX vs NTS MM Vehicle. Data was measured as mean + SEM.

3.5 Effects of Glucocorticoids in the Nucleus of the Solitary Tract with Concomitant Peripheral Sympathetic Blockade

3.5.1 Sympathetic nervous system antagonism negates the hindbrain glucocorticoid effects to trigger hepatic lipid secretion.

Thus far, we demonstrated that NTS GCs stimulate hepatic VLDL-TG secretion, and that this is associated with an increase in circulating FFAs and increased pHSL:HSL protein levels in WAT. With the knowledge that increased sympathetic activity stimulates WAT lipolysis and consequently increases FFA levels in the plasma, we postulated whether NTS GCs may activate the sympathetic nervous system (SNS), which may contribute to the hyperlipidemic effects of NTS GCs. Thus, our next goal was to examine if the NTS DEX hyperlipidemic effects were mediated via peripheral sympathetic outflow (Figure 3.5.1A). The requirement of the SNS was tested by administering an alpha- and beta-adrenergic antagonist cocktail (SNSi) intravenously, to pharmacologically inhibit the SNS, 10 minutes prior to the start of VLDL secretion experiments as described previously[268,269]. As expected, when given the control 15% dimethyl sulfoxide (DMSO) compound intravenously, NTS DEX effects to increase plasma TG (Figure 3.5.1B) is maintained along with a strong trend to increase VLDL-TG secretion rate ($P = 0.057$) (Figure 3.5.1C) compared to NTS Vehicle. Whereas intravenous administration of the SNSi alone did not influence plasma TG or VLDL-TG secretion rate (NTS Vehicle + i.v. SNSi), SNSi blocked NTS DEX's ability to increase plasma TG (NTS DEX + i.v. SNSi) (Figure 3.5.1B), and the VLDL-TG secretion rate (Figure 3.5.1C), suggesting that the SNS mediates the actions of NTS DEX to stimulate VLDL-TG secretion. When analyzing plasma FFAs, peripheral sympathetic inhibition prevented the NTS DEX-induced increase (Figure 3.5.1D). All changes observed were independent of plasma glucose at end of experiment (Figure 3.5.1E) and body weight (Figure 3.5.1F). Overall, this data suggests that NTS DEX triggers the SNS to induce its lipid-increasing effects.

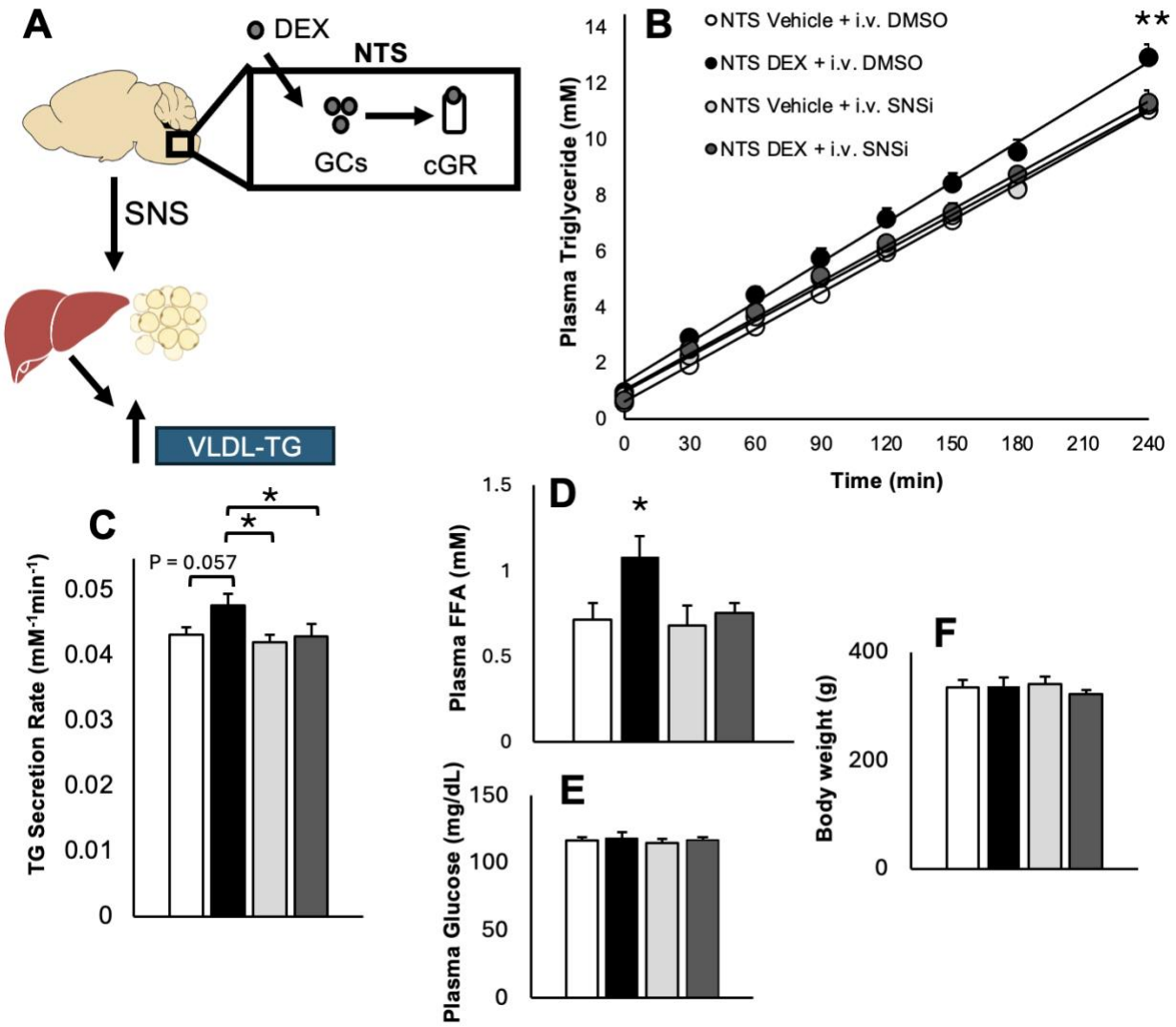

Figure 3.5.1. Peripheral blockade of sympathetic nervous system negates NTS glucocorticoid effects. A) Schematical representation of working hypothesis. **B)** Plasma TG concentration and **C)** hepatic triglyceride secretion rate for animals that received NTS Vehicle + i.v. DMSO (white; n =8), NTS DEX + i.v. DMSO (black; n = 9), NTS Vehicle + i.v. SNSi (light gray; n = 6), and NTS DEX + i.v. SNSi (dark gray; n = 9). Plasma **D)** FFAs, and **E)** glucose at end of experiment. **F)** Body weight. For **B)**, NTS DEX + i.v. DMSO vs NTS Vehicle + i.v. DMSO, NTS Vehicle + i.v. SNSi, and NTS DEX + i.v. SNSi *P < 0.01 for effect of time, treatment, and interaction between time and treatment using a two-way ANOVA test; **P < 0.01 at t=240 min using Fisher's posthoc test for NTS DEX + i.v. DMSO vs NTS Vehicle + i.v. DMSO, NTS Vehicle + i.v. SNSi,

and NTS DEX + i.v. SNSi. For **C)**, one-way ANOVA was conducted, before a Fisher's posthoc test; *P < 0.05 for NTS DEX + i.v. DMSO vs NTS Vehicle + i.v. SNSi, and *P < 0.05 for NTS DEX + i.v. DMSO vs NTS DEX + i.v. SNSi, P = 0.057 for NTS DEX + i.v. DMSO vs NTS Vehicle + i.v. DMSO. **D)** a one-way ANOVA test was done, prior to conducting a Fisher's posthoc test; *P < 0.05 for NTS DEX + i.v. DMSO vs NTS Vehicle + i.v. DMSO, NTS Vehicle + i.v. SNSi, and NTS DEX + i.v. SNSi. Data was measured as mean + SEM.

3.5.2 Investigation of white adipose tissue protein changes in sympathetically inhibited animals with hindbrain glucocorticoids.

Given that we observed a change pHSL:HSL in the NTS DEX group, we next wanted to assess this enzyme's protein levels for the pharmacologically sympathetic denervated animals. As expected, the NTS DEX + SNSi treated rats was able to reverse the pHSL:HSL changes induced by NTS DEX treatment (Figure 3.5.2A, B). Taken together with the data showing that SNSi reverses the increase in plasma FFA levels in the NTS DEX-treated rats (Figure 3.5.1F), this suggests that hindbrain GC action may activate the SNS to stimulate lipolysis in WAT. Thus, this data further supports that NTS DEX hyperlipidemic effects could be mediated through the sympathetic nervous system.

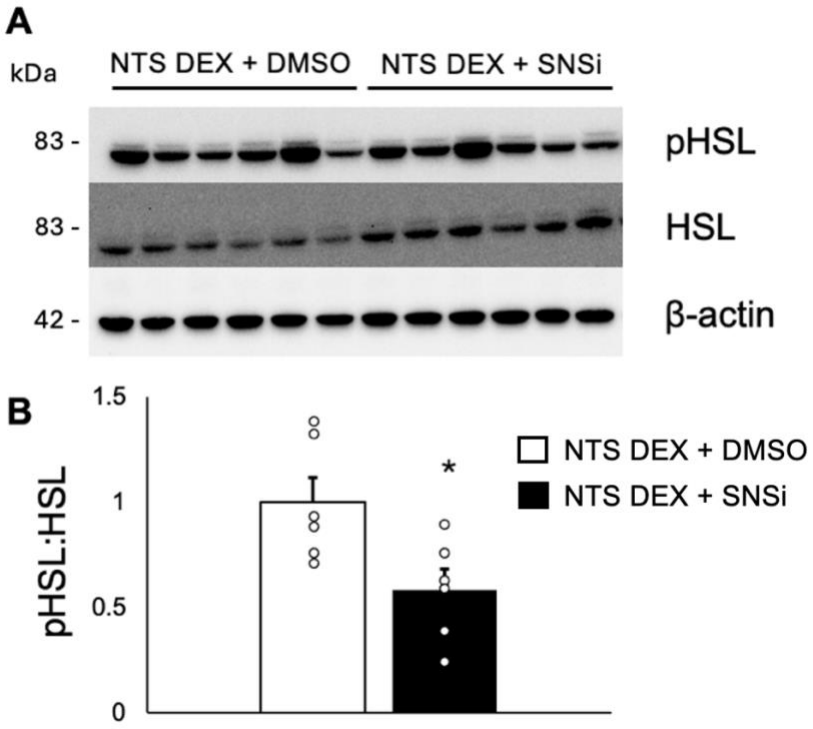

Figure 3.5.2. Peripheral blockade of sympathetic nervous system blocks the NTS dexamethasone-induced increased levels of phosphorylated-hormone sensitive lipase in white adipose tissue A) Western blot chemiluminescent image for white adipose tissue. **B)** quantification of phosphorylated-hormone sensitive lipase (pHSL) to total hormone sensitive lipase (HSL) for animals that received NTS DEX + i.v. DMSO (white; n =6) vs NTS DEX + i.v.SNSi (black; n = 6). Using a Student's t test, *P < 0.05 for NTS DEX + i.v. SNSi vs NTS DEX + i.v. DMSO. Data measured in mean + SEM.

Chapter 4: Aim 1 Discussion

4.1 Significance of Results

Obesity and diabetes affect a large number of individuals worldwide and are becoming a significant healthcare problem[1,2,5,6,9]. A common characteristic of these diseases is dyslipidemia, in part due to overproduction and circulating levels of VLDL-TGs[13,16,20,21,23,24]. Research on dysregulation of hepatic VLDL-TG secretion has thus far primarily focused on peripheral mechanisms. However, the brain is emerging as a critical regulator of whole-body metabolism. Specifically, the hypothalamus and brainstem can sense nutrients (e.g. glucose[206,227,228,249], fatty acids[209,249], and amino acids[233,234,256]) and hormones (e.g. GCs[237,238,240], insulin[226,250,251], GLP-1[268–271], NPY[225,246,272]) to regulate peripheral metabolism. It has been shown that if the central sensing mechanisms of these factors becomes disrupted, this can lead to dysregulated glucose and lipid metabolism, as well as the development of metabolic diseases[231,273,274]. Thus, the brain's ability to respond to circulating hormones and nutrients is a critical part of regulating metabolic homeostasis.

It is well known that excessive GC levels and action can negatively impact metabolism via direct action on peripheral organs[110,116,177], however, central GC signaling effects on metabolism remain largely unexplored. This is particularly relevant given that the activity of these stress-related hormones are known to be elevated in metabolic diseases such as obesity[110,118] and diabetes[118,189] and may contribute to the dysregulated lipid homeostasis that is characteristic to both of these diseases. Here, we provide evidence for the first time that GCs within the NTS can regulate hepatic TG secretion by acting on NTS GRs or mGRs. Our research contributes to the knowledge of NTS regulation of peripheral lipid metabolism, and it furthers our understanding of central GC effects and potential mechanisms on the development of dyslipidemia.

4.2 Discussion of Results

4.2.1 Glucocorticoids act on canonical glucocorticoid receptors in the nucleus of the solitary tract to stimulate hepatic triglyceride secretion.

Our results revealed that direct, acute infusion of dexamethasone, a synthetic GC, in the NTS of 10-hour fasted, conscious, freely moving rats stimulates an increase in

VLDL-TG secretion from the liver via NTS GRs as both pharmacological (with GR antagonist mifepristone) and genetic knockdown (with GR shRNA) to selectively inhibit GRs in NTS negated this effect. To the best of our knowledge, this is the first study that assessed the effects of hindbrain GC action on lipid homeostasis and hepatic TG secretion. Previous work in the Yue laboratory demonstrated that acute infusion of GCs into the hypothalamus also triggers hepatic VLDL-TG secretion[240] under similar conditions to the present study which supports the notion that GCs can act in various regions of the brain to affect lipid metabolism. Future studies may reveal whether GCs acting concurrently in both hypothalamic and brainstem regions simultaneously have additive or redundant effects and may uncover the relative contribution of GCs acting centrally within the brain versus peripherally on liver and adipose tissue on the regulation of lipid homeostasis. Additionally, in line with our results demonstrating a central role of GCs on metabolism, a study done by Zakrzewska et al. showed that a chronic, 3-day intracerebroventricular (ICV) GC infusion targeting the hypothalamus in rats induces increased plasma TG levels[237]. It should be noted that VLDL-TG secretion was not measured in this study, and food intake was also increased, which could have contributed to the elevated plasma TGs[237]. GCs can also affect glucose metabolism via central pathways. Studies have revealed GC action in the arcuate nucleus (ARC) can impair hepatic insulin resistance and induce endogenous glucose production under hyperinsulinemic-euglycemic clamp conditions[238,243]. On top of this, chronic ICV dexamethasone treatment leads to hyperinsulinemia[237,246], suggesting that central GC action can contribute to the development of insulin resistance and impair glucose homeostasis. However, there remains a gap in literature as to whether GCs acting in the NTS can affect glucose homeostasis.

Interestingly, many central GC effects are dependent on NPY co-expression in the hypothalamus. For instance, Yi et al. confirmed that acute dexamethasone treatment in the ARC leads to insulin resistance, but this was reversed with a NPY receptor antagonist co-administered into the ARC[243]. Conversely, for ICV NPY infusion in adrenalectomized rats to induce hyperphagia, body weight gain, hypertriglyceridemia, and hyperinsulinemia, ICV GC must also be administered[246]. Importantly, in our follow-up of the study by Cardoso et al. which looked at MBH GC infusion on VLDL-TG

secretion[240], we also found elevated NPY expression in the hypothalamus, suggesting that in the hypothalamus, the effects of GCs to induce hypertriglyceridemia are also associated with an increase in hypothalamic NPY, although the necessity of NPY on MBH GC infusion to modulate hepatic VLDL-TG secretion was not tested directly[240]. These studies that looked at hypothalamic GC action to regulate peripheral metabolism reveal a link with NPY action. In contrast, our study which assessed NTS GC action on lipid metabolism revealed no change in NPY expression within the DVC in the hindbrain (see Chapter 5, Figure 5.1.2). Thus, this suggests that despite the same hormone having similar effects on metabolism, the underlying mechanisms may differ depending on the brain region it acts upon.

To confirm our data was indeed as a result of GR activation in the NTS, we measured GR activity markers in the DVC wedges (which contain the NTS), namely PDK4 and FKBP51 gene expression. Our results showed that DEX treatment in the NTS induces the expression for both of these genes, confirming that NTS GRs were activated. Of note, co-administration of mifepristone, the GR antagonist, was only able to negate PDK4 expression, but not FKBP51, suggesting that this GR antagonist may block some DEX-induced changes in GR activity but not others, which may occur via a mifepristone-independent effect. Mifepristone has been shown to reverse some, but not all, GC-induced increases in FKBP51 expression in both *in vitro* and *in vivo* studies[275–277]. For example, one study found animals treated with dexamethasone expectedly experienced increases in FKBP51 expression in various tissues assessed, such as the liver, adrenal, pituitary gland, and hippocampus[277]. Prior treatment with mifepristone, however, was only able to reverse the increase in FKBP51 in the liver, adrenals, and within the brain's hippocampus, but not in the pituitary gland[277]. Additionally, our laboratory found that acute infusion of GCs into the MBH increases hypothalamic FKBP51 expression, but co-infusion with mifepristone does not reverse this. Thus, there could be areas in the brain where GCs induce FKBP51 expression through GR-independent pathways, though more research on this is required.

This study confirmed the presence of GRs in the DVC through western blots, and others have indeed confirmed the expression of GRs in the NTS[259,278,279]. Another

question that remains is what neural populations in the NTS are responsible for mediating NTS GC action. The NTS is comprised of glutamatergic, GABAergic, dopaminergic, and noradrenergic neurons[169,248,279–282]. Multiple lines of evidence suggest that GCs interact with noradrenergic neurons in the NTS to mediate their effects. For instance, it was reported that GC infusion into the NTS modulated memory consolidation via the activation of GRs in A2-noradrenergic NTS neurons projecting to the amygdala[283]. Another study also investigated how elevated GC levels led to the activation of A2-noradrenergic neurons in the NTS as well[281]. Furthermore, despite the NTS predominantly being involved in suppressing food intake via glutamatergic neurons[248,284,285], it is also able to stimulate food intake via noradrenergic neurons projecting to the ARC to activate local AgRP/NPY neurons[286,287]. In line with this, preliminary data generated in our laboratory has revealed that dexamethasone infusion into the NTS stimulates food intake (data not shown). This effect could therefore be induced by GR-expressing noradrenergic neurons in the NTS. Although there is evidence to suggest NTS noradrenergic neurons mediate NTS GC effects, there have been reports which indicate that NTS GCs can also modulate local GABA or glutamate signaling[169,288]. Thus, further investigation on the specific neuronal populations in the NTS that respond to GCs is needed, particularly in the context of NTS GCs to modulate hepatic VLDL-TG release.

Our results suggested that NTS GC action increased VLDL-TG levels by neurotransmission via the sympathetic nervous system (SNS). First, we found that plasma FFA levels were elevated with NTS dexamethasone treatment, and this was corroborated with an increase in phosphorylated-hormone sensitive lipase (pHSL) levels in the white adipose tissue (WAT) in the same animals. This data is characteristic with enhanced sympathetic outflow to the adipose tissue[289,290]. We next directly assessed the requirement of the SNS for NTS GCs to modulate VLDL-TG secretion by giving an i.v. injection of adrenergic receptor antagonists to the animals. Our results revealed that blocking peripheral alpha- and beta-adrenergic receptors negates NTS GC effects to increase plasma TG, which supports that NTS GC action to stimulate hepatic VLDL-TG secretion is dependent on the SNS. Importantly, peripheral SNS denervation was also able to reverse the increase in plasma FFAs and pHSL as well. In line with our data,

hormones and nutrients acting in the brain to regulate peripheral metabolism have been shown to mediate their effects through the autonomic nervous system (ANS). For example, insulin infusion into the MBH suppresses WAT lipolysis by dampening sympathetic innervation[226]. Mighiu et al. reported that glucagon acting in the MBH lowers hepatic glucose production via the parasympathetic vagus nerve[214]. ICV3 NPY infusion increases VLDL-TG release via hepatic sympathetic innervation[225]. Finally, dexamethasone acting in the ARC impairs hepatic insulin sensitivity through the SNS[243]. Though these studies focused on the hypothalamus, the NTS has also been shown to regulate metabolism through the parasympathetic nervous system in response to hormone and nutrient sensing. For example, leptin infusion into the DVC increased hepatic TG release via the vagus nerve[223]. It was also shown that glycine acting in NTS lowered VLDL-TG through parasympathetic outflow[256]. Of note, there is no literature currently that directly supports the NTS regulating peripheral metabolism through the sympathetic system, thus our study is the first, to our knowledge that demonstrates an effect of NTS regulation of metabolism via the SNS. Aside from metabolism, Shigematsu et al. revealed that the NTS can activate the SNS during heart failure[291]. A potential mechanism for this could be through the locus coeruleus (LC). Briefly, the LC is a brainstem nucleus that is the main producer of norepinephrine (NE) in the brain, and importantly, is involved in activating the SNS[242,292]. It is established that the NTS delivers extensive projections towards the LC[293,294]. Therefore, it is possible the SNS could be stimulated through some of these projections. Thus, we report for the first time that the NTS can also regulate peripheral lipid metabolism via the SNS.

Continuing, the hyperlipidemic effects of NTS GCs were found to be independent to changes in hepatic pACC to total ACC, FAS, and MTP protein levels. ICV3 NPY administration, which also results in increased VLDL-TG secretion in 4h fasted animals, also occurred independent of changes to liver pACC, FAS, or MTP protein levels[224]. In contrast, ICV3 leptin stimulated VLDL-TG via increased MTP, and decreased FAS levels in the liver in 6h fasted rats[223]. Moreover, when analyzing the mRNA expression of genes involved in hepatic lipid metabolism, we found no difference in *Srebf1c*, *Scd1*, *Dgat1*, *Dgat2*, *Lpin2*, *Arf1*, *Ppara*, *Ampk*, or *Cpt1a*. Opposite to our findings, a study on ICV3 NPY that triggers VLDL-TG secretion showed an increase in hepatic *Scd1* and

Arf1 mRNA expression which supports VLDL assembly and release[224]. Another similar study that infused NPY into ICV3 in sham-operated rats elevated plasma TGs due to an increase in *Arf1* mRNA expression, and decreased *Cpt1a* mRNA expression, which are consistent with increased VLDL-TG as well[225]. One potential explanation for the differences with our results is that in both of these studies, liver tissues were collected 2 hours after giving NPY into the brains, whereas in the present study, tissues were collected at the end of the experiment following 6 hours of dexamethasone treatment. Thus, potential changes in gene expression may have occurred earlier to contribute to the NTS DEX-induced increase in hepatic VLDL-TG secretion. Despite not seeing a change in liver protein or mRNA levels, we cannot rule that some of these proteins may be more active post NTS GC action. Assessing SCD1 protein activity may be worthwhile as this protein is important for the synthesis of TGs and overall VLDL production[209,256,295,296]. Additionally, doing an MTP activity assay could prove valuable as it was reported that ICV GLP-1 infusion lowered postprandial chylomicron secretion due to a reduction in intestinal MTP activity[268].

The liver relies on the availability of TGs to synthesize and secrete VLDL-TG. TGs come from various sources, such as hepatic lipid stores, *de novo* lipogenesis (DNL), or re-esterification of fatty acids into TGs. Our data showed that hepatic TG content did not change with NTS GCs despite the liver releasing more VLDL-TG, which indicates TG synthesis may be upregulated. Since the animals were fasted, liver ACC and FAS were both unchanged, and there was no difference in plasma glucose, DNL is unlikely to contribute to the increase in TG production. Recall, we found that NTS GCs elevated plasma FFAs by stimulating WAT pHSL-induced lipolysis. These FFAs could be used by hepatocytes and esterified into TGs for VLDL packaging[297]. Studies that used the intralipid-heparin i.v. infusion technique to raise plasma FFAs by heparin-induced activation of lipoprotein lipase to breakdown the infused TGs into FFAs revealed that elevations in circulating FFAs increases VLDL-TG secretion[26,249]. Therefore, this could potentially be a peripheral mechanism responsible for the increased VLDL-TG secretion observed with NTS GC treatment. In line with this hypothesis, we next assessed CD36, FATP2, and FATP5 levels in the liver as these are all fatty acid transporters involved in the uptake of FFAs, but we found no change. Previous work revealed that

overexpression of hepatic CD36 resulted in increased liver TG levels and VLDL-TG secretion[298]. The reverse is also true as liver-specific CD36 knockout mice experience lower hepatic VLDL-TG release[299]. Knocking out FATP in liver has also been shown to lower VLDL secretion[300]. In spite of us not finding a difference in the levels for these proteins, we cannot rule out that the liver is indeed taking-up more FFAs. A better confirmation of this would be to extract the acyl-CoAs (up-taken fatty acids are converted to acyl-CoAs before being shuttled to various biochemical pathways) from liver tissue using solid-phase extraction and quantify with high-performance liquid chromatography (HPLC)[301,302]. If our hypothesis is true, we would expect higher levels of acyl-CoAs in the livers of NTS GC animals. Our laboratory will undertake these analyses in the future.

Apolipoprotein B (ApoB) constitutes the major apoprotein component of VLDL particles[86–88]. In rat livers, VLDL particles are made with either one ApoB100 or one ApoB48 protein[86], and therefore, measuring plasma ApoB levels provides an estimate for VLDL particle numbers in the circulation. In this study, we assessed the levels of ApoB in plasma collected from the VLDL secretion experiments. We found that plasma at time 0 (plasma obtained prior to poloxamer injection, but after a 90-minute pre-infusion of dexamethasone in the NTS) displayed no difference between ApoB100 or ApoB48 levels compared to vehicle. This was also true for plasma at the end of the experiment (time 240). This data appears to suggest that NTS GCs increase VLDL-TG secretion not by increasing the number of VLDL particles secreted, but rather by increasing its lipid content. To verify this, we performed fast-protein liquid chromatography (FPLC) on plasma from our experiments. This technique has been used previously to fractionate plasma lipoproteins based on size, and then measure TG content in the VLDL-specific fractions[224,303]. Indeed, NTS GC animals displayed higher TG levels in their VLDL-containing fractions, supporting our theory. Importantly, work done in our laboratory that assessed MBH GC effects on VLDL-TG secretion revealed that after a pre-infusion with dexamethasone (time 0) into the MBH there was a significant increase in plasma ApoB100 compared to control[240]. Hence, this further supports that central GC action to regulate VLDL-TG secretion may have differing peripheral mechanisms based on the brain region they act on. It should be noted that

there are some caveats with these analyses. One, we do not have a loading control for our plasma ApoB western blots, so we could not confirm that each sample was diluted evenly. Albumin has previously been used as a loading control for plasma ApoB[304,305], and this could be used in future studies. The other caveat is with FPLC, which is a technique that separates lipoproteins by their size[303]. VLDL particles vary in size and their ranges can overlap with chylomicron sizes[306]. Thus, our FPLC data may have some chylomicron-TG contamination. A more accurate assessment of lipoprotein size would require nuclear magnetic resonance (NMR) spectroscopy[307–309].

Heat shock protein 90 (Hsp90) is a chaperone protein involved in maintaining cellular homeostasis through the regulation of various cellular functions[310–312], including GR signaling[138,139]. Using pharmacological and genetic manipulations in the NTS, we revealed that NTS GC effects on VLDL-TG secretion are reliant on functional Hsp90. Similar to our results, studies that looked at the effects of MBH GCs to increase VLDL-TG[240] or induce hepatic insulin resistance[238] were both negated by Hsp90 blockade. Recent advances in Hsp90 knowledge has also linked this chaperone protein to the pathophysiology of diabetes and obesity. For instance, inhibiting Hsp90 in insulin-resistant myocyte cell lines improved insulin signaling by increasing phosphorylated-Akt (pAkt) levels[313]. Work by Jing et al. suggests that, at least in the muscles, it is the Hsp90β isoform that contributes to insulin resistance[314]. When challenged with inflammatory cytokine treatment, the INS-1 β-cell line underwent increased apoptosis; however, this was significantly reduced with Hsp90 inhibition[313]. It was also reported that treating *db*/*db* mice (a mouse model of diabetes and obesity) with a Hsp90 inhibitor for 2 weeks resulted in lower glycemia, improved glucose and insulin tolerance[313]. In corroboration with this, Hsp90 antagonism in rat islets exposed to high concentrations of glucose led to increased insulin secretion due to an upregulation of genes related to glucose sensing, insulin production, and exocytosis[315]. Continuing, Hsp90 is also associated with obesity and lipid metabolism. To illustrate, Hsp90 inhibition was able to reverse body weight gain, dyslipidemia, and liver steatosis in mice fed a western-type diet[316]. Both diabetes in *db*/*db* mice and HFD-feeding are associated with higher levels of GCs, thus it would be intriguing to determine whether improved metabolic outcomes are associated with reduced GC action in the brain with whole-body Hsp90 inhibition.

Another study reported that treating mice on a high fat diet (HFD) with geldanamycin (a Hsp90 antagonist) reduces adipose tissue expansion, and this was associated with reduced adipocyte GR expression[317]. In addition, rats on a 3-day HFD experienced elevated GC levels and/or action which resulted in hypertriglyceridemia; however, acute and/or chronic Hsp90 antagonism in the MBH negated this effect, likely due to GR dysfunction[240]. Thus, inhibiting Hsp90 either peripherally or centrally may improve metabolic outcomes possibly through impairments in GR signaling. In fact, this could be a potential future therapeutic target for diseases such as diabetes and obesity.

Another accessory protein for the GR that we investigated was FK506 binding protein 51 (FKBP51). Giving this protein's role of repressing GR activation[140–142], we hypothesized that knocking down FKBP51 in the NTS would lead to overactivated GRs which would increase VLDL-TG secretion. Indeed, NTS FKBP5 shRNA animals had significantly higher plasma TG levels and VLDL-TG secretion rate compared to NTS mismatch controls, indicative of increased NTS GR activation. Although, it's important to note that we did not directly confirm that NTS GRs were more active in FKBP5 shRNA-treated animals in the present study. Our next step is to measure *Pdk4* gene expression, a GR activity marker[265], in DVC tissue of FKBP5 shRNA-infused rats to assess whether NTS GRs are in fact more active. In line with of our results, a study by Häusl et al. generated paraventricular nucleus (PVN)-specific FKBP51 knockout mice and found that this results in enhanced-negative feedback of the HPA axis as a consequence of greater GR activation in the PVN[143]. Similar findings on increased GR sensitivity were also reported in full FKBP51 knockout mice studies as well[318,319]. Beyond its role of regulating GR signaling, FKBP51 is also involved in immunoregulation, protein folding, and trafficking[320]. This protein is also expressed in various tissues, namely the brain, adipose tissue, and skeletal muscle[320]. Recent studies have also linked excessive FKBP51 expression to metabolic dysfunction[321–325], as well as some psychiatric disorders[141,326,327]. Soukas and colleagues revealed that *ob*/*ob* mice (obese mouse model) had increased FKBP51 expression[322]. Later studies showed that FKBP51 activates peroxisome proliferator-activated receptor γ (PPARγ) which promotes adipogenesis[320,321] and could contribute to adipose mass gain. As a corollary, FKBP51 knockout mice were protected against diet-induced obesity,

hypertriglyceridemia, hyperglycemia, and hyperinsulinemia[323]. Other studies with FKBP51 knockout mice showed increased phosphorylated-Akt levels in skeletal muscle compared to wild-type, indicative of enhanced insulin sensitivity[325]. Analyses on human diabetic WAT donor tissue with elevated FKBP51 levels corroborate those findings as these tissues experience decreased insulin sensitivity[328]. Finally, FKBP51 also has an interesting role in the brain. Fasting induces increased levels of FKBP51 in the arcuate nucleus (ARC), ventral medial nucleus (VMH), and PVN of the hypothalamus[329]. One theory is that central GC action promotes feeding behaviors, which is beneficial in a fasted state. By raising FKBP51 levels in the hypothalamus, you diminish GR sensitivity and dampen negative feedback on the HPA axis, resulting in a hyperactive axis and elevated GC levels. Indeed, when overexpressing FKBP51 in the hypothalamus, GC levels increase in the plasma[143,329]. However, hypothalamic FKBP51 has other mechanisms by which it affects metabolism, because it was found that overexpression of FKBP51 around the VMH and ARC led to an increase in body weight in mice on HFD and impaired glucose tolerance[329]. Continuing, higher mRNA levels of *Fkbp5* specifically in the VMH is correlated to increased body weight and food intake[330]. Intriguingly, Brix et al. demonstrated that both overexpression or knockout of FKBP51 in the VMH causes increased body weight gain on a HFD[331]. To further showcase the complexity of hypothalamic FKBP51, mice overexpressing *Fkbp5* in the MBH and fed a HFD are protected from diet-induced obesity and glucose intolerance and exhibit lower food intake[332]. Conversely, MBH *Fkbp5* knockout mice fed a regular chow diet leads to obesity, increased food intake and glucose intolerance[332]. In contrast, we reported that knocking down FKBP51 in the NTS for 2 weeks does not affect body weight but does evoke hepatic TG secretion. Overall, there is sufficient data to suggest that high levels of FKBP51 in the periphery negatively impacts metabolism; however, it is more ambiguous for central FKBP51, and further research on this topic is warranted.

Chapter 5: Aim 2 Results

The second aim for this thesis involved testing whether infusing a membrane-impermeable DEX directly into NTS to activate NTS mGRs would also regulate hepatic VLDL-TG release. We also aimed to test potential downstream intracellular signaling mediators involved. *We hypothesize that using membrane-impermeant DEX will activate mGRs, and require downstream intracellular signaling mediators, in the NTS to stimulate hepatic VLDL-TG secretion* (Figure 1.5).

5.1 Membrane-Associated Glucocorticoid Receptor Role in the Nucleus of the Solitary Tract to Regulate Lipid Metabolism

5.1.1 Membrane-impermeant glucocorticoid action in the nucleus of the solitary tract stimulates very-low density lipoprotein secretion from the liver.

Given that NTS GCs were able to stimulate TG secretion from the liver, we next sought to see if novel membrane-bound GRs (mGRs) were also implicated (Figure 5.1.1A). Since DEX theoretically binds with either the canonical GR in the cytosol or mGR[150,153,154,262,333], we used a commercially available DEX-conjugated to bovine serum albumin (BSA-DEX) that has been previously tested and validated[263,334] to isolate mGR action. The bovine serum albumin moiety prevents the DEX molecules bound to it from crossing the plasma membrane, and therefore limits their effects to the exterior of the cell[165,170,262,334,335].

Our data shows that infusion of BSA-DEX into the NTS was able to recapitulate the lipostimulatory effects of regular NTS DEX for both plasma TG (Figure 5.1.1B) and VLDL-TG secretion (Figure 5.1.1C) compared to NTS saline-infused controls. Thus, mGRs may, at least in part, contribute to the NTS DEX's ability to modulate hepatic lipid homeostasis. Although we found that NTS BSA-DEX treatment trended to increase TG content in the VLDL-containing fractions (Figure 5.1.1D), we found no difference in plasma ApoB100 or ApoB48 protein levels (Figure 5.1.1E). Hepatic TG content was assessed as well, but no change was observed (Figure 5.1.1F). However, we did find that NTS BSA-DEX treatment significantly increased plasma FFAs (Figure 5.1.1G), similar to NTS DEX. We also measured end of experiment plasma glucose (Figure 5.1.1H) and insulin (Figure 5.1.1I), and body weight (Figure 5.1.1J), but no differences between groups was found.

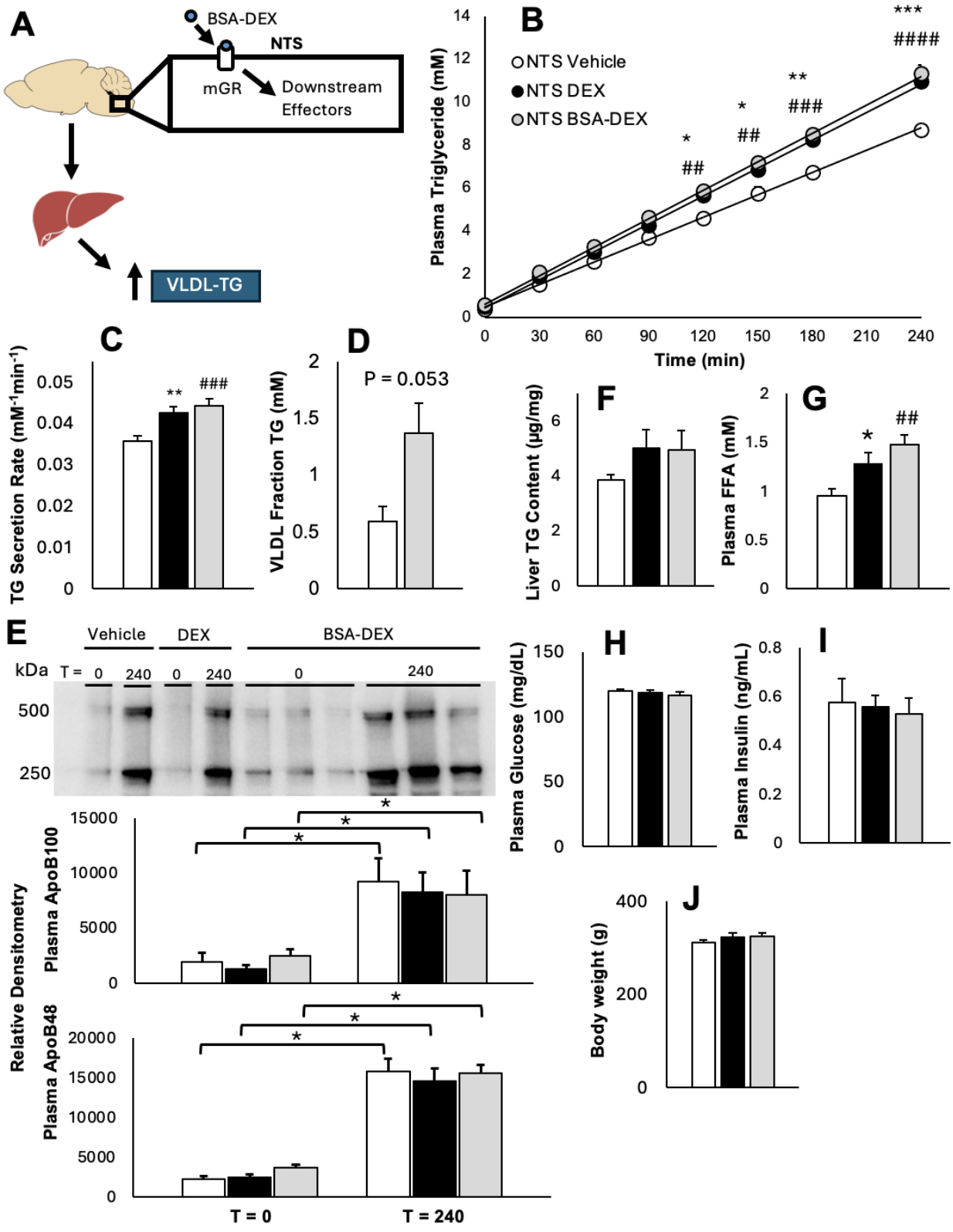
A
BSA-DEX
NTS
mGR
Downstream Effectors
VLDL-TG
B
NTS Vehicle
NTS DEX
NTS BSA-DEX
Plasma Triglyceride (mM)
Time (min)
C
TG Secretion Rate (mM-1min-1)
D
VLDL Fraction TG (mM)
P = 0.053
E
Vehicle
DEX
BSA-DEX
kDa
T =
500
250
Relative Densitometry
Plasma ApoB100
Plasma ApoB48
T = 0
T = 240
F
Liver TG Content (µg/mg)
G
Plasma FFA (mM)
H
Plasma Glucose (mg/dL)
I
Plasma Insulin (ng/mL)
J
Body weight (g)

Figure 5.1.1. Acute NTS membrane-impermeant glucocorticoid infusion increases plasma triglycerides similar to NTS DEX. A) Schematical representation of working hypothesis. **B)** Plasma TG concentration and **C)** hepatic triglyceride secretion rate for animals that received NTS Vehicle (white; n = 10), NTS DEX (black; n = 9), and NTS bovine serum albumin-conjugated DEX (BSA-DEX) (light gray; n =12). **D)** Triglyceride levels in very-low density lipoprotein fraction; NTS Vehicle and NTS MIF were combined (white; n = 4), and NTS BSA-DEX (light gray; n = 4). **E)** Western blot for plasma ApoB100 and ApoB48 at beginning (t = 0) and end (t = 240) of experiment and quantification (NTS Vehicle n = 5; NTS DEX n = 5; NTS BSA-DEX n = 6). **F)** Liver triglyceride levels. **G)** Plasma free fatty acids (FFA), **H)** glucose (NTS Vehicle n = 10; NTS DEX n = 9; NTS BSA-DEX n = 12), and **I)** insulin at end (t = 240) of experiment. **J)** Body weight at the start of the experiment. For **B)** NTS Vehicle, NTS DEX, and NTS BSA-DEX **P < 0.01 for effect of time, treatment, and interaction between time and treatment using a two-way ANOVA, ***P < 0.001 at t=240min and **P < 0.01 at t=180min, *P < 0.05 at t=150 and t=120 minutes for NTS DEX vs NTS Vehicle using Fisher's posthoc test. ####P < 0.0001 at t=240min, ###P < 0.001 at t=180min, and ##P < 0.01 at t=150 and t=120 min for NTS BSA-DEX vs NTS Vehicle. For **C)**, ANOVA was conducted prior to a Fisher's posthoc test; **P < 0.01 for NTS DEX vs NTS Vehicle; ###P < 0.001 for NTS BSA-DEX vs NTS Vehicle. For **G)**, ANOVA was conducted prior to a Fisher's posthoc test; *P < 0.05 for NTS DEX vs NTS Vehicle; ##P < 0.01 for NTS BSA-DEX vs NTS Vehicle. For **E)**, ApoB100 and ApoB48 graphs: *P < 0.05 for effect of time only, treatment effect n.s., and interaction between time and treatment n.s. Data was measured as mean + SEM.

5.1.2 Assessement of changes in the nucleus of the solitary tract upon membrane-impermeant glucocorticoid treatment.

To measure whether BSA-DEX infusion into the NTS altered the expression of genes within neural cells compared with NTS vehicle or DEX infusions, we conducted qPCR on rat DVC tissues. Similar to NTS DEX, BSA-DEX administration was able to increase the mRNA of the *Fkbp5* gene (Figure 5.1.2A). This data suggests that *Fkbp5* upregulation can be used as a marker of activity not just for the canonical GR, but mGRs as well. Expression for *Npy* in the DVC was also assessed due to its importance for hypothalamic DEX's ability to control metabolism[236,237,240,243,244], but no significant difference among groups was found, indicating NTS GC effects on metabolism occur independently to NPY (Figure 5.1.2B).

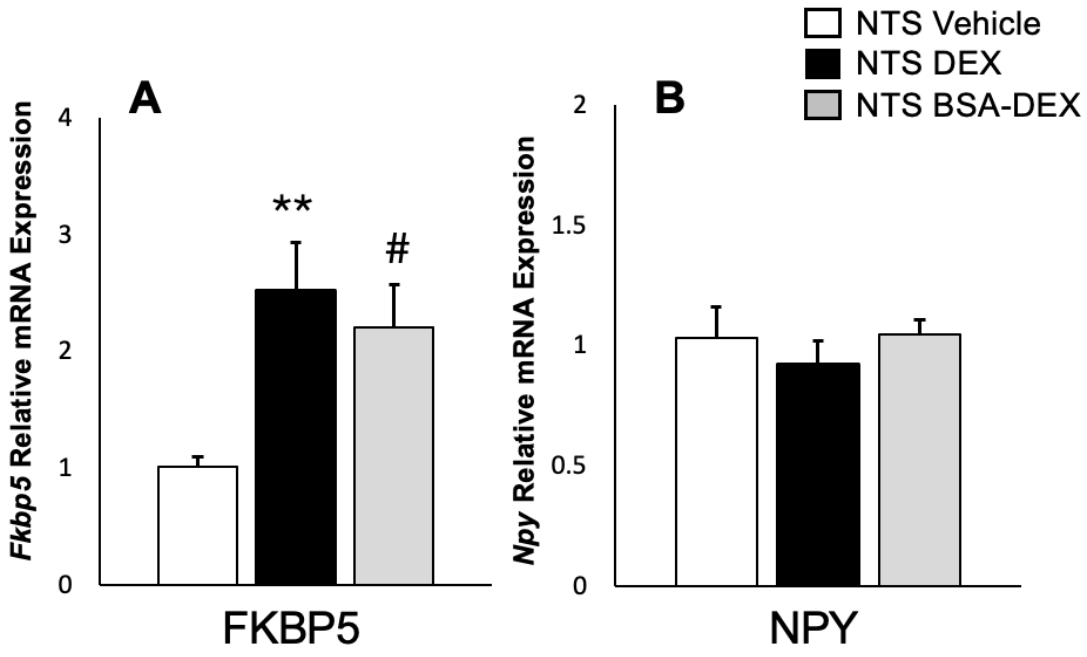

Figure 5.1.2. Assessment of genes related to glucocorticoid receptor action in the dorsal vagal complex. A) Relative expression of *Fkbp5* in dorsal vagal complex (DVC) tissue between NTS Vehicle (white; n = 5), NTS DEX (black; n = 6), NTS BSA-DEX (light gray; n = 4). **B)** Relative expression of *Npy* in DVC tissue between NTS Vehicle, NTS DEX, NTS BSA-DEX. For **A)**, One-way ANOVA was conducted, followed by a Fisher's posthoc; **P < 0.01 NTS DEX vs NTS Vehicle, and #P < 0.05 for NTS BSA-DEX vs NTS Vehicle. Data was measured as mean + SEM.

5.1.3 Assessment of hepatic mechanisms involved in mediating the hyperlipidemic effects induced by membrane-associated glucocorticoid receptor agonism in the nucleus of the solitary tract via western blotting.

To try and start to delineate hepatic mechanisms which may underlie how BSA-DEX acting in the NTS leads to higher plasma TG, we began to examine liporegulatory protein levels in the liver via western blots. Liver pACC to ACC (Figure 5.1.3B), FAS (Figure 5.1.3C), MTP (Figure 5.1.3D), and Arf1 (Figure 5.1.3E) were all unchanged between groups. This data implies that NTS BSA-DEX effects to increase VLDL-TG secretion is unrelated in these proteins involved in *de novo* lipogenesis, VLDL assembly or secretion.

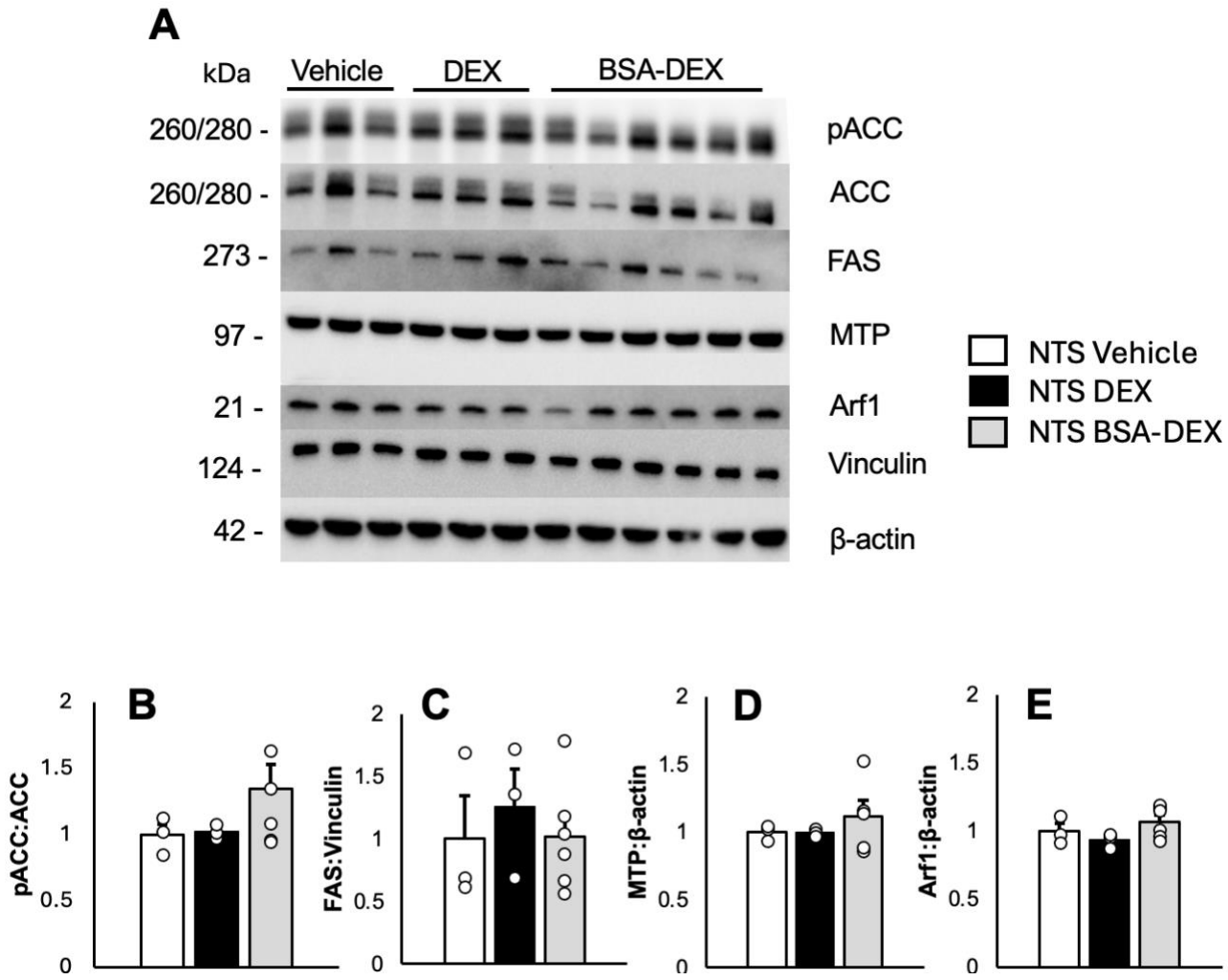

Figure 5.1.3. NTS membrane-bound glucocorticoid receptor agonism effects on hepatic triglyceride secretion are independent to hepatic lipid metabolism-related protein levels. A) Representative western blots between NTS Vehicle, NTS DEX, and NTS BSA-DEX for liver tissue. Quantified levels of **B)** phosphorylated acetyl-CoA carboxylase: acetyl-CoA carboxylase (pACC:ACC), **C)** fatty acid synthase (FAS), **D)** microsomal triglyceride transfer protein (MTP), **E)** ADP-ribosylation factor 1 (Arf1). Data was given as mean + SEM.

5.1.4 Assessment of hepatic mechanisms involved in mediating the hyperlipidemic effects induced by membrane-associated glucocorticoid receptor agonism in the nucleus of the solitary tract via PCR.

Quantitative PCR analyses were also conducted on all the hepatic genes we previously assessed in Section 3.1.4. For most genes, no difference was found, however, *Srebf1c* (Figure 5.1.4B) and *Ppara* (Figure 5.1.4H) mRNA levels were significantly lowered by NTS BSA-DEX treatment, as compared to NTS vehicle controls. Notably, this is different from NTS DEX, in which NTS DEX likewise increased VLDL-TG secretion without affecting the hepatic mRNA levels of *Srebf1c* (Figure 3.1.4B) and *Ppara* (Figure 3.1.4H). Therefore, BSA-DEX may induce its hyperlipidemic effects by altering lipogenic and fatty acid oxidation pathways in the liver in a manner separate from that of NTS DEX.

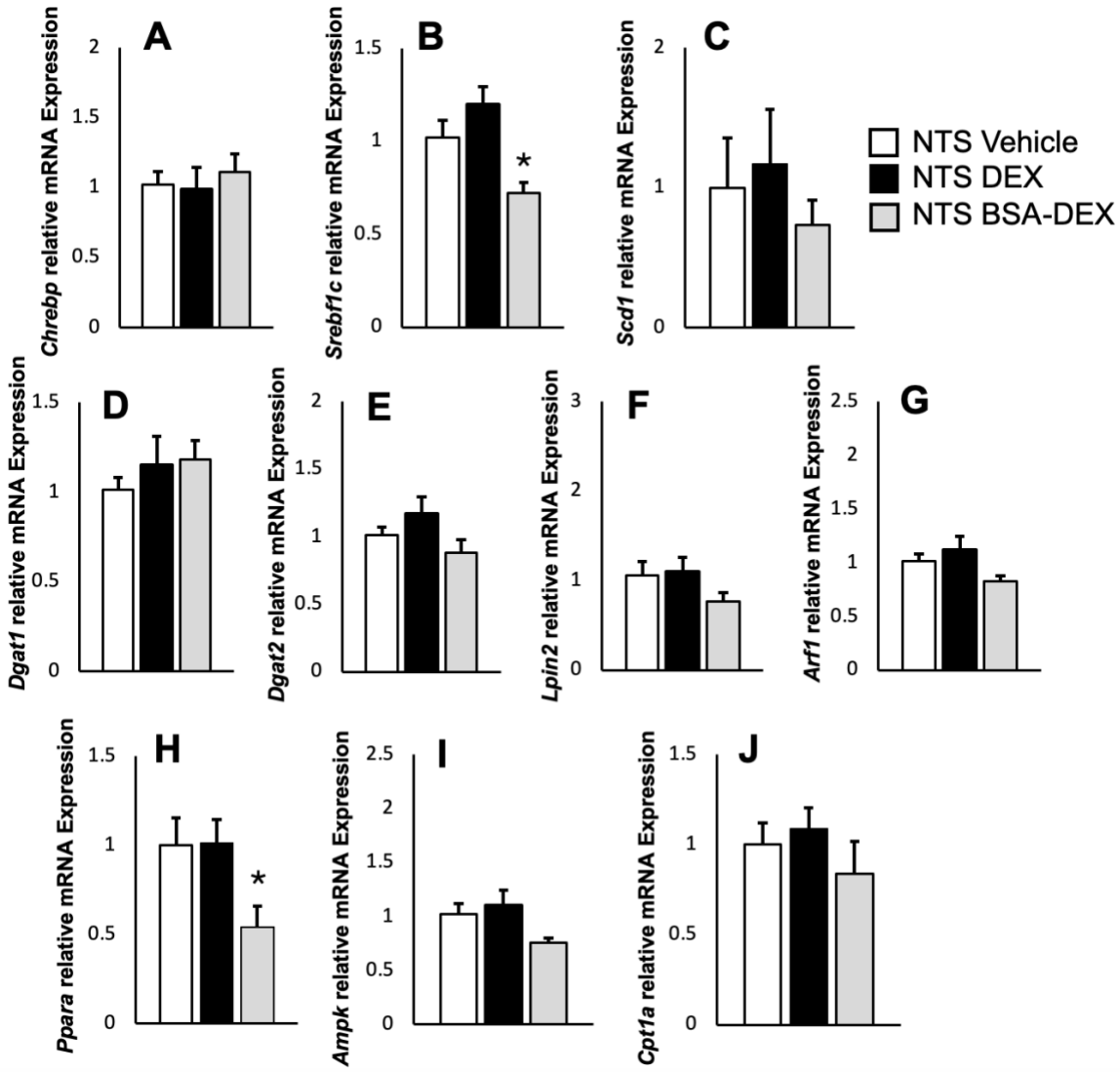

Figure 5.1.4. Assessment of hepatic genes related to lipid metabolism to delineate the mechanisms of membrane-bound glucocorticoid receptor agonism in the NTS. Relative expression for **A)** carbohydrate response element binding protein (*ChREBP*), **B)** sterol regulatory element-binding transcription factor 1c (*Srebf1c*), **C)** stearoyl-CoA desaturase 1 (*Scd1*), **D)** diacylglycerol acyltransferase 1 (*Dgat1*), **E)** *Dgat2*, **F)** lipin 2 (*Lpin2*), **G)** ADP-ribosylation factor 1 (*Arf1*), **H)** peroxisome proliferator-activated receptor α (*Ppara*), **I)** AMP-activated kinase (*Ampk*), and **J)** carnitine palmitoyltransferase 1α (*Cpt1a*) for NTS Vehicle (white; n = 6), NTS DEX (black; n = 6), and NTS BSA-DEX (light gray; n = 6). For **B)** and **H)**, one-way ANOVA was conducted, followed by a Fisher's posthoc; *P < 0.05 NTS BSA-DEX vs NTS Vehicle and NTS DEX. Data was measured as mean + SEM.

5.1.5 Assessment of white adipose tissue mechanisms involved in mediating the hyperlipidemic effects induced by membrane-associated glucocorticoid receptor agonism in the nucleus of the solitary tract.

Since the increase of hepatic VLDL-secretion observed upon BSA-DEX infusion in the NTS was associated with significantly higher plasma FFAs, we next probed the WAT. Unlike NTS DEX (Figure 3.1.5B), NTS BSA-DEX treatment did not affect the levels of pHSL to total HSL (Figure 5.1.5B). Interestingly, NTS BSA-DEX did increase ATGL levels relative to control (Figure 5.1.5C), which corroborates the observed increase in plasma FFAs we also observed. NTS BSA-DEX did not affect CGI-58 (Figure 5.1.5D) and perilipin (Figure 5.1.5E) protein levels in WAT. Thus, unlike NTS DEX, which increased pHSL:HSL in WAT, the increased plasma FFA levels observed with NTS BSA-DEX were associated with increased ATGL in WAT, potentially representing another difference by which DEX and BSA-DEX act differently within the NTS to induce hyperlipidemia.

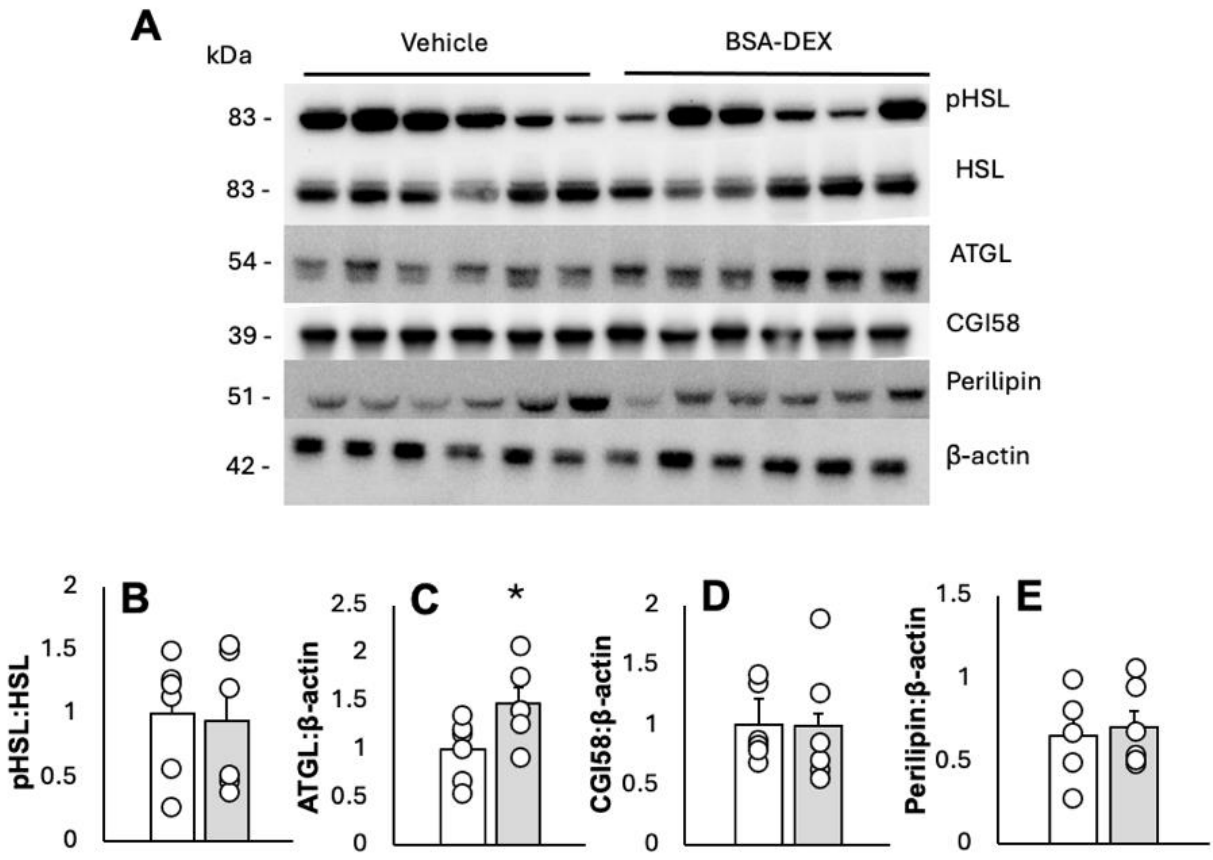

Figure 5.1.5. Changes in VLDL-TG secretion induced by NTS BSA-DEX infusion altered lipolytic enzyme levels in white adipose tissue. A) Representative western blots for white adipose tissue. Levels of **B)** phosphorylated hormone sensitive lipase: total hormone sensitive lipase (pHSL:HSL), **C)** adipose triglyceride lipase (ATGL), **D)** comparative gene identification-58 (CGI-58), **E)** perilipin. For **C)**, a Student's t test was done, *P < 0.05 NTS BSA-DEX vs NTS Vehicle. Data was given as mean + SEM.

5.2 Investigation of the Role of Glucocorticoid Receptor shRNA on the Membrane-Associated Glucocorticoid Receptor in the Nucleus of the Solitary Tract

5.2.1. Genetically disrupting the glucocorticoid gene does not impact membrane-associated glucocorticoid receptor action in the nucleus of the solitary tract.

As NTS GR shRNA, which reduced GR protein levels by ~50% (Figure 3.2.1B), reversed the hyperlipidemic effects of NTS DEX (Figure 3.2.1C, D), we next sought to find out whether NTS GR shRNA would also block the NTS BSA-DEX effects on hepatic TG secretion (Figure 5.2.1A). As expected, in animals that received a control shRNA, BSA-DEX infusion was still able to trigger increased plasma TG and hepatic VLDL-TG release (Figure 5.2.1B, C). Interestingly, the effects of BSA-DEX effects persisted in animals that received NTS GR shRNA (Figure 5.2.1B, C). These effects were independent to end of experiment plasma glucose levels (Figure 5.2.1D) and start of experiment body weight (Figure 5.2.1E). Taken together, this data shows that NTS GR shRNA blocks NTS DEX, but not NTS BSA-DEX, to stimulate VLDL-TG and suggests that the canonical GR (which is inhibited by GR shRNA) that mediates the effects of NTS DEX is different from the mGR that mediates the effects of NTS BSA-DEX on lipid regulation.

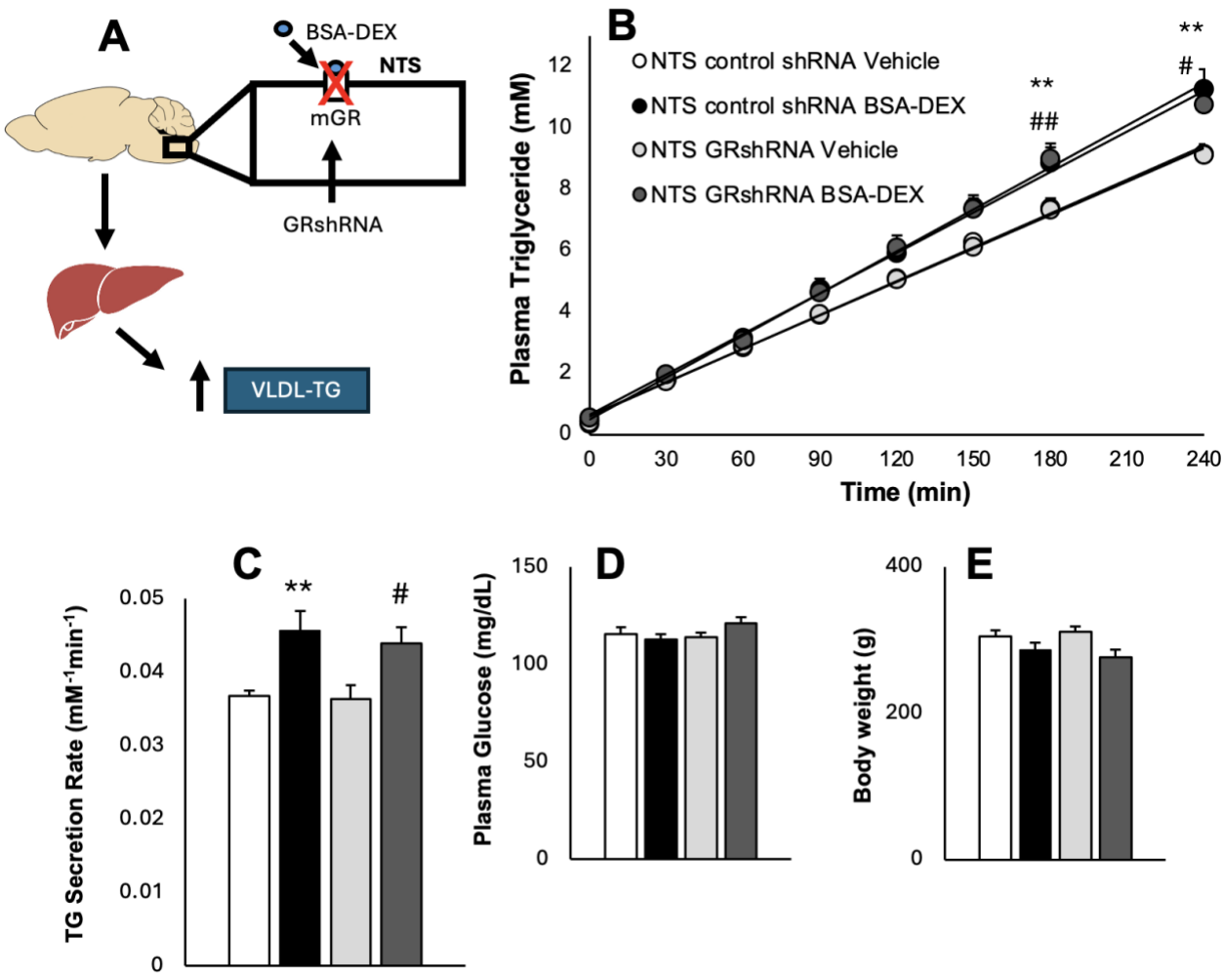

Figure 5.2.1. Knockdown of NTS glucocorticoid receptors does not negate NTS BSA-DEX effects on plasma triglycerides. A) Schematical representation of working hypothesis. **B)** Plasma TG concentration and **C)** hepatic triglyceride secretion rate for animals that received NTS control shRNA Vehicle (white; n = 7), NTS control shRNA BSA-DEX (black; n = 7), NTS GR shRNA Vehicle (light gray; n = 5), and NTS GR shRNA BSA-DEX (dark gray; n = 6). **D)** End of experiment plasma glucose. **E)** Start of experiment body weight. For **B)**, NTS control shRNA BSA-DEX, NTS control shRNA Vehicle, NTS GR shRNA Vehicle, and NTS GR shRNA BSA-DEX **P < 0.01 for effect of time, treatment, and interaction between time and treatment (two-way ANOVA). Fisher's posthoc test: **P < 0.01 at t=240 and t=180 min for NTS control shRNA BSA-DEX vs NTS control shRNA Vehicle and NTS GR shRNA Vehicle. #P < 0.05 at t=240 min and ##P < 0.01 at t=180 min for NTS GR shRNA BSA-DEX vs NTS control shRNA Vehicle

and NTS GR shRNA Vehicle. For **C)**, **P < 0.01 for NTS control shRNA BSA-DEX vs NTS control shRNA Vehicle and NTS GR shRNA Vehicle, and #P < 0.05 for NTS GR shRNA BSA-DEX vs NTS control shRNA Vehicle and NTS GR shRNA Vehicle (one-way ANOVA, followed by a Fisher's posthoc test). Data was measured as mean + SEM.

5.3 Investigation of the Role of Heat Shock Protein 90 on the Membrane-Associated Glucocorticoid Receptor in the Nucleus of the Solitary Tract

5.3.1. Heat shock protein 90 is not required for the membrane-associated glucocorticoid receptor.

Previously, we observed that blocking the action of Hsp90 blocked the lipostimulatory effects of NTS DEX (Figure 3.3.1B, C), demonstrating the importance of this chaperone protein on GR function. To the best of our knowledge, there have been no studies done assessing whether Hsp90 is also required for the mGRs, thus this was our next goal (Figure 5.3.1A).

Using *in vivo* VLDL secretion experiments, we again showed that administering our pharmacological antagonist of Hsp90 alone into the NTS had no effects on plasma TG or VLDL secretion (Figure 5.3.1B, C). However, unlike its inhibitory effect on NTS DEX, Hsp90i was unable to negate the NTS BSA-DEX effects on lipid metabolism when co-infused together, suggesting mGRs work through Hsp90-independent pathways (Figure 5.3.1B, C). End of experiment plasma glucose levels (Figure 5.3.1D) and start of experiment body weight (Figure 5.3.1E) remained unchanged as well.

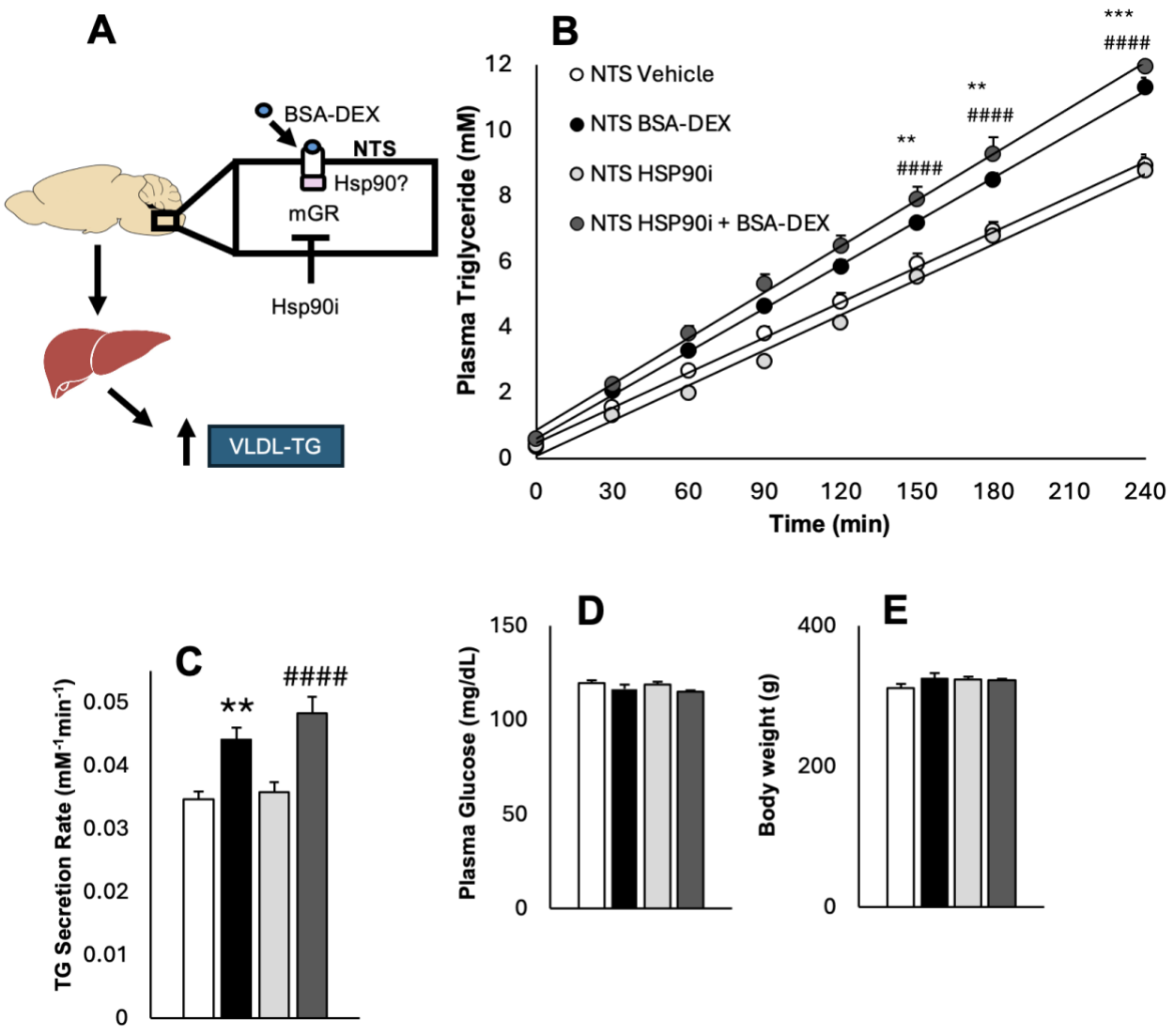

Figure 5.3.1. Blocking Hsp90 in the NTS does not reverse NTS BSA-DEX effects on plasma triglycerides. A) Schematical representation of working hypothesis. **B)** Plasma TG concentration and **C)** hepatic triglyceride secretion rate for animals that received NTS Vehicle (white; n = 10), NTS BSA-DEX (black; n = 12), NTS Hsp90i (light gray; n = 10), and NTS Hsp90i + BSA-DEX (dark gray; n = 9). **D)** End of experiment plasma glucose levels. **E)** Start of experiment body weight. For **B)**, NTS Vehicle, NTS BSA-DEX, NTS Hsp90i, and NTS Hsp90i + BSA-DEX ****P < 0.0001 for effect of time, treatment, and interaction between time and treatment (two-way ANOVA). Fisher's posthoc test: ***P < 0.001 at t=240 min, and **P < 0.01 at t=180 and t=150 min for NTS BSA-DEX vs NTS Vehicle and NTS Hsp90i. ####P < 0.0001 at t=240, t=180, and t=150

min for NTS Hsp90i + BSA-DEX vs NTS Vehicle and NTS Hsp90i. For **C)**, **P < 0.01 for NTS BSA-DEX vs NTS Vehicle and NTS Hsp90i. ####P < 0.0001 for NTS Hsp90i + BSA-DEX vs NTS Vehicle and NTS Hsp90i (one-way ANOVA, followed by a Fisher's posthoc test). Data was measured as mean + SEM.

5.4 Examination of Downstream Effectors for the Membrane-Associated Glucocorticoid Receptor Role in the Nucleus of the Solitary Tract

5.4.1 Protein Kinase A is not required for hindbrain membrane-associated glucocorticoid receptor's ability to stimulate very-low density lipoprotein secretion from the liver.

The importance of PKA for the mGR's signaling has been documented in several studies[154,157,336]. Thus, we conducted *in vivo* experiments to test the necessity of NTS PKA on NTS BSA-DEX's effects on VLDL-TG secretion (Figure 5.4.1A). We first showed that inhibiting PKA alone in the NTS using Rp-CAMPs (Rp) had no impact on lipid metabolism (Figure 5.4.1B, C). This is analogous to a parallel study in our laboratory which examined the role of NTS PKA in mediating the effects of the hormone glucagon on hepatic VLDL-TG secretion[253]. Additionally, this separate project in our laboratory demonstrated that the same administration (concentration and duration) of Rp infused into the NTS of rats blocked both the effects of glucagon acting via its GPCR and direct PKA activation within the NTS, to modulate liver TG secretion, showing the efficacy of this compound to inhibit PKA-mediated signaling within the NTS. However, in the present study, co-infusing both Rp and BSA-DEX together into the NTS did not block the ability of BSA-DEX to stimulate VLDL-TG secretion (Figure 5.4.1B, C), indicating that PKA may not be a downstream effector for the NTS mGRs. Again, plasma glucose at the end of experiment (Figure 5.4.1D) and the body weight at the start of the experiment (Figure 5.4.1E) were not different between groups. It is possible that a higher concentration of PKA is required to block BSA-DEX, thus future studies to test additional doses of Rp, or direct assessments of Rp on NTS PKA activity to confirm PKA inhibition, are warranted.

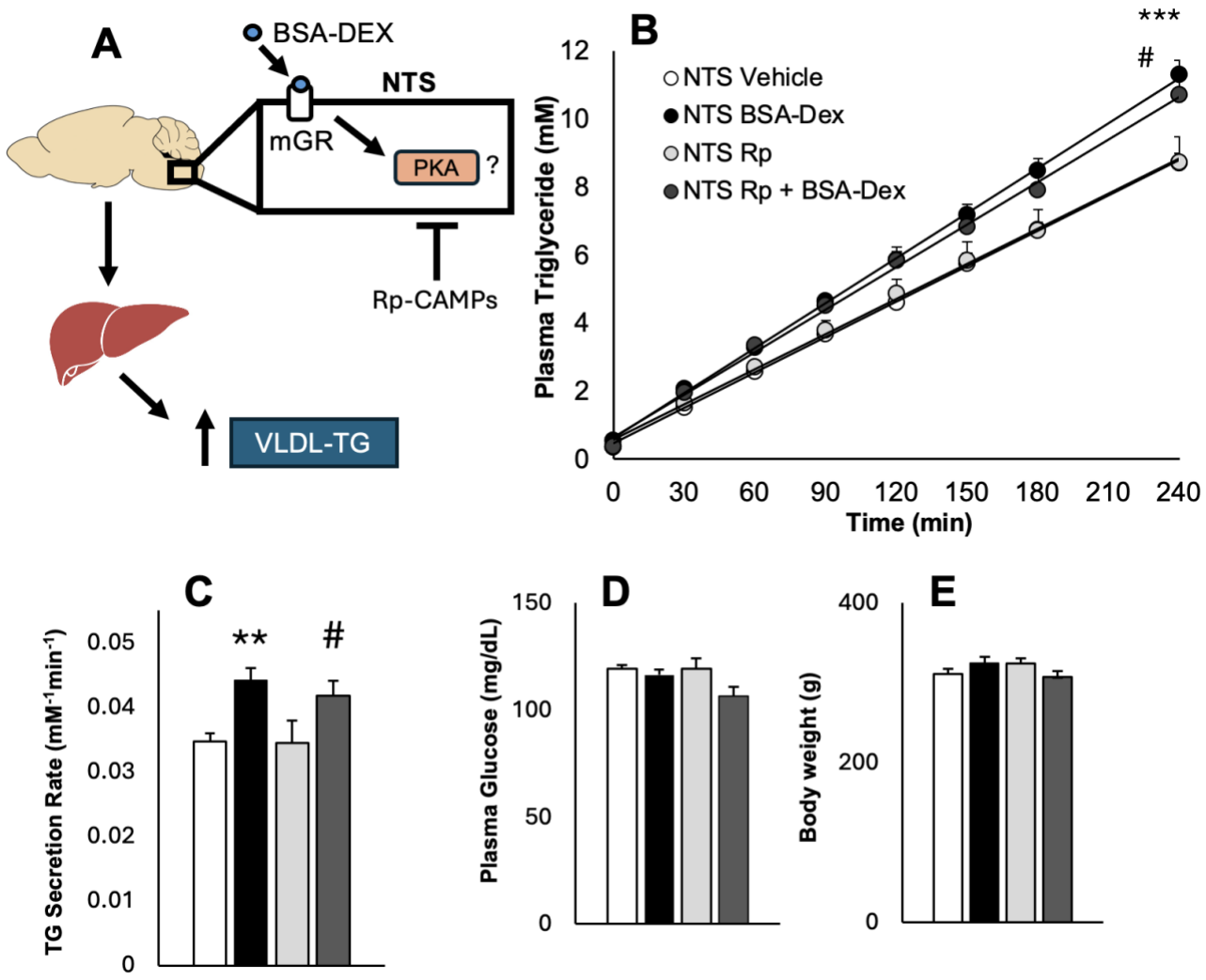

Figure 5.4.1. NTS BSA-DEX effects on plasma triglycerides are independent to NTS PKA action. A) Schematical representation of working hypothesis. **B)** Plasma TG concentration and **C)** hepatic triglyceride secretion rate for animals that received NTS Vehicle (white; n = 10), NTS BSA-DEX (black; n = 12), NTS Rp-CAMPs (Rp) (light gray; n = 7), and NTS Rp + BSA-DEX (dark gray; n = 7). **D)** End of experiment plasma glucose levels. **E)** Start of experiment body weight. For **B)**, NTS Vehicle, NTS BSA-DEX, NTS Rp, and NTS Rp + BSA-DEX **P < 0.01 for effect of time, treatment, and interaction between time and treatment (two-way ANOVA). Fisher's posthoc test: ***P < 0.001 at t=240 min for NTS BSA-DEX vs NTS Vehicle and NTS Rp. #P < 0.05 at t=240 min for NTS Rp + BSA-DEX vs NTS Vehicle and NTS Rp. For **C)**, a one-way ANOVA

was conducted, followed by a Fisher's posthoc test; **P < 0.01 for NTS BSA-DEX vs NTS Vehicle and NTS Rp. #P < 0.05 for NTS Rp + BSA-DEX vs NTS Vehicle and NTS Rp. Data was measured as mean + SEM.

5.4.2 Hindbrain membrane-associated glucocorticoid receptor's ability to stimulate very-low density lipoprotein secretion requires protein kinase C.

Another downstream target that has been described for mGR's signaling is PKC[155,168,337]. Thus, we next tested the requirement of NTS PKC on mediating the effects of NTS BSA-DEX using a pharmacological PKC inhibitor, Bisindolylmaleimide I (BIMI) (Figure 5.4.2A). NTS BIMI did not impact VLDL-TG secretion (Figure 5.4.2B, C). However, concomitant infusion of both BIMI and BSA-DEX into the NTS blocked the stimulatory ability of BSA-DEX on VLDL-TG secretion, indicating that PKC is required for the effects of BSA-DEX and suggesting that PKC may be acting as a downstream effector of the mGRs (Figure 5.4.2B, C). End of experiment plasma glucose levels (Figure 5.4.2D) and start of experiment body weight (Figure 5.4.2E) remained unchanged between groups. In future studies, a PKC protein activity assay[338,339] could be used to assess DVC tissues (which contain the NTS) to confirm the efficacy of BIMI on the inhibition of this kinase.

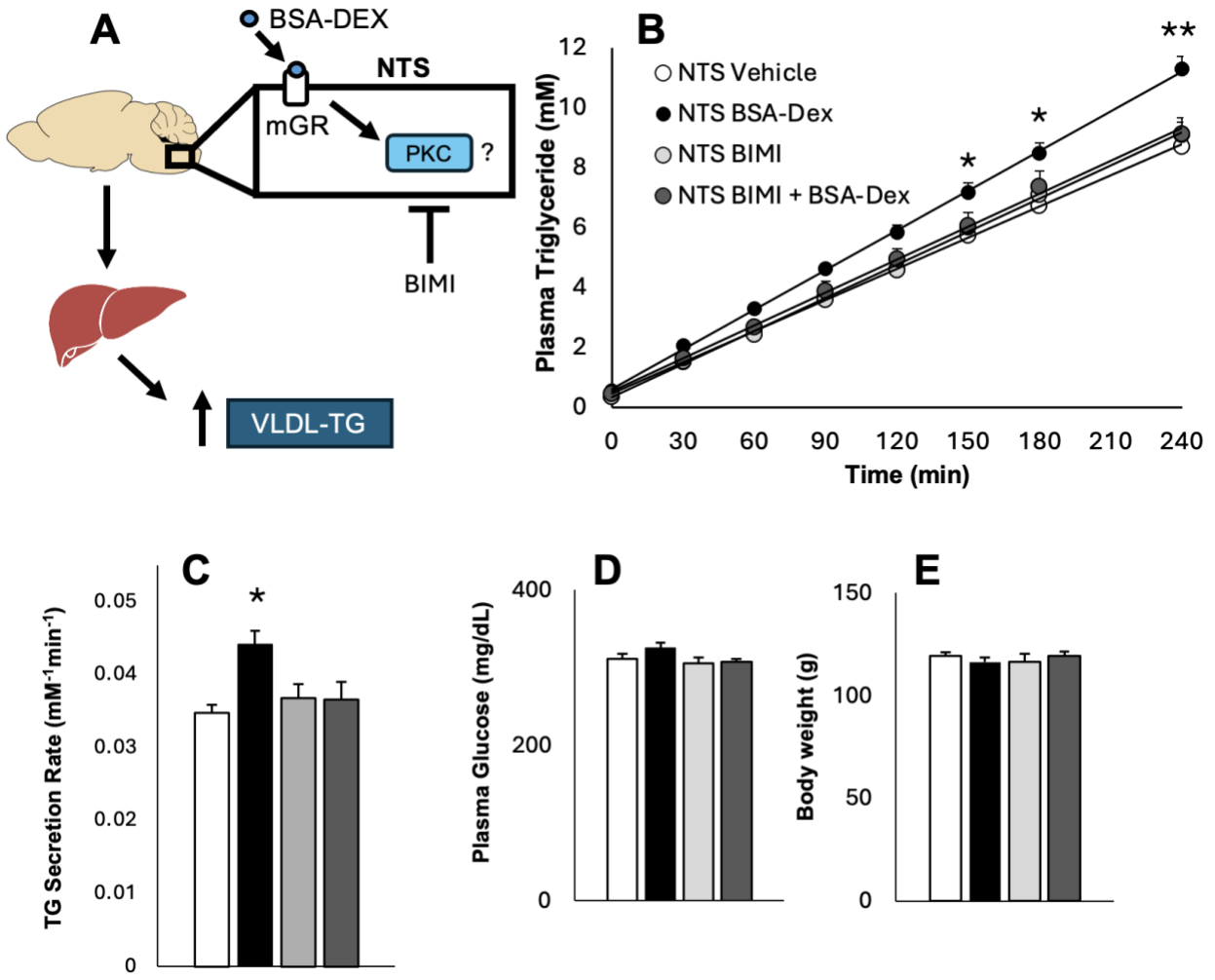

Figure 5.4.2. NTS BSA-DEX effects on plasma triglycerides require NTS PKC. A) Schematical representation of working hypothesis. **B)** Plasma TG concentration and **C)** hepatic triglyceride secretion rate for animals that received NTS Vehicle (white; n = 10), NTS BSA-DEX (black; n = 12), NTS BIMI (light gray; n = 12), and NTS BIMI + BSA-DEX (dark gray; n = 7). **D)** End of experiment plasma glucose levels **E)** Start of experiment body weight. For **B)**, NTS BSA-DEX vs NTS Vehicle, NTS BIMI, and NTS BIMI + BSA-DEX ***P < 0.001 for effect of time, treatment, and interaction between time and treatment (two-way ANOVA). Fisher's posthoc test: **P < 0.01 at t=240 min and *P < 0.05 at t=180 and t=150 min for NTS BSA-DEX vs NTS Vehicle, NTS BIMI, and NTS BIMI + BSA-DEX. For **C)**, a one-way ANOVA was conducted, followed by a Fisher's posthoc; *P < 0.05 for NTS BSA-DEX vs NTS Vehicle, NTS BIMI, and NTS BIMI + BSA-DEX. Data was measured as mean + SEM.

5.4.3 Mitogen-activated protein kinase function is needed for membrane-associated glucocorticoid receptor's ability to stimulate hepatic lipoprotein secretion.

The third and final kinase that was assessed for NTS mGR signaling is MAPK as this effector has also been linked to the mGR signaling cascade[159,171,263] (Figure 5.4.3A). To start, we infused the MEK inhibitor, PD98059 (PD), into the NTS of the animals and observed no changes in hepatic lipid secretion (Figure 5.4.3B, C). Using PD to block MEK, prevents MEK-induced activation of MAPK. Confirmation of the efficacy of PD is still required for this study, potentially with a MAPK activity assay[340]. Next, we tested a co-infusion of PD with BSA-DEX and observed that PD negated the lipostimulatory effects of NTS BSA-DEX (Figure 5.4.3B, C). This supports that MAPK signaling could be involved in mediating NTS mGR hyperlipidemic effects. The observed changes in lipid metabolism were also independent to the end of experiment plasma glucose levels (Figure 5.4.3D) and body weight (Figure 5.4.3E).

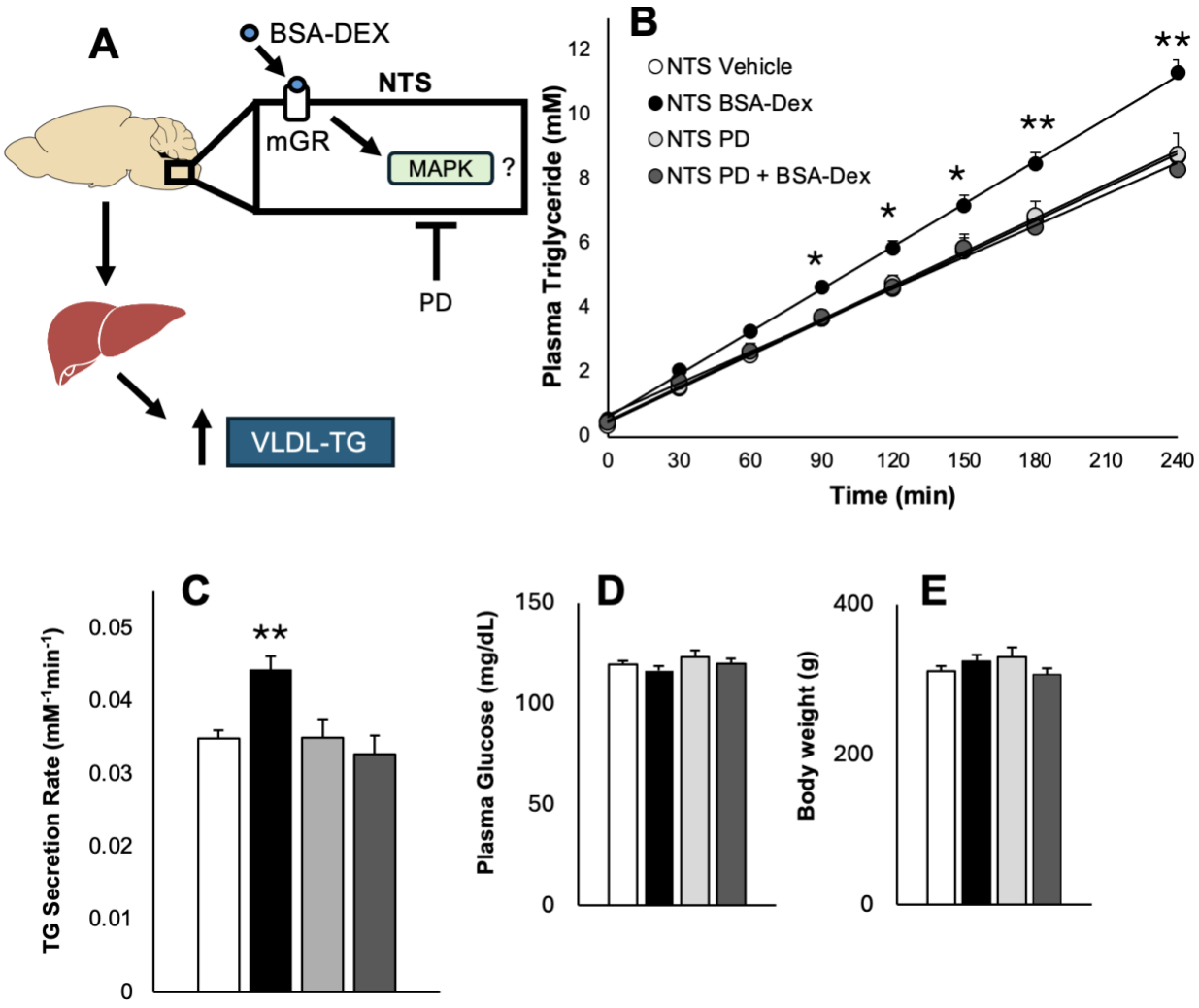

Figure 5.4.3. NTS BSA-DEX effects require NTS MAPK. A) Schematical representation of working hypothesis. **B)** Plasma TG concentration and **C)** hepatic triglyceride secretion rate for animals that received NTS Vehicle (white; n = 10), NTS BSA-DEX (black; n = 12), NTS PD98059 (PD) (light gray; n = 6), and NTS PD + BSA-DEX (dark gray; n = 8). **D)** End of experiment plasma glucose levels. **E)** Start of experiment body weight. For **B)**, NTS BSA-DEX vs NTS Vehicle, NTS PD, and NTS PD + BSA-DEX **P < 0.01 for effect of time, treatment, and interaction between time and treatment (two-way ANOVA). Fisher's posthoc test: **P < 0.01 at t=240 and t=180 min, and *P < 0.05 at t=180, t=150, t=120, and t=90 min for NTS BSA-DEX vs NTS Vehicle, NTS PD, and NTS PD + BSA-DEX. For **C)**, a one-way ANOVA was conducted, followed by a Fisher's posthoc; **P < 0.01 for NTS BSA-DEX vs NTS Vehicle, NTS PD, and NTS PD + BSA-DEX. Data was measured as mean + SEM.

Chapter 6: Aim 2 Discussion

6.1 Significance of Results

As mentioned earlier, excessive levels of GCs can contribute to the development of metabolic diseases, and importantly, there is an associated upregulation of GR expression[110,111,114–118]. Understanding how GCs signal and mediate their actions is an important step for the development of future therapeutics. Beyond their classical genomic mechanisms (via cGRs), GCs can also mediate nongenomic effects via putative membrane-associated GRs (mGRs)[165,180]. However, the relative contribution of cGRs and mGRs in development of metabolic disorders remains unresolved. Knowing the exact effects from each receptor and their relative contribution in diseased states will be crucial for the treatment of these conditions. An interesting report revealed that human monocytes derived from individuals with rheumatoid arthritis had increasing mGR levels with disease progression[341], suggesting that mGRs are also implicated in pathophysiological states. In the present thesis, we report for the first time that administering a membrane-impermeant form of DEX, to specifically target the mGRs, into the NTS can induce hyperlipidemia, indicating that NTS mGRs may be implicated in the development of dyslipidemia in individuals experiencing excessive GC levels and/or action. Thus, our research furthers the knowledge on these putative mGRs and their role in regulating lipid metabolism via central hindbrain pathways.

6.2 Use of the BSA-DEX compound

It has been revealed that GCs can mediate some of their effects via nongenomic mechanisms which involves a membrane-associated glucocorticoid receptor (mGR)[342,343]. Literature suggests that dexamethasone is capable of interacting with either the cGR or mGR[150,153,344,345]. Future, it has been reported that the levels of mGRs present on a cell are much lower than cGRs, by about a 1000-fold less[160,341]. To discriminate between the activation of both receptors, we used a commercially available and previously validated membrane-impermeant dexamethasone conjugated to bovine serum albumin (BSA-DEX)[334]. This compound contains DEX molecules which are covalently linked to a BSA moiety. The ratio of DEX:BSA of the BSA-DEX compound used is 37:1 with a molecular weight of 83,233.61g/mol (where the molecular weight of BSA is 65,000g/mol). We used a dose of BSA-DEX analogous to that which was used *in vivo* in rats in which BSA-DEX [for mGR activation] was shown to mediate rapid

inhibition of the HPA axis when infused into the hypothalamus' PVN[346]. As stated in the Methods (Chapter 2), the concentration of our NTS DEX infusate was at 100µg/µL (255µM), whereas the concentration of the NTS BSA-DEX infusate was at 2.35µg/µL (28.2µM). Thus, the molarity of the BSA-DEX infusate was approximately one-tenth that of the DEX infusate. For this present study, we used a commercially available BSA-DEX (Steraloids P0516) that was previously validated through NMR studies[334]. Specifically, the BSA-DEX used in this thesis was shown to be stable over time and at increasing temperatures (i.e. DEX does not unbind BSA under varying conditions)[334]. This study also found that 95.5% of the total DEX molecules remain covalently bound to BSA, whereas only 4.5% are noncovalently bound 'free' DEX[334]. Importantly, the 'free' DEX was determined to not be biologically available as those molecules were trapped within hydrophobic pockets of the BSA protein[334]. While our laboratory is not specialized in molecular and cellular biological techniques to recapitulate the analyses to confirm the impermeant properties of this compound, a future direction to test whether this BSA-DEX compound is indeed not activating cGRs and triggering genomic signaling, could be through a luciferase reporter assay on the GC-response elements. In one paper that performed this test, it was revealed that DEX increased the luciferase activity by activating cGRs, but BSA-DEX was unable to evoke a genomic response due to its inability to enter cells[263]. Overall, whilst most steroid-conjugated compounds are unstable, evidence suggests that the commercially available BSA-DEX utilized in the present study is a suitable agonist for the mGRs under acute conditions.

6.3 Discussion of the liporegulatory effects of NTS BSA-DEX (Aim 2) results.

We report for the first time that acute infusion of BSA-DEX into the NTS stimulates VLDL-TG secretion. These results indicate that, at least in part, NTS GCs can trigger hepatic TG release via NTS mGRs. Further, we revealed that NTS BSA-DEX's hyperlipidemic effects are dependent on NTS PKC and MAPK, suggesting that these are downstream effectors of the NTS mGRs. Previous *in vitro* studies of nongenomic GC effects on skin wound healing[168], spinal cord neuronal transmission[347], and hippocampal neural excitability[155] also implicated PKC to mediate mGR signaling.

Therefore, there is now both *in vitro* and *in vivo* evidence in different tissues and cell types suggesting that mGRs trigger PKC-dependent signaling cascades. We also found that pre-treatment with PD98059, a MEK inhibitor used to prevent MAPK activation, negates BSA-DEX effects. Briefly, MAPK is a kinase activated by the Ras-Raf-MEK-ERK (ERK is another name for MAPK) pathway[348]. In support of this, Gutièrrez-Mecinas and colleagues subjected Wister rats to an acute stress challenge and found that phosphorylated-ERK levels were rapidly upregulated in the hippocampus via nongenomic GR signaling[349], providing evidence for MAPK signaling downstream of mGR. Other *in vitro* analyses on myocytes[171,345] and immune cells[159] also reported an mGR - MAPK signaling cascade. While it is possible that mGRs trigger multiple cascades at the same time, it is also plausible that NTS mGRs activate a single pathway of mGR - PKC - MAPK arranged in series. It is well established that MAPK is activated by Ras/Raf signaling[348,350–352]. Importantly, PKC is capable of activating MAPK indirectly via Raf activation[353,354]. However, we have yet to directly test whether PKC activation precedes MAPK activation following BSA-DEX infusion, but future investigation is warranted. Interestingly, PKA was also reported to be a downstream effector for the mGRs in cultured rat hypothalamic neurons[154,157], but our data did not support this since co-infusion of PKA inhibitor Rp-cAMPs into the NTS failed to block the hyperlipidemic effects of NTS BSA-DEX. It is possible that forebrain and hindbrain regions possess different signaling pathways for hormones, as has been shown for differential insulin signaling in the regulation of glucose metabolism in the hypothalamus as compared to the dorsal vagal complex[250] . An additional potential explanation for different downstream targets for mGRs may be that different tissues or even different cell types within the same tissue possess different mGR isoforms each with their own cascades, such as adrenergic receptors[355,356].

6.4 Similarities and differences between NTS DEX and NTS BSA-DEX effects.

6.4.1 Similarities and differences between NTS DEX and NTS BSA-DEX effects on lipid metabolic readouts.

As mentioned, BSA-DEX treatment in the NTS induced hepatic VLDL-TG secretion, similar to NTS DEX. Our data showed extensive similarities between both compounds. For instance, NTS DEX and NTS BSA-DEX each increased plasma TG

and VLDL-TG secretion. We found that NTS DEX treatment increased TG content in VLDL fractions, and there was a strong trend (P = 0.056) for NTS BSA-DEX to also increase it. Plasma ApoB was unchanged in both groups as well. In Aim 1 (Chapter 3), we discussed our evidence which suggests that NTS DEX effects to increase VLDL-TG secretion likely involves elevations in circulating FFAs, and results from the studies performed to test Aim 2 suggest that NTS BSA-DEX's hyperlipidemic phenotype is also associated with increased FFAs.

6.4.2 Similarities and differences between NTS DEX and NTS BSA-DEX effects on molecular analyses.

Furthermore, western blotting and PCR data also showed similarities and differences in different tissues between the two NTS infusates. First, both DEX and BSA-DEX elicited an upregulation in *Fkbp5* expression in DVC wedges. While it has been established that DEX induces *Fkbp5*[146,147,149], this is the first study that explored and reports an effect of BSA-DEX on FKBP51 expression.

For peripheral tissues, liver western blotting for proteins involved in DNL and VLDL assembly/secretion did not show any change with either DEX or BSA-DEX treatment at the end of VLDL-TG secretion experiments, suggesting that the increase in VLDL-TG secretion observed with both of these infusates is independent of these hepatic pathways. Gene expression assessment in liver tissue of NTS DEX treated animals was not changed; however, hepatic *Srebf1c* and *Ppara* mRNA levels were decreased with NTS BSA-DEX treatment, showing a liver-specific difference as a result of NTS treatments following VLDL-TG secretion experiments. Clinically, PPARα agonists are used to manage hypertriglyceridemia[357–359], and these drugs have been reported to lower plasma VLDL-TG[358,359]. Furthermore, *in vivo* studies have reported that hepatic PPARα levels are reduced in insulin-resistant rats with dyslipidemia[360]. These results were corroborated in liver-specific PPARα knockout mice on a HFD, as these animals showed elevated plasma TG and ApoB, indicative of higher VLDL levels[361]. As PPARα is involved in β-oxidation of fatty acids, a reduction in the levels of this protein could mean that the acyl-CoAs in the liver may be redirected to other pathways, such as VLDL packaging. On the other hand, *Srebf1c* mRNA was lower in the NTS BSA-DEX group.

This was surprising as SREBP1c is generally associated with VLDL-TG secretion[362–365]. We cannot explain how downregulation of hepatic SREBP1c relates to the hyperlipidemic effects of NTS BSA-DEX, thus more research is warranted. Since plasma FFAs were also increased in the BSA-DEX group, we next assessed lipolytic enzymes in WAT tissue. Surprisingly, we did not find any change in pHSL:HSL levels in this group, as was observed with NTS DEX. Instead, we found ATGL levels upregulated in the NTS BSA-DEX animals, further suggesting that NTS DEX and NTS BSA-DEX mediate their lipostimulatory effects through different mechanisms in WAT.

6.4.3 Similarities and differences between NTS DEX and NTS BSA-DEX effects with different manipulations.

Infusing either DEX or BSA-DEX into the NTS, we found differences between both compounds during our *in vivo* experiments. For example, knocking down NTS GR protein levels, or antagonizing Hsp90, negated NTS DEX effects on lipid metabolism, whereas these manipulations did not alter NTS BSA-DEX effects, revealing differential mechanisms likely specifically related to the receptors for DEX and BSA-DEX. These findings were interesting since it is believed that DEX can act on either the cGR and/or mGR[154,157,159,168]. Our data suggests that DEX does not interact with the mGRs, given all the differences observed between the BSA-DEX and DEX groups. For instance, if DEX was able to activate the NTS mGRs to stimulate VLDL-TG secretion, it's lipostimulatory effects would not have been blocked with Hsp90 blockade, similar to how co-infusing a Hsp90 inhibitor did not negate the NTS BSA-DEX hyperlipidemic effects. Also, we would not have found any differences in our molecular analyses between DEX and BSA-DEX if DEX was able to stimulate mGRs. In support of this, Strehl et al. performed *in vitro* tests on HEK 293T cells and showed that applying BSA-DEX to the cells induced MAPK activation, whereas DEX treatment did not[263]. Data from an ongoing project in our laboratory that investigates the effects of NTS GCs on modulating hepatic insulin sensitivity also suggests that DEX is unlikely to interact with mGRs[366]. In agreement with these results, Nahar et al. investigated the binding affinities of GCs to either the membrane GRs versus the cytosolic GRs[335]. Their data showed that DEX had a 25- and a 21-fold higher K_d for membrane binding compared to cytoplasmic binding in hypothalamic membrane fractions of mice and rats,

respectively[335]. The same trend was also seen with CORT, where CORT had a 4-fold (mouse) and 11-fold (rat) higher K_d for membrane binding compared to cytoplasmic binding in hypothalamic membrane fractions[335]. Given that the higher the dissociation constant (K_d) is, the lower the binding affinity is, these results suggest that endogenous or synthetic GCs preferentially bind to intracellular components (e.g. cGRs) compared to membrane components (e.g. mGRs). Therefore, there is a growing body of evidence that indicates DEX may not be able to trigger mGR signaling, or at least it prefers binding the cGR, however further research is needed.

6.5 Potential identity of the mGR.

The identity of the mGR is yet to be elucidated; both the genetic and protein structures of this receptor remain a mystery. There has been three major hypotheses for the identity of the mGR: 1) it is a GPCR[150,153–158]; 2) it is the cGR interacting with cellular proteins to initiate signaling cascades prior to nuclear translocation[159–164]; 3) it is not a receptor itself, but rather GCs intercalating themselves in the membrane and altering the physicochemical properties of the plasma membrane to trigger signaling pathways[109,367,368]. Starting with the first of these three hypotheses, there are many studies that support the mGR being a GPCR. Though the papers did not specifically identify a G-protein, it was found that using GPCR inhibitors was able to negate GC effects[153–155,157,158,347]. For example, Malcher-Lopes and colleagues revealed that treating cultured hypothalamic neurons with GCs rapidly reduces their firing, however this can be negated by administering antibodies targeting the $G\alpha_s$-subunit, and this was further supported by Rp-CAMPs (PKA inhibitor) treatment also blocking the GC effects[157]. Furthermore, other studies showed that BSA-DEX can suppress the firing of pyramidal neurons from amygdala slices; however, direct intracellular application of DEX had no effect[153]. Thus, although there is evidence to support that mGRs may work through a GPCR, no study has been able to purify and determine its identity as of yet.

The second hypothesis is that the 'mGR' is the cGR, *per se*, activating signaling pathways. It has been reported that the cytosolic glucocorticoid receptors can associate with caveolin[161]. This is a protein which is required for the formation of caveolae

(invaginations in the plasma membrane), a type of lipid raft. One important role that plasma membrane lipid rafts do is signal transduction by recruiting signaling proteins[369]. Thus, it is feasible that some rapid nongenomic effects mediated by glucocorticoid receptors are dependent on the cytosolic receptor to interact with caveolae lipid rafts. Further supporting this hypothesis, is a study done by Lu et al. on the estrogen receptor[370]. Estrogen receptors are another steroid receptor that also mediate nongenomic actions[172–174]. It was discovered that activated cytosolic estrogen receptors (cERs) bind to caveolin on the membrane and lead to the activation of ERK upon posttranslational palmitoylation, whereas mutant cERs that cannot undergo palmitoylation could not bind the membrane and activate ERK, but were still able to translocate to the nucleus and mediate gene transcription[371,372]. Importantly, this palmitoylation event of cER occurred at a conserved amino acid sequence found in other steroid receptors, including glucocorticoid receptors[371]. A third study supporting this hypothesis was done by Oppong and co., where they showed that activated cGRs first migrate towards the plasma membrane and increase the phosphorylation of ERK, before translocating into the nucleus to mediate genomic effects[159]. Overall, these results suggest that the cGR participates in nongenomic signaling of GCs prior to proceeding with genomic mechanisms.

Finally, the last hypothesis for what the 'mGR' might be is not an actual receptor. It has been suggested that GCs can intercalate into the plasma membrane and alter its physicochemical properties. In detail, due to GCs' hydrophobic structure and properties, they embed themselves between the phospholipid bilayer and affect the membrane fluidity, which in turn alters the functions of membrane-associated proteins[109,367,368]. Signaling from alterations in membrane fluidity has been previously reported regarding changes in membrane cholesterol levels[373,374]. Dindia et al. reported that treating trout liver cells with cortisol increased membrane fluidity, but not when treating them with estradiol or testosterone, suggesting a GC-specific effect, rather than steroid-specific effects[367]. These changes in membrane physicochemical properties were associated with activation of downstream signaling mediators: PKA, PKC, and AKT in response to cortisol-induced increased membrane fluidity[367]. These studies have helped us to appreciate the complexity of glucocorticoid action and extended the traditional view of

cytosolic GRs only. Of note, these is still a gap in our knowledge of how mGRs may regulate metabolism. Taking together the knowledge gained from the studies that corroborate these three hypotheses, our present data does not support the second hypothesis where the cGR is involved with mediating the nongenomic signaling. This is because we see an effect with BSA-DEX in the presence of Hsp90 inhibition (an important chaperone for the cGR). As for the first and third hypotheses, our data does not necessarily disprove either as of right now. For future tests, we could co-administer a G-protein antagonist alongside BSA-DEX to directly test the first hypothesis of whether BSA-DEX signals via a GPCR.

When we administered BSA-DEX into the NTS alongside an inhibitor of Hsp90, the effects of BSA-DEX to stimulate hyperlipidemia persisted, implying that mGRs work through a Hsp90-independent mechanism. To the best of our knowledge, this was the first study that looked at Hsp90 requirement for BSA-DEX effects. In line with our results, two other studies that investigated nongenomic GC signaling also reported that Hsp90 was not required[161,163]. To illustrate, *in vitro* analyses showed that dexamethasone treatment rapidly increased the phosphorylation of Akt, and this effect remained after Hsp90 inhibition[161]. In brief, there is now both *in vivo* and *in vitro* data that suggest mGRs do not require Hsp90.

One of our interesting findings was that GR shRNA injected into the NTS (which we confirmed was able to knockdown GRs and negate DEX effects) could not reverse NTS BSA-DEX's ability to trigger VLDL-TG secretion. This data implies that the genetic origin of the mGR may differ from that of the cGR. In contrast to our data, a previous report showed that various GR shRNA sequences targeting different exons was able to knockdown the levels on mGRs in HEK 293T cells as determined with an anti-GR antibody via flow cytometry with liposome-based immunofluorescence amplification[263]. This study concluded that cGRs and mGRs originate from the same gene and that posttranslational modifications allow the cGR to interact with the plasma membrane[263]. Furthermore, work which report the presence of mGRs on plasma membranes all use general anti-GR antibodies[160,263,335,375], and all these studies conclude that there is high sequence homology between the mGR and cGR, supporting that both receptors come

from the same gene. In addition, no reports have indicated that the GR protein sequence contains a transmembrane domain to allow the GR to insert in the plasma membrane[160,263]. This suggests that the mGR could be the cGR interacting with the membrane directly (potentially via posttranslational palmitoylation). Overall, the genetic background and protein identity of the mGR remains unresolved and further investigation is warranted.

Chapter 7: General Discussion

7.1 Synopsis

Glucocorticoids are known to regulate metabolism via their direct actions on GRs in peripheral tissues (e.g. liver, adipose)[189–191], but they can also modulate peripheral metabolism through central hypothalamic mechanisms[237,238,240]. The NTS in the hindbrain has emerged as another brain region that can also regulate metabolism[209,223,250,253], but there remains a gap in literature as to whether GCs can regulate metabolism via the NTS. In the present thesis, we investigated the importance of GC signaling in the hindbrain of SD rats to regulate hepatic VLDL-TG secretion. Specifically, we tested two different types of GRs in the NTS, the cGR and mGR, and their roles in lipid metabolism. Our results revealed novel mechanisms in which central GC action can modulate hepatic VLDL-TG, and overall plasma TGs (Figure 7.1).

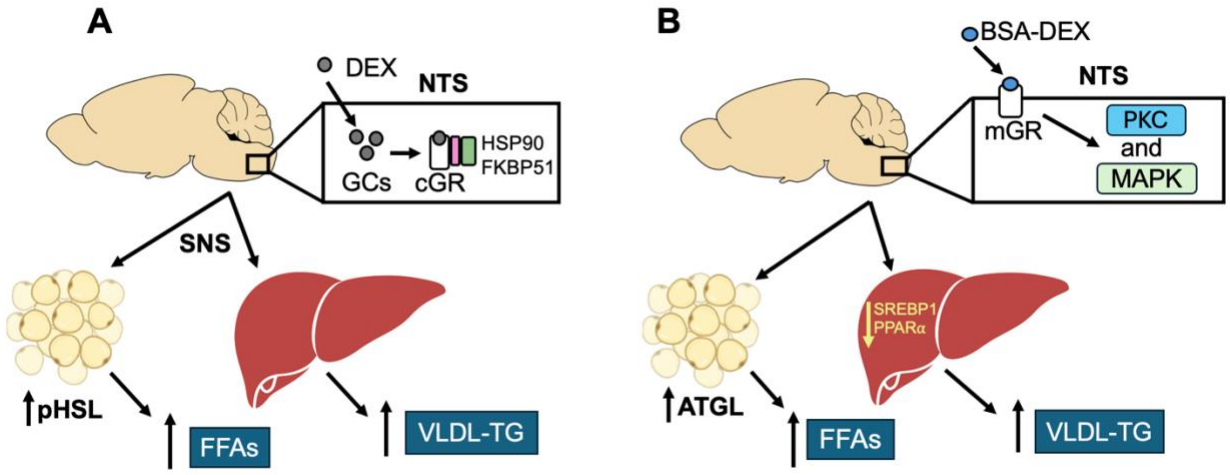

Figure 7.1: Summary of Thesis Results. A) NTS DEX stimulates hepatic VLDL-TG secretion via NTS cGRs and increased sympathetic outflow. Adipose tissue lipolysis is also likely increased due to greater pHSL levels and elevated plasma FFAs. **B)** BSA-DEX infused into the NTS interacts with NTS mGRs to trigger a PKC and MAPK-dependent pathway in the NTS to stimulate VLDL secretion from the liver. While hepatic expression of SREBP1 and PPARα was reduced with NTS BSA-DEX treatment, ATGL levels were increased in the adipose tissue likely contributing to the greater plasma FFAs also observed in these animals.

7.2 Future Directions for Aim 1

7.2.1 Further confirmation for the requirement for the sympathetic nervous system for NTS GC hyperlipidemic effects.

Despite the finding that pharmacological inhibition of the SNS negated the lipostimulatory effects of NTS GC action, additional investigation is needed to delineate the peripheral mechanism for the changes in VLDL-TG secretion, which would require knowing whether the liver or WAT or both, require sympathetic innervation to mediate the effects of NTS GCs. Our data suggests there is enhanced sympathetic tone in the WAT to stimulate lipolysis as i.v. administration of SNSi reversed the NTS GC-induced increase in pHSL and plasma FFAs. Measuring local norepinephrine (NE) levels in WAT tissue would support this hypothesis, as differences in local NE is indicative of changes to sympathetic innervation[225,376]. Other studies investigated the role of GCs in the ARC to reduce liver insulin sensitivity highlighted the requirement for the hepatic sympathetic branch[243]. Similarly, ICV NPY's effects to stimulate VLDL-TG secretion were also elicited by direct sympathetic innervation to the liver[225]. It is therefore possible that SNS innervation to the liver may also play a role in our study, and future studies will analyze whether severing the hepatic sympathetic branch alters NTS GC lipostimulatory effects.

7.2.2 Test whether NTS GCs contribute to triglyceride hypersecretion in high fat diet animals.

So far, we have only tested how GCs acting in the NTS regulate VLDL-TG secretion in regular chow-fed animals. The next steps are to investigate if NTS GCs contribute to hepatic TG release in a pre-obese model. A 3-day HFD has previously been reported to induce mild hyperglycemia and insulinemia, as well as hypertriglyceridemia and elevated VLDL-TG, without inducing obesity[209,214,238,240,253,254,256]. A 3-day HFD also significantly increases plasma CORT in rats[238]. Recall that excessive GC action is associated with obesity and diabetes[110,114,118]. Interestingly, previous work that investigated the effects of MBH GCs on VLDL-TG secretion revealed that 3-day HFD-fed rats had increased plasma TG and hepatic VLDL-TG release, but chronic GR knockdown in the MBH negated this effect[240]. It was also found that a 3-day HFD induced hepatic insulin resistance, although MIF application to the MBH or MBH GR knockdown reversed this[238]. Thus, future

investigation on the effects of NTS GCs to modulate lipid metabolism under a 3-day HFD are warranted.

7.3 Limitations of Aim 1

7.3.1 VLDL-TG may not be the only source for the increase in plasma TG.

Our results revealed that acute NTS GCs increase plasma TG under a 10-hour fast. Though majority of these plasma TGs are VLDL-TGs, a part of them may be chylomicron (CM)-TGs. CMs are generally released during the absorptive state, however it has been reported that delayed CMs can also be secreted under fasting conditions as well[377,378]. In fact, one study showed that acute elevation of plasma FFAs can trigger CM secretion under fasting conditons[378]. Recall we found that dexamethasone treatment in the NTS increases circulating FFAs, thus it is possible that CMs may contribute to the increase in plasma TG. To mitigate this limitation, we could perform the same *in vivo* TG secretion experiments in the fed state to assess whether NTS GCs alter CM production and secretion.

7.3.2 Lack of confirmation of FFA fluxes to the liver.

As described above, NTS GC's hyperlipidemic effects are possibly related to changes in circulating FFAs. The level of FFAs in the plasma represents the net effect of FFA release (via lipolysis) and uptake by peripheral tissues. Given that we found an upregulation of phosphorylated-HSL levels in WAT, and elevated plasma FFAs, we concluded that FFA release was increased. However, we hypothesize that these FFAs are also being taken up by the liver to be used for VLDL packaging. Although we do not have confirmation that FFA fluxes to the liver are altered with NTS GC action, we are planning on measuring acyl-CoA levels in liver tissue to shed light on this. Another important thing to consider with the measuring of acyl-CoAs is if uptake is increased, that does not necessarily mean that these acyl-CoAs are being used up to TG synthesis and overall VLDL production. It is possible that those acyl-CoAs are being shuttled to different biochemical pathways within the hepatocyte such as β-oxidation. Therefore, it would be also beneficial to measure plasma ketones as well to rule that possibility out,

since ketone levels in the plasma are proportional to the rate of mitochondrial β-oxidation[379].

7.3.3 Hsp90 inhibition.

To pharmacologically block the actions of Hsp90 *in vivo*, we used 17-AAG, which is a less toxic derivative of geldanamycin[380]. 17-AAG antagonizes Hsp90 by competitively binding to its ATP-binding site and inducing a conformational change in Hsp90 which results in its ubiquination and degradation by the proteasome[381]. Despite being less toxic than galdanamycin, 17-AAG still possesses cytotoxic and pro-apoptotic properties[380–382]. Since we administer this inhibitor acutely however, and no behavioral or metabolic changes are observed with 17-AAG infusion alone, it is unlikely that cell death in the NTS is occurring or that 17-AAG toxicity is affecting our measured outcomes. Additionally, Hsp90 is one of the most abundant molecular chaperones in eukaryotes, and participates in numerous physiological pathways as a result of its involvement in protein folding, stability, and transport[383]. Due to its diverse actions, Hsp90 has also been associated with cancer[381], neurodegenerative diseases[384,385], obesity[316], and diabetes[313]. Thus, our Hsp90 inhibition may not have been specific to the GRs only, although both pharmacological and shRNA inhibition of Hsp90 blocked the effects of NTS DEX. Another limitation is that we are yet to confirm whether our Hsp90i worked, besides its effects to block NTS DEX. One test we could do is measure Hsp70 or Hsp40 levels in DVC tissue following NTS Hsp90i infusion, where the animals receiving the Hsp90i would be expected to have greater Hsp70 and Hsp40 levels compared to control. Once Hsp90 is blocked, it unbinds heat shock factor-1 which then enables this protein to upregulate the expression of Hsp70 and Hsp40[380]. Another method we employed to block Hsp90 action in the NTS *in vivo* is through the genetic loss-of-function technique using Hsp90 shRNA. Here, we induced a chronic, 2-week knockdown of Hsp90 protein in the NTS. Given the length of time which Hsp90 was knocked down, feasibly there could have been cell death that occurred in the NTS of these animals, however we have not assessed for this. Measuring the plasma levels of lactate dehydrogenase, a biomarker for cell death[386], can be used to see if cell death may be occurring in our Hsp90 shRNA-infused animals. Finally, we were unsuccessful at confirming whether the knockdown of Hsp90 indeed occurred. Possibly, this was due

to us analyzing the DVC wedge which might have diluted the effect, as our virus injections are very localized to the NTS with minimal spread. It is worth mentioning though that both pharmacological inhibition and knockdown of Hsp90 negated the NTS GC effects to increase VLDL-TG suggesting Hsp90 was indeed blocked, but confirmation of decreased Hsp90 specifically in the NTS may be warranted.

7.3.4 Sex difference.

In the present study, our *in vivo* experiments were exclusively done on male Sprague Dawley rats. We cannot rule out the potential involvement of sex hormones in the regulation of VLDL-TG secretion. It is known that estrogen, the major sex hormone in females, can regulate lipid metabolism[387,388]. For instance, women have higher rates of VLDL-TG secretion with greater clearance of these lipoproteins and estrogen signaling in the liver was shown to promote fatty acid oxidation[387]. Furthermore, estrogen acting on its receptor in various brain regions (e.g. hypothalamus and NTS) can control metabolism[389]. When knocking out the estrogen receptors in the brain's hypothalamus, female mice were shown to develop obesity and hyperphagia[390]. Another study which investigated the role of estrogen receptors in the NTS in female rats revealed these receptors play a role in regulating food intake[391]. Thus, it is possible that the hormonal differences between females and males could impact the metabolic effects induced by glucocorticoid signaling in the NTS.

7.4 Future Directions for Aim 2

7.4.1 Further confirmation for the requirement of PKC and/or MAPK for NTS BSA-DEX hyperlipidemic effects.

Our *in vivo* data revealed that NTS BSA-DEX triggers hepatic lipid secretion via NTS PKC and MAPK signaling. Future experiments will test the requirements for both of these kinases. Studies will include direct stimulation, as well as knockdown of PKC or MAPK in the NTS. We will also test whether PKC and MAPK are arranged in a series fashion, and if so, which kinase is upstream or downstream of one another. Equally, we would like to determine the specific isoform of PKC which leads to the hyperlipidemic

effects. The PKCθ isoform has been extensively shown to be involved in metabolic disorders[392–396].

7.4.2 More tests to support the validity of our BSA-DEX and further probe whether DEX can activate the membrane glucocorticoid receptor.

One way we can show our BSA-DEX compound is not inducing genomic changes due to 'free' DEX, is by co-administering a gene transcription inhibitor (e.g. actinomycin D) or a protein synthesis inhibitor (e.g. cycloheximide) with BSA-DEX. This would theoretically negate any 'free' DEX that may arise from unbinding BSA. In detail, assuming that 'free' DEX will cross the membrane and activate cGRs, blocking gene transcription or protein synthesis would negate the effects of any 'free' DEX. As discussed above, a luciferase reporter assay is another analysis that could be performed to see if our BSA-DEX is not entering inside the cells. Finally, our findings suggest that DEX cannot interact with mGRs. One other test that could be conducted is to administer both DEX and BSA-DEX in the NTS at the same time to see whether that can increase VLDL-TG even more than either compound by itself. Although, this would only work as long as either compound does not max out VLDL-TG secretion when infused alone.

7.5 Limitations for Aim 2

7.5.1 Insufficient understanding of membrane glucocorticoid receptors.

A major limitation in our study is the lack of understanding and knowledge on this putative mGR. One reason for this is the contrasting and inconsistent data reported in literature, as highlighted throughout this thesis. Another example is with mifepristone, a GR antagonist, where some papers report that it can block mGR effects[164,168], whereas other studies show that it does not[150,153,368]. Nonetheless, it is generally accepted that GRs can signal through nongenomic mechanisms. Although the data we presented in this thesis also had inconsistencies with other literature reports, we were able to show that mGR signaling in the NTS could contribute to GC-induced dyslipidemia.

Along the same line is a lack of proper tools to selectively block just the mGR or cGR. This could be achieved once the identity of the mGR is known. Being able to

specifically block one or the other could allow us to better study the contributions of that receptor to mediate GC actions on lipid metabolism. This could consequently provide the groundwork for future investigations into how GC-mediated actions are affected in metabolic disease conditions where elevated GCs contribute to dysregulated lipid metabolism.

7.5.2 BSA-DEX compound.

Another reason why the studies on the mGR are limited, is because of the lack of reliable methods to discriminate between the activation of the mGR and cGR. In this study, we use commercially available BSA-DEX, and although this compound was found to have a small percentage (4.5%) of 'free' DEX associated with the BSA moiety which is believed to be biologically unavailable[334], one wonders if traces of DEX unbound to BSA may permeate the cell and act on cGRs. In addition to our current control groups, another control could be a BSA alone infusate at the same concentration of BSA that is administered to our BSA-DEX group. Other *in vitro* studies have shown that BSA administration has no effect, however[160,397]. Furthermore, parallel *in vivo* studies in our laboratory demonstrate that whereas NTS BSA-DEX infusion induces hepatic insulin resistance and inhibits the suppressive actions of insulin on glucose production during hyperinsulinemic-euglycemic clamp experiments, NTS BSA administration *per se* at the same concentration as that which is administered into the NTS in our BSA-DEX infusions has no effect on whole-body insulin sensitivity or glucose metabolism as assessed in hyperinsulinemic-euglycemic clamp experiments compared to NTS vehicle administration. Although NTS BSA was observed to have vehicle-like effects on glucose metabolism, future studies to confirm this in VLDL-secretion experiments is warranted, given that compounds within the NTS may differentially affect glucose and lipid metabolism.

7.5.3 No confirmation for kinase or Hsp90 inhibition.

We tested the requirement of three kinases in the NTS for the lipostimulatory of effects of BSA-DEX. While both PKC and MAPK inhibition showed an effect to block BSA-DEX, we have not directly confirmed that our inhibitors specifically inhibited the kinase activity of these kinases. Commercially available kits exist to test the activity of

these kinases. We also tested the requirement of PKA but found that Rp-CAMPs co-infusion had no effect, again, we did not assess whether our PKA inhibitor worked. As mentioned, our laboratory has previously used the same NTS administration (dose and time) of Rp-CAMPs and confirmed its efficacy to block the actions of a different hormone[253], although we have yet to do so for this project. PKA activity kit assays could be used to mitigate this limitation. Similar to Aim 1, Hsp90 inhibition has not been confirmed, though measuring the levels of Hsp70 or Hsp40 in the DVC wedges via PCR or western blotting may help to provide validation of Hsp90 inhibition. Performing this is crucial as our results indicated that Hsp90 blockade did not negate NTS BSA-DEX effects.

7.6 Conclusion

In summary, we report for the first time that hindbrain GC action triggers hepatic lipid secretion mediated via both NTS cGRs or mGRs. Additionally, we demonstrate that mGRs require both PKC and MAPK downstream signaling to regulate lipid metabolism in the liver. We also provide evidence to suggest that mGRs may arise from a different gene than the canonical GR, as well as that these novel receptors work through Hsp90-indepedent pathways. Given that excessive GC levels and/or actions are linked with metabolic diseases, including states of dyslipidemia[110,114,115,118], this research sheds new information about the potential mechanisms involved. The pathways we elucidated in this thesis could potentially provide targets for future therapeutics to look at when developing therapies for dyslipidemia.

References

1. Obesity and overweight. https://www.who.int/news-room/fact-sheets/detail/obesity-and-overweight.
2. Diabetes. https://www.who.int/health-topics/diabetes.
3. Diabetes in Canada - Diabetes Canada. *DiabetesCanadaWebsite* https://www.diabetes.ca/advocacy---policies/advocacy-reports/national-and-provincial-backgrounders/diabetes-in-canada.
4. The top 10 causes of death. https://www.who.int/news-room/fact-sheets/detail/the-top-10-causes-of-death.
5. Ong, K. L. *et al.* Global, regional, and national burden of diabetes from 1990 to 2021, with projections of prevalence to 2050: a systematic analysis for the Global Burden of Disease Study 2021. *The Lancet* **402**, 203–234 (2023).
6. Collaborators, T. G. 2015 O. Health Effects of Overweight and Obesity in 195 Countries over 25 Years. *N. Engl. J. Med.* **377**, 13–27 (2017).
7. Cusi, K. Nonalcoholic Fatty Liver Disease in Diabetes: A Call to Action. *Diabetes Spectr.* **37**, 5–7 (2024).
8. Cardiovascular diseases (CVDs). https://www.who.int/news-room/fact-sheets/detail/cardiovascular-diseases-(cvds).
9. Government of Canada, S. C. An overview of weight and height measurements on World Obesity Day. https://www.statcan.gc.ca/o1/en/plus/5742-overview-weight-and-height-measurements-world-obesity-day (2024).
10. Understanding Type 1 Diabetes | ADA. https://diabetes.org/about-diabetes/type-1.
11. Home *et al.* IDF Diabetes Atlas. https://diabetesatlas.org/.
12. Bommer, C. *et al.* Global Economic Burden of Diabetes in Adults: Projections From 2015 to 2030. *Diabetes Care* **41**, 963–970 (2018).
13. Singla, P., Bardoloi, A. & Parkash, A. A. Metabolic effects of obesity: A review. *World J. Diabetes* **1**, 76–88 (2010).
14. Shoelson, S. E., Herrero, L. & Naaz, A. Obesity, Inflammation, and Insulin Resistance. *Gastroenterology* **132**, 2169–2180 (2007).

15. Scherer, P. E. Adipose Tissue: From Lipid Storage Compartment to Endocrine Organ. *Diabetes* **55**, 1537–1545 (2006).
16. Alves-Bezerra, M. & Cohen, D. E. Triglyceride metabolism in the liver. *Compr. Physiol.* **8**, 1–8 (2017).
17. Cai, D. *et al.* Local and systemic insulin resistance resulting from hepatic activation of IKK-β and NF-κB. *Nat. Med.* **11**, 183–190 (2005).
18. Hotamisligil, G. S. *et al.* IRS-1-Mediated Inhibition of Insulin Receptor Tyrosine Kinase Activity in TNF-α- and Obesity-Induced Insulin Resistance. *Science* **271**, 665–670 (1996).
19. Klover, P. J., Clementi, A. H. & Mooney, R. A. Interleukin-6 Depletion Selectively Improves Hepatic Insulin Action in Obesity. *Endocrinology* **146**, 3417–3427 (2005).
20. Wilcox, G. Insulin and Insulin Resistance. *Clin. Biochem. Rev.* **26**, 19–39 (2005).
21. Petersen, M. C. & Shulman, G. I. Mechanisms of Insulin Action and Insulin Resistance. *Physiol. Rev.* **98**, 2133–2223 (2018).
22. Spiller, S., Blüher, M. & Hoffmann, R. Plasma levels of free fatty acids correlate with type 2 diabetes mellitus. *Diabetes Obes. Metab.* **20**, 2661–2669 (2018).
23. Henderson, G. C. Plasma Free Fatty Acid Concentration as a Modifiable Risk Factor for Metabolic Disease. *Nutrients* **13**, 2590 (2021).
24. I. S. Sobczak, A., A. Blindauer, C. & J. Stewart, A. Changes in Plasma Free Fatty Acids Associated with Type-2 Diabetes. *Nutrients* **11**, 2022 (2019).
25. Boden, G. Obesity and Free Fatty Acids. *Endocrinol. Metab. Clin. North Am.* **37**, 635–646 (2008).
26. Lewis, G. F., Uffelman, K. D., Szeto, L. W., Weller, B. & Steiner, G. Interaction between free fatty acids and insulin in the acute control of very low density lipoprotein production in humans. *J. Clin. Invest.* **95**, 158–166 (1995).
27. Barthel, A. & Schmoll, D. Novel concepts in insulin regulation of hepatic gluconeogenesis. *Am. J. Physiol.-Endocrinol. Metab.* **285**, E685–E692 (2003).
28. Hatting, M., Tavares, C. D. J., Sharabi, K., Rines, A. K. & Puigserver, P. Insulin regulation of gluconeogenesis. *Ann. N. Y. Acad. Sci.* **1411**, 21–35 (2018).
29. Xu, X., So, J.-S., Park, J.-G. & Lee, A.-H. Transcriptional Control of Hepatic Lipid Metabolism by SREBP and ChREBP. *Semin. Liver Dis.* **33**, 301–311 (2013).

30. Denechaud, P.-D., Dentin, R., Girard, J. & Postic, C. Role of ChREBP in hepatic steatosis and insulin resistance. *FEBS Lett.* **582**, 68–73 (2008).
31. Eroglu, N., Yerlikaya, F. H., Onmaz, D. E. & Colakoglu, M. C. Role of ChREBP and SREBP-1c in gestational diabetes: two key players in glucose and lipid metabolism. *Int. J. Diabetes Dev. Ctries.* **43**, 587–591 (2023).
32. Iqbal, J. & Hussain, M. M. Intestinal lipid absorption. *Am. J. Physiol.-Endocrinol. Metab.* **296**, E1183–E1194 (2009).
33. Jackson, A. D. & McLaughlin, J. Digestion and absorption. *Surg. Oxf.* **27**, 231–236 (2009).
34. Tso, P. Gastrointestinal Digestion and Absorption of Lipid. in *Advances in Lipid Research* (eds. Paoletti, R. & Kritchevsky, D.) vol. 21 143–186 (Elsevier, 1985).
35. Golding, M. & Wooster, T. J. The influence of emulsion structure and stability on lipid digestion. *Curr. Opin. Colloid Interface Sci.* **15**, 90–101 (2010).
36. Singh, H., Ye, A. & Horne, D. Structuring food emulsions in the gastrointestinal tract to modify lipid digestion. *Prog. Lipid Res.* **48**, 92–100 (2009).
37. Rehfeld, J. F. Cholecystokinin. *Best Pract. Res. Clin. Endocrinol. Metab.* **18**, 569–586 (2004).
38. Niot, I., Poirier, H., Tran, T. T. T. & Besnard, P. Intestinal absorption of long-chain fatty acids: Evidence and uncertainties. *Prog. Lipid Res.* **48**, 101–115 (2009).
39. Cifarelli, V. & Abumrad, N. A. Intestinal CD36 and Other Key Proteins of Lipid Utilization: Role in Absorption and Gut Homeostasis. *Compr. Physiol.* **8**, 493–507 (2018).
40. Buttet, M. *et al.* From fatty-acid sensing to chylomicron synthesis: Role of intestinal lipid-binding proteins. *Biochimie* **96**, 37–47 (2014).
41. Gugliucci, A. The chylomicron saga: time to focus on postprandial metabolism. *Front. Endocrinol.* **14**, (2024).
42. Xiao, C. & Lewis, G. F. Regulation of chylomicron production in humans. *Biochim. Biophys. Acta BBA - Mol. Cell Biol. Lipids* **1821**, 736–746 (2012).
43. Sanders, F. W. B. & Griffin, J. L. De novo lipogenesis in the liver in health and disease: more than just a shunting yard for glucose. *Biol. Rev.* **91**, 452–468 (2016).

44. Song, Z., Xiaoli, A. M. & Yang, F. Regulation and Metabolic Significance of De Novo Lipogenesis in Adipose Tissues. *Nutrients* **10**, 1383 (2018).
45. Ameer, F., Scandiuzzi, L., Hasnain, S., Kalbacher, H. & Zaidi, N. *De novo* lipogenesis in health and disease. *Metabolism* **63**, 895–902 (2014).
46. Softic, S., Cohen, D. E. & Kahn, C. R. Role of Dietary Fructose and Hepatic De Novo Lipogenesis in Fatty Liver Disease. *Dig. Dis. Sci.* **61**, 1282–1293 (2016).
47. Moore, J. B., Gunn, P. J. & Fielding, B. A. The Role of Dietary Sugars and De novo Lipogenesis in Non-Alcoholic Fatty Liver Disease. *Nutrients* **6**, 5679–5703 (2014).
48. Richter, E. A. & Hargreaves, M. Exercise, GLUT4, and Skeletal Muscle Glucose Uptake. *Physiol. Rev.* **93**, 993–1017 (2013).
49. Zangari, J., Petrelli, F., Maillot, B. & Martinou, J.-C. The Multifaceted Pyruvate Metabolism: Role of the Mitochondrial Pyruvate Carrier. *Biomolecules* **10**, 1068 (2020).
50. Ng, F. & Tang, B. L. Pyruvate dehydrogenase complex (PDC) export from the mitochondrial matrix. *Mol. Membr. Biol.* **31**, 207–210 (2014).
51. Los, D. A. & Murata, N. Structure and expression of fatty acid desaturases. *Biochim. Biophys. Acta BBA - Lipids Lipid Metab.* **1394**, 3–15 (1998).
52. Jakobsson, A., Westerberg, R. & Jacobsson, A. Fatty acid elongases in mammals: Their regulation and roles in metabolism. *Prog. Lipid Res.* **45**, 237–249 (2006).
53. Piccinin, E. *et al.* Role of Oleic Acid in the Gut-Liver Axis: From Diet to the Regulation of Its Synthesis via Stearoyl-CoA Desaturase 1 (SCD1). *Nutrients* **11**, 2283 (2019).
54. Watkins, P. A. Very-long-chain Acyl-CoA Synthetases *. *J. Biol. Chem.* **283**, 1773–1777 (2008).
55. Soupene, E. & Kuypers, F. A. Mammalian Long-Chain Acyl-CoA Synthetases. *Exp. Biol. Med.* **233**, 507–521 (2008).
56. Hellerstein, M. De novo lipogenesis in humans: metabolic and regulatory aspects. *Eur. J. Clin. Nutr.* **53**, s53–s65 (1999).
57. Smith, U. & Kahn, B. B. Adipose tissue regulates insulin sensitivity: role of adipogenesis, de novo lipogenesis and novel lipids. *J. Intern. Med.* **280**, 465–475 (2016).

58. Solinas, G., Borén, J. & Dulloo, A. G. De novo lipogenesis in metabolic homeostasis: More friend than foe? *Mol. Metab.* **4**, 367–377 (2015).
59. Stone, S. J. Mechanisms of intestinal triacylglycerol synthesis. *Biochim. Biophys. Acta BBA - Mol. Cell Biol. Lipids* **1867**, 159151 (2022).
60. Lee, J. & Ridgway, N. D. Substrate channeling in the glycerol-3-phosphate pathway regulates the synthesis, storage and secretion of glycerolipids. *Biochim. Biophys. Acta BBA - Mol. Cell Biol. Lipids* **1865**, 158438 (2020).
61. Takeuchi, K. & Reue, K. Biochemistry, physiology, and genetics of GPAT, AGPAT, and lipin enzymes in triglyceride synthesis. *Am. J. Physiol.-Endocrinol. Metab.* **296**, E1195–E1209 (2009).
62. Kawano, Y. & Cohen, D. E. Mechanisms of hepatic triglyceride accumulation in non-alcoholic fatty liver disease. *J. Gastroenterol.* **48**, 434–441 (2013).
63. Nguyen, P. *et al.* Liver lipid metabolism. *J. Anim. Physiol. Anim. Nutr.* **92**, 272–283 (2008).
64. Lamiquiz-Moneo, I. *et al.* Glycerol kinase deficiency in adults: Description of 4 novel cases, systematic review and development of a clinical diagnostic score. *Atherosclerosis* **315**, 24–32 (2020).
65. Watford, M. Functional Glycerol Kinase Activity and the Possibility of a Major Role for Glyceroneogenesis in Mammalian Skeletal Muscle. *Nutr. Rev.* **58**, 145–148 (2009).
66. Zammit, V. A. Hepatic triacylglycerol synthesis and secretion: DGAT2 as the link between glycaemia and triglyceridaemia. *Biochem. J.* **451**, 1–12 (2013).
67. Bhatt-Wessel, B., Jordan, T. W., Miller, J. H. & Peng, L. Role of DGAT enzymes in triacylglycerol metabolism. *Arch. Biochem. Biophys.* **655**, 1–11 (2018).
68. Yen, C.-L. E., Nelson, D. W. & Yen, M.-I. Intestinal triacylglycerol synthesis in fat absorption and systemic energy metabolism. *J. Lipid Res.* **56**, 489–501 (2015).
69. Cases, S. *et al.* Cloning of DGAT2, a Second Mammalian Diacylglycerol Acyltransferase, and Related Family Members *. *J. Biol. Chem.* **276**, 38870–38876 (2001).

70. DeVita, R. J. & Pinto, S. Current Status of the Research and Development of Diacylglycerol *O* -Acyltransferase 1 (DGAT1) Inhibitors: Miniperspective. *J. Med. Chem.* **56**, 9820–9825 (2013).
71. Turkish, A. & Sturley, S. L. Regulation of Triglyceride Metabolism. I. Eukaryotic neutral lipid synthesis: “Many ways to skin ACAT or a DGAT”. *Am. J. Physiol.-Gastrointest. Liver Physiol.* **292**, G953–G957 (2007).
72. Gluchowski, N. L., Becuwe, M., Walther, T. C. & Farese, R. V. Lipid droplets and liver disease: from basic biology to clinical implications. *Nat. Rev. Gastroenterol. Hepatol.* **14**, 343–355 (2017).
73. Borén, J., Taskinen, M.-R., Olofsson, S.-O. & Levin, M. Ectopic lipid storage and insulin resistance: a harmful relationship. *J. Intern. Med.* **274**, 25–40 (2013).
74. Reue, K. A Thematic Review Series: Lipid droplet storage and metabolism: from yeast to man. *J. Lipid Res.* **52**, 1865–1868 (2011).
75. Birsoy, K., Festuccia, W. T. & Laplante, M. A comparative perspective on lipid storage in animals. *J. Cell Sci.* **126**, 1541–1552 (2013).
76. Ohsaki, Y., Suzuki, M. & Fujimoto, T. Open Questions in Lipid Droplet Biology. *Chem. Biol.* **21**, 86–96 (2014).
77. Dolinsky, V. W., Gilham, D., Alam, M., Vance, D. E. & Lehner, R. Triacylglycerol hydrolase: role in intracellular lipid metabolism. *Cell. Mol. Life Sci.* **61**, (2004).
78. Quiroga, A. D. & Lehner, R. Liver triacylglycerol lipases. *Biochim. Biophys. Acta BBA - Mol. Cell Biol. Lipids* **1821**, 762–769 (2012).
79. Duncan, R. E., Ahmadian, M., Jaworski, K., Sarkadi-Nagy, E. & Sul, H. S. Regulation of Lipolysis in Adipocytes. *Annu. Rev. Nutr.* **27**, 79–101 (2007).
80. Tahri-Joutey, M. *et al.* Mechanisms Mediating the Regulation of Peroxisomal Fatty Acid Beta-Oxidation by PPARα. *Int. J. Mol. Sci.* **22**, 8969 (2021).
81. Houten, S. M. & Wanders, R. J. A. A general introduction to the biochemistry of mitochondrial fatty acid β-oxidation. *J. Inherit. Metab. Dis.* **33**, 469–477 (2010).
82. Houten, S. M., Violante, S., Ventura, F. V. & Wanders, R. J. A. The Biochemistry and Physiology of Mitochondrial Fatty Acid β-Oxidation and Its Genetic Disorders. *Annu. Rev. Physiol.* **78**, 23–44 (2016).

83. Abumrad, N. A. & Goldberg, I. J. CD36 actions in the heart: Lipids, calcium, inflammation, repair and more? *Biochim. Biophys. Acta BBA - Mol. Cell Biol. Lipids* **1861**, 1442–1449 (2016).
84. Kim, T. T. & Dyck, J. R. B. The role of CD36 in the regulation of myocardial lipid metabolism. *Biochim. Biophys. Acta BBA - Mol. Cell Biol. Lipids* **1861**, 1450–1460 (2016).
85. Nagendran, J., Waller, T. J. & Dyck, J. R. B. AMPK signalling and the control of substrate use in the heart. *Mol. Cell. Endocrinol.* **366**, 180–193 (2013).
86. Sundaram, M. & Yao, Z. Recent progress in understanding protein and lipid factors affecting hepatic VLDL assembly and secretion. *Nutr. Metab.* **7**, 35 (2010).
87. Kang, S. & Davis, R. A. Cholesterol and hepatic lipoprotein assembly and secretion. *Biochim. Biophys. Acta BBA - Mol. Cell Biol. Lipids* **1529**, 223–230 (2000).
88. Gibbons, G. F. Assembly and secretion of hepatic very-low-density lipoprotein. *Biochem. J.* **268**, 1–13 (1990).
89. Shelness, G. S. & Sellers, J. A. Very-low-density lipoprotein assembly and secretion. *Curr. Opin. Lipidol.* **12**, 151 (2001).
90. Olofsson, S.-O., Stillemark-Billton, P. & Asp, L. Intracellular Assembly of VLDL: Two Major Steps in Separate Cell Compartments. *Trends Cardiovasc. Med.* **10**, 338–345 (2000).
91. Mangat, R. *et al.* Chylomicron and apoB48 metabolism in the JCR:LA corpulent rat, a model for the metabolic syndrome. *Biochem. Soc. Trans.* **35**, 477–481 (2007).
92. Mansbach, C. M. & Siddiqi, S. A. The Biogenesis of Chylomicrons. *Annu. Rev. Physiol.* **72**, 315–333 (2010).
93. Sacks, F. M. The apolipoprotein story. *Atheroscler. Suppl.* **7**, 23–27 (2006).
94. Mahley, R. W., Innerarity, T. L., Rall, S. C. & Weisgraber, K. H. Plasma lipoproteins: apolipoprotein structure and function. *J. Lipid Res.* **25**, 1277–1294 (1984).
95. Hatters, D. M., Peters-Libeu, C. A. & Weisgraber, K. H. Apolipoprotein E structure: insights into function. *Trends Biochem. Sci.* **31**, 445–454 (2006).

96. Kei, A. A., Filippatos, T. D., Tsimihodimos, V. & Elisaf, M. S. A review of the role of apolipoprotein C-II in lipoprotein metabolism and cardiovascular disease. *Metabolism* **61**, 906–921 (2012).
97. Norata, G. D., Tsimikas, S., Pirillo, A. & Catapano, A. L. Apolipoprotein C-III: From Pathophysiology to Pharmacology. *Trends Pharmacol. Sci.* **36**, 675–687 (2015).
98. Lehner, R., Lian, J. & Quiroga, A. D. Lumenal Lipid Metabolism. *Arterioscler. Thromb. Vasc. Biol.* **32**, 1087–1093 (2012).
99. White, D. A., Bennett, A. J., Billett, M. A. & Salter, A. M. The assembly of triacylglycerol-rich lipoproteins: an essential role for the microsomal triacylglycerol transfer protein. *Br. J. Nutr.* **80**, 219–229 (1998).
100. Tiwari, S. & Siddiqi, S. A. Intracellular Trafficking and Secretion of VLDL. *Arterioscler. Thromb. Vasc. Biol.* **32**, 1079–1086 (2012).
101. Sirwi, A. & Hussain, M. M. Lipid transfer proteins in the assembly of apoB-containing lipoproteins. *J. Lipid Res.* **59**, 1094–1102 (2018).
102. Ye, J. *et al.* Cideb, an ER- and Lipid Droplet-Associated Protein, Mediates VLDL Lipidation and Maturation by Interacting with Apolipoprotein B. *Cell Metab.* **9**, 177–190 (2009).
103. Asp, L., Claesson, C., Borén, J. & Olofsson, S.-O. ADP-ribosylation Factor 1 and Its Activation of Phospholipase D Are Important for the Assembly of Very Low Density Lipoproteins *. *J. Biol. Chem.* **275**, 26285–26292 (2000).
104. Olofsson, S.-O. & Borèn, J. Apolipoprotein B: a clinically important apolipoprotein which assembles atherogenic lipoproteins and promotes the development of atherosclerosis. *J. Intern. Med.* **258**, 395–410 (2005).
105. Saponaro, C., Gaggini, M., Carli, F. & Gastaldelli, A. The Subtle Balance between Lipolysis and Lipogenesis: A Critical Point in Metabolic Homeostasis. *Nutrients* **7**, 9453–9474 (2015).
106. Angelier, F. & Wingfield, J. C. Importance of the glucocorticoid stress response in a changing world: Theory, hypotheses and perspectives. *Gen. Comp. Endocrinol.* **190**, 118–128 (2013).
107. Russell, G. & Lightman, S. The human stress response. *Nat. Rev. Endocrinol.* **15**, 525–534 (2019).

108. Frew, A. J. 86 - Glucocorticoids. in *Clinical Immunology (Fifth Edition)* (eds. Rich, R. R. et al.) 1165-1175.e1 (Elsevier, London, 2019). doi:10.1016/B978-0-7020-6896-6.00086-7.
109. Buttgereit, F. & Scheffold, A. Rapid glucocorticoid effects on immune cells. *Steroids* **67**, 529–534 (2002).
110. Fardet, L., Nazareth, I. & Petersen, I. Long-term systemic glucocorticoid therapy and weight gain: a population-based cohort study. *Rheumatology* **60**, 1502–1511 (2021).
111. Chan, E. D., Chan, M. M., Chan, M. M. & Marik, P. E. Use of glucocorticoids in the critical care setting: Science and clinical evidence. *Pharmacol. Ther.* **206**, 107428 (2020).
112. Buckley, L. & Humphrey, M. B. Glucocorticoid-Induced Osteoporosis. *N. Engl. J. Med.* **379**, 2547–2556 (2018).
113. Lukert, B. P. & Raisz, L. G. Glucocorticoid-Induced Osteoporosis: Pathogenesis and Management. *Ann. Intern. Med.* **112**, 352–364 (1990).
114. Oray, M., Samra, K. A., Ebrahimiadib, N., Meese, H. & Foster, C. S. Long-term side effects of glucocorticoids. *Expert Opin. Drug Saf.* (2016).
115. de Guia, R. M. Stress, glucocorticoid signaling pathway, and metabolic disorders. *Diabetes Metab. Syndr. Clin. Res. Rev.* **14**, 1273–1280 (2020).
116. Suh, S. & Park, M. K. Glucocorticoid-Induced Diabetes Mellitus: An Important but Overlooked Problem. *Endocrinol. Metab.* **32**, 180–189 (2017).
117. Liu, Y. *et al.* Increased Glucocorticoid Receptor and 11␣-Hydroxysteroid Dehydrogenase Type 1 Expression in Hepatocytes May Contribute to the Phenotype of Type 2 Diabetes in db/db Mice. **54**, (2005).
118. Liu, Y. *et al.* Reduction of hepatic glucocorticoid receptor and hexose-6-phosphate dehydrogenase expression ameliorates diet-induced obesity and insulin resistance in mice. (2008) doi:10.1677/JME-08-0004.
119. LeDoux, J. The amygdala. *Curr. Biol.* **17**, R868–R874 (2007).
120. Tafet, G. E. & Nemeroff, C. B. Pharmacological Treatment of Anxiety Disorders: The Role of the HPA Axis. *Front. Psychiatry* **11**, (2020).

121. Tsigos, C. & Chrousos, G. P. Hypothalamic–pituitary–adrenal axis, neuroendocrine factors and stress. *J. Psychosom. Res.* **53**, 865–871 (2002).
122. Rao, R. & Androulakis, I. P. The physiological significance of the circadian dynamics of the HPA axis: Interplay between circadian rhythms, allostasis and stress resilience. *Horm. Behav.* **110**, 77–89 (2019).
123. Stulnig, T. M. & Waldhäusl, W. 11β-Hydroxysteroid dehydrogenase Type 1 in obesity and Type 2 diabetes. *Diabetologia* **47**, 1–11 (2004).
124. White, P. C., Rogoff, D., McMillan, D. R. & Lavery, G. G. Hexose 6-phosphate dehydrogenase (H6PD) and corticosteroid metabolism. *Mol. Cell. Endocrinol.* **265–266**, 89–92 (2007).
125. Krozowski, Z. The 11β-hydroxysteroid dehydrogenases: functions and physiological effects. *Mol. Cell. Endocrinol.* **151**, 121–127 (1999).
126. Kalsbeek, A. *et al.* Circadian rhythms in the hypothalamo–pituitary–adrenal (HPA) axis. *Mol. Cell. Endocrinol.* **349**, 20–29 (2012).
127. Spiga, F. & Lightman, S. L. Dynamics of adrenal glucocorticoid steroidogenesis in health and disease. *Mol. Cell. Endocrinol.* **408**, 227–234 (2015).
128. Timmermans, S., Souffriau, J. & Libert, C. A General Introduction to Glucocorticoid Biology. *Front. Immunol.* **10**, (2019).
129. Vinson, G. p. Adrenocortical zonation and ACTH. *Microsc. Res. Tech.* **61**, 227–239 (2003).
130. Nicolaides, N. C., Willenberg, H. S., Bornstein, S. R. & Chrousos, G. P. Adrenal Cortex: Embryonic Development, Anatomy, Histology and Physiology. in *Endotext* (eds. Feingold, K. R. et al.) (MDText.com, Inc., South Dartmouth (MA), 2000).
131. Rodrigues, A. R., Almeida, H. & Gouveia, A. M. Intracellular signaling mechanisms of the melanocortin receptors: current state of the art. *Cell. Mol. Life Sci.* **72**, 1331–1345 (2015).
132. Stahn, C., Löwenberg, M., Hommes, D. W. & Buttgereit, F. Molecular mechanisms of glucocorticoid action and selective glucocorticoid receptor agonists. *Mol. Cell. Endocrinol.* **275**, 71–78 (2007).

133. Oakley, R. H. & Cidlowski, J. A. The biology of the glucocorticoid receptor: New signaling mechanisms in health and disease. *J. Allergy Clin. Immunol.* **132**, 1033–1044 (2013).
134. Vandevyver, S., Dejager, L. & Libert, C. Comprehensive Overview of the Structure and Regulation of the Glucocorticoid Receptor. *Endocr. Rev.* **35**, 671–693 (2014).
135. Heitzer, M. D., Wolf, I. M., Sanchez, E. R., Witchel, S. F. & DeFranco, D. B. Glucocorticoid receptor physiology. *Rev. Endocr. Metab. Disord.* **8**, 321–330 (2007).
136. Kadmiel, M. & Cidlowski, J. A. Glucocorticoid receptor signaling in health and disease. *Trends Pharmacol. Sci.* **34**, 518–530 (2013).
137. Schoneveld, O. J. L. M., Gaemers, I. C. & Lamers, W. H. Mechanisms of glucocorticoid signalling. *Biochim. Biophys. Acta BBA - Gene Struct. Expr.* **1680**, 114–128 (2004).
138. Segnitz, B. & Gehring, U. The Function of Steroid Hormone Receptors Is Inhibited by the hsp90-specific Compound Geldanamycin *. *J. Biol. Chem.* **272**, 18694–18701 (1997).
139. Agyeman, A. S. *et al.* Hsp90 Inhibition Results in Glucocorticoid Receptor Degradation in Association with Increased Sensitivity to Paclitaxel in Triple-Negative Breast Cancer. *Horm. Cancer* **7**, 114–126 (2016).
140. Davies, T. H., Ning, Y.-M. & Sánchez, E. R. A New First Step in Activation of Steroid Receptors: HORMONE-INDUCED SWITCHING OF FKBP51 AND FKBP52 IMMUNOPHILINS *. *J. Biol. Chem.* **277**, 4597–4600 (2002).
141. Binder, E. B. The role of FKBP5, a co-chaperone of the glucocorticoid receptor in the pathogenesis and therapy of affective and anxiety disorders. *Psychoneuroendocrinology* **34**, S186–S195 (2009).
142. Vandevyver, S., Dejager, L. & Libert, C. On the Trail of the Glucocorticoid Receptor: Into the Nucleus and Back. *Traffic* **13**, 364–374 (2012).
143. Häusl, A. S. *et al.* The co-chaperone Fkbp5 shapes the acute stress response in the paraventricular nucleus of the hypothalamus of male mice. *Mol. Psychiatry* **26**, 3060–3076 (2021).

144. Maiarù, M. *et al.* The stress regulator FKBP51 drives chronic pain by modulating spinal glucocorticoid signaling. *Sci. Transl. Med.* **8**, (2016).
145. Jääskeläinen, T., Makkonen, H. & Palvimo, J. J. Steroid up-regulation of FKBP51 and its role in hormone signaling. *Curr. Opin. Pharmacol.* **11**, 326–331 (2011).
146. Fries, G. R., Gassen, N. C. & Rein, T. The FKBP51 Glucocorticoid Receptor Co-Chaperone: Regulation, Function, and Implications in Health and Disease. *Int. J. Mol. Sci.* **18**, 2614 (2017).
147. Menke, A. *et al.* Dexamethasone Stimulated Gene Expression in Peripheral Blood is a Sensitive Marker for Glucocorticoid Receptor Resistance in Depressed Patients. *Neuropsychopharmacology* **37**, 1455–1464 (2012).
148. Stechschulte, L. A. & Sanchez, E. R. FKBP51 — a selective modulator of glucocorticoid and androgen sensitivity. *Curr. Opin. Pharmacol.* **11**, 332–337 (2011).
149. Vermeer, H., Hendriks-Stegeman, B. I., van der Burg, B., van Buul-Offers, S. C. & Jansen, M. Glucocorticoid-Induced Increase in Lymphocytic FKBP51 Messenger Ribonucleic Acid Expression: A Potential Marker for Glucocorticoid Sensitivity, Potency, and Bioavailability. *J. Clin. Endocrinol. Metab.* **88**, 277–284 (2003).
150. Di, S., Malcher-Lopes, R., Halmos, K. Cs. & Tasker, J. G. Nongenomic Glucocorticoid Inhibition via Endocannabinoid Release in the Hypothalamus: A Fast Feedback Mechanism. *J. Neurosci.* **23**, 4850–4857 (2003).
151. Straub, R. H. & Cutolo, M. Glucocorticoids and chronic inflammation. *Rheumatology* **55**, ii6–ii14 (2016).
152. Hinz, B. & Hirschelmann, R. Rapid Non-Genomic Feedback Effects of Glucocorticoids on CRF-Induced ACTH Secretion in Rats. *Pharm. Res.* **17**, 1273–1277 (2000).
153. Di, S. *et al.* Acute Stress Suppresses Synaptic Inhibition and Increases Anxiety via Endocannabinoid Release in the Basolateral Amygdala. *J. Neurosci.* **36**, 8461–8470 (2016).
154. Di, S., Maxson, M. M., Franco, A. & Tasker, J. G. Glucocorticoids Regulate Glutamate and GABA Synapse-Specific Retrograde Transmission via Divergent Nongenomic Signaling Pathways. *J. Neurosci.* **29**, 393–401 (2009).

155. Ffrench-Mullen, J. Cortisol inhibition of calcium currents in guinea pig hippocampal CA1 neurons via G-protein-coupled activation of protein kinase C. *J. Neurosci.* **15**, 903–911 (1995).
156. Nahar, J. *et al.* Rapid Nongenomic Glucocorticoid Actions in Male Mouse Hypothalamic Neuroendocrine Cells Are Dependent on the Nuclear Glucocorticoid Receptor. *Endocrinology* **156**, 2831–2842 (2015).
157. Malcher-Lopes, R. *et al.* Opposing Crosstalk between Leptin and Glucocorticoids Rapidly Modulates Synaptic Excitation via Endocannabinoid Release. *J. Neurosci.* **26**, 6643–6650 (2006).
158. Maier, C. *et al.* G-protein-coupled glucocorticoid receptors on the pituitary cell membrane. *J. Cell Sci.* **118**, 3353–3361 (2005).
159. Oppong, E. *et al.* Localization and Dynamics of Glucocorticoid Receptor at the Plasma Membrane of Activated Mast Cells. *Small* **10**, 1991–1998 (2014).
160. Vernocchi, S. *et al.* Membrane Glucocorticoid Receptor Activation Induces Proteomic Changes Aligning with Classical Glucocorticoid Effects. *Mol. Cell. Proteomics* **12**, 1764–1779 (2013).
161. Matthews, L. *et al.* Caveolin Mediates Rapid Glucocorticoid Effects and Couples Glucocorticoid Action to the Antiproliferative Program. *Mol. Endocrinol.* **22**, 1320–1330 (2008).
162. Grote, H., Ioannou, I., Voigt, J. & Sekeris, C. E. Localization of the glucocorticoid receptor in rat liver cells: Evidence for plasma membrane bound receptor. *Int. J. Biochem.* **25**, 1593–1599 (1993).
163. Croxtall, J. D., Choudhury, Q. & Flower, R. J. Glucocorticoids act within minutes to inhibit recruitment of signalling factors to activated EGF receptors through a receptor-dependent, transcription-independent mechanism. *Br. J. Pharmacol.* **130**, 289–298 (2000).
164. Hafezi-Moghadam, A. *et al.* Acute cardiovascular protective effects of corticosteroids are mediated by non-transcriptional activation of endothelial nitric oxide synthase. *Nat. Med.* **8**, 473–479 (2002).
165. Tasker, J. G., Di, S. & Malcher-Lopes, R. Rapid Glucocorticoid Signaling via Membrane-Associated Receptors. *Endocrinology* **147**, 5549–5556 (2006).

166. Harris, C., Weiss, G. L., Di, S. & Tasker, J. G. Cell signaling dependence of rapid glucocorticoid-induced endocannabinoid synthesis in hypothalamic neuroendocrine cells. *Neurobiol. Stress* **10**, 100158 (2019).
167. Harrison, L. M. & Tasker, J. G. Multiplexed membrane signaling by glucocorticoids. *Curr. Opin. Endocr. Metab. Res.* **26**, 100390 (2022).
168. Jozic, I. *et al.* Stress Signals, Mediated by Membranous Glucocorticoid Receptor, Activate PLC/PKC/GSK-3β/β-catenin Pathway to Inhibit Wound Closure. *J. Invest. Dermatol.* **137**, 1144–1154 (2017).
169. Wang, L.-L., Ou, C.-C. & Chan, J. Y. H. Receptor-Independent Activation of GABAergic Neurotransmission and Receptor-Dependent Nontranscriptional Activation of Phosphatidylinositol 3-kinase/Protein Kinase Akt Pathway in Short-Term Cardiovascular Actions of Dexamethasone at the Nucleus Tractus Solitarii of the Rat. *Mol. Pharmacol.* **67**, 489–498 (2005).
170. Rainville, J. R. *et al.* Membrane-initiated nuclear trafficking of the glucocorticoid receptor in hypothalamic neurons. *Steroids* **142**, 55–64 (2019).
171. Boncompagni, S. *et al.* Membrane glucocorticoid receptors are localised in the extracellular matrix and signal through the MAPK pathway in mammalian skeletal muscle fibres. *J. Physiol.* **593**, 2679–2692 (2015).
172. Nadal, A. *et al.* Nongenomic actions of estrogens and xenoestrogens by binding at a plasma membrane receptor unrelated to estrogen receptor α and estrogen receptor β. *Proc. Natl. Acad. Sci.* **97**, 11603–11608 (2000).
173. Thomas, P., Pang, Y., Filardo, E. J. & Dong, J. Identity of an Estrogen Membrane Receptor Coupled to a G Protein in Human Breast Cancer Cells. *Endocrinology* **146**, 624–632 (2005).
174. Levin, E. R. Cellular functions of plasma membrane estrogen receptors. *Steroids* **67**, 471–475 (2002).
175. Cain, D. W. & Cidlowski, J. A. Immune regulation by glucocorticoids. *Nat. Rev. Immunol.* **17**, 233–247 (2017).
176. Rizzoli, R. & Biver, E. Glucocorticoid-induced osteoporosis: who to treat with what agent? *Nat. Rev. Rheumatol.* **11**, 98–109 (2015).

177. Fardet, L. & Fève, B. Systemic Glucocorticoid Therapy: a Review of its Metabolic and Cardiovascular Adverse Events. *Drugs* **74**, 1731–1745 (2014).
178. Nicolaides, N. C., Galata, Z., Kino, T., Chrousos, G. P. & Charmandari, E. The human glucocorticoid receptor: Molecular basis of biologic function. *Steroids* **75**, 1–12 (2010).
179. Lu, N. Z. & Cidlowski, J. A. Glucocorticoid receptor isoforms generate transcription specificity. *Trends Cell Biol.* **16**, 301–307 (2006).
180. Quax, R. A. *et al.* Glucocorticoid sensitivity in health and disease. *Nat. Rev. Endocrinol.* **9**, 670–686 (2013).
181. Walker, B. R. Glucocorticoids and Cardiovascular Disease*. *Eur. J. Endocrinol.* **157**, 545–559 (2007).
182. Mangos, G. J. *et al.* Cortisol inhibits cholinergic vasodilatation in the human forearm*: *Am. J. Hypertens.* **13**, 1155–1160 (2000).
183. Costello, R. E., Yimer, B. B., Roads, P., Jani, M. & Dixon, W. G. Glucocorticoid use is associated with an increased risk of hypertension. *Rheumatology* **60**, 132–139 (2021).
184. Panoulas, V. F. *et al.* Long-term exposure to medium-dose glucocorticoid therapy associates with hypertension in patients with rheumatoid arthritis. *Rheumatology* **47**, 72–75 (2008).
185. Raggatt, L. J. & Partridge, N. C. Cellular and Molecular Mechanisms of Bone Remodeling *. *J. Biol. Chem.* **285**, 25103–25108 (2010).
186. Compston, J. Management of glucocorticoid-induced osteoporosis. *Nat. Rev. Rheumatol.* **6**, 82–88 (2010).
187. Lafage-Proust, M. H., Boudignon, B. & Thomas, T. Glucocorticoid-induced osteoporosis: pathophysiological data and recent treatments. *Joint Bone Spine* **70**, 109–118 (2003).
188. Kim, M.-H., Lee, G.-S., Jung, E.-M., Choi, K.-C. & Jeung, E.-B. The negative effect of dexamethasone on calcium-processing gene expressions is associated with a glucocorticoid-induced calcium-absorbing disorder. *Life Sci.* **85**, 146–152 (2009).
189. Li, J.-X. & Cummins, C. L. Fresh insights into glucocorticoid-induced diabetes mellitus and new therapeutic directions. *Nat. Rev. Endocrinol.* **18**, 540–557 (2022).

190. Dirlewanger, M. *et al.* Effects of glucocorticoids on hepatic sensitivity to insulin and glucagon in man. *Clin. Nutr.* **19**, 29–34 (2000).
191. Rahimi, L., Rajpal, A. & Ismail-Beigi, F. Glucocorticoid-Induced Fatty Liver Disease. *Diabetes Metab. Syndr. Obes. Targets Ther.* **Volume 13**, 1133–1145 (2020).
192. Dolinsky, V. W., Douglas, D. N., Lehner, R. & Vance, D. E. Regulation of the enzymes of hepatic microsomal triacylglycerol lipolysis and re-esterification by the glucocorticoid dexamethasone. *Biochem. J.* **378**, 967–974 (2004).
193. Krausz, Y., Bar-On, H. & Shafrir, E. Origin and pattern of glucocorticoid-induced hyperlipidemia in rats dose-dependent bimodal changes in serum lipids and lipoproteins in relation to hepatic lipogenesis and tissue lipoprotein lipase activity. *Biochim. Biophys. Acta BBA - Lipids Lipid Metab.* **663**, 69–82 (1981).
194. Piroli, G. G. *et al.* Corticosterone Impairs Insulin-Stimulated Translocation of GLUT4 in the Rat Hippocampus. *Neuroendocrinology* **85**, 71–80 (2007).
195. Coderre, L., Vallega, G. A., Pilch, P. F. & Chipkin, S. R. In vivo effects of dexamethasone and sucrose on glucose transport (GLUT-4) protein tissue distribution. *Am. J. Physiol.-Endocrinol. Metab.* **271**, E643–E648 (1996).
196. Bujalska, I. J., Kumar, S., Hewison, M. & Stewart, P. M. Differentiation of Adipose Stromal Cells: The Roles of Glucocorticoids and 11β-Hydroxysteroid Dehydrogenase*. *Endocrinology* **140**, 3188–3196 (1999).
197. Morton, N. M. *et al.* Novel Adipose Tissue–Mediated Resistance to Diet-Induced Visceral Obesity in 11β-Hydroxysteroid Dehydrogenase Type 1–Deficient Mice. *Diabetes* **53**, 931–938 (2004).
198. Lee, M.-J., Pramyothin, P., Karastergiou, K. & Fried, S. K. Deconstructing the roles of glucocorticoids in adipose tissue biology and the development of central obesity. *Biochim. Biophys. Acta BBA - Mol. Basis Dis.* **1842**, 473–481 (2014).
199. Slavin, B. G., Ong, J. M. & Kern, P. A. Hormonal regulation of hormone-sensitive lipase activity and mRNA levels in isolated rat adipocytes. *J. Lipid Res.* **35**, 1535–1541 (1994).
200. Geer, E. B., Islam, J. & Buettner, C. Mechanisms of Glucocorticoid-Induced Insulin Resistance. *Endocrinol. Metab. Clin. North Am.* **43**, 75–102 (2014).

201. Wing, S. S. & Goldberg, A. L. Glucocorticoids activate the ATP-ubiquitin-dependent proteolytic system in skeletal muscle during fasting. *https://doi.org/10.1152/ajpendo.1993.264.4.E668* (1993) doi:10.1152/ajpendo.1993.264.4.E668.
202. Isozaki, U., Mitch, W. E., England, B. K. & Price, S. R. Protein degradation and increased mRNAs encoding proteins of the ubiquitin-proteasome proteolytic pathway in BC3H1 myocytes require an interaction between glucocorticoids and acidification. *Proc. Natl. Acad. Sci.* **93**, 1967–1971 (1996).
203. Kayali, A. G., Young, V. R. & Goodman, M. N. Sensitivity of myofibrillar proteins to glucocorticoid-induced muscle proteolysis. *https://doi.org/10.1152/ajpendo.1987.252.5.E621* (1987) doi:10.1152/ajpendo.1987.252.5.E621.
204. Wang, X. J., Song, Z. G., Jiao, H. C. & Lin, H. Dexamethasone facilitates lipid accumulation in chicken skeletal muscle. *Stress* **15**, 443–456 (2012).
205. Nakken, G. N., Jacobs, D. L., Thomson, D. M., Fillmore, N. & Winder, W. W. Effects of excess corticosterone on LKB1 and AMPK signaling in rat skeletal muscle. *J. Appl. Physiol.* **108**, 298–305 (2010).
206. Belgardt, B. F., Okamura, T. & Brüning, J. C. Hormone and glucose signalling in POMC and AgRP neurons. *J. Physiol.* **587**, 5305–5314 (2009).
207. Saper, C. B. & Lowell, B. B. The hypothalamus. *Curr. Biol.* **24**, R1111–R1116 (2014).
208. Scherer, T., Sakamoto, K. & Buettner, C. Brain insulin signalling in metabolic homeostasis and disease. *Nat. Rev. Endocrinol.* **17**, 468–483 (2021).
209. Yue, J. T. Y. *et al.* A fatty acid-dependent hypothalamic–DVC neurocircuitry that regulates hepatic secretion of triglyceride-rich lipoproteins. *Nat. Commun.* **6**, 5970 (2015).
210. Ganong, W. F. Circumventricular Organs: Definition And Role In The Regulation Of Endocrine And Autonomic Function. *Clin. Exp. Pharmacol. Physiol.* **27**, 422–427 (2000).
211. Osterstock, G. *et al.* Ghrelin Stimulation of Growth Hormone-Releasing Hormone Neurons Is Direct in the Arcuate Nucleus. *PLoS ONE* **5**, e9159 (2010).

212. Shin, A. C. *et al.* Insulin Receptor Signaling in POMC, but Not AgRP, Neurons Controls Adipose Tissue Insulin Action. *Diabetes* **66**, 1560–1571 (2017).
213. Secher, A. *et al.* The arcuate nucleus mediates GLP-1 receptor agonist liraglutide-dependent weight loss. *J. Clin. Invest.* **124**, 4473–4488 (2014).
214. Mighiu, P. I. *et al.* Hypothalamic glucagon signaling inhibits hepatic glucose production. *Nat. Med.* **19**, 766–772 (2013).
215. Buettner, C. *et al.* Leptin controls adipose tissue lipogenesis via central, STAT3–independent mechanisms. *Nat. Med.* **14**, 667–675 (2008).
216. Könner, A. C. *et al.* Insulin Action in AgRP-Expressing Neurons Is Required for Suppression of Hepatic Glucose Production. *Cell Metab.* **5**, 438–449 (2007).
217. Valassi, E., Scacchi, M. & Cavagnini, F. Neuroendocrine control of food intake. *Nutr. Metab. Cardiovasc. Dis.* **18**, 158–168 (2008).
218. Jais, A. & Brüning, J. C. Arcuate Nucleus-Dependent Regulation of Metabolism—Pathways to Obesity and Diabetes Mellitus. *Endocr. Rev.* **43**, 314–328 (2022).
219. Loh, K. *et al.* Insulin controls food intake and energy balance via NPY neurons. *Mol. Metab.* **6**, 574–584 (2017).
220. Schwartz, M. W. *et al.* CENTRAL INSULIN ADMINISTRATION REDUCES NEUROPEPTIDE Y mRNA EXPRESSION IN THE ARCUATE NUCLEUS OF FOOD-DEPRIVED LEAN (Fa/Fa) BUT NOT OBESE (fa/fa) ZUCKER RATS. *Endocrinology* **128**, 2645–2647 (1991).
221. Gao, S. *et al.* Leptin activates hypothalamic acetyl-CoA carboxylase to inhibit food intake. *Proc. Natl. Acad. Sci.* **104**, 17358–17363 (2007).
222. Bruijnzeel, A. W., Corrie, L. W., Rogers, J. A. & Yamada, H. Effects of insulin and leptin in the ventral tegmental area and arcuate hypothalamic nucleus on food intake and brain reward function in female rats. *Behav. Brain Res.* **219**, 254–264 (2011).
223. Hackl, M. T. *et al.* Brain leptin reduces liver lipids by increasing hepatic triglyceride secretion and lowering lipogenesis. *Nat. Commun.* **10**, 2717 (2019).
224. Stafford, J. M. *et al.* Central Nervous System Neuropeptide Y Signaling Modulates VLDL Triglyceride Secretion. *Diabetes* **57**, 1482–1490 (2008).

225. Bruinstroop, E. *et al.* Hypothalamic Neuropeptide Y (NPY) Controls Hepatic VLDL-Triglyceride Secretion in Rats via the Sympathetic Nervous System. *Diabetes* **61**, 1043–1050 (2012).
226. Scherer, T. *et al.* Brain Insulin Controls Adipose Tissue Lipolysis and Lipogenesis. *Cell Metab.* **13**, 183–194 (2011).
227. Lam, T. K. T., Gutierrez-Juarez, R., Pocai, A. & Rossetti, L. Regulation of Blood Glucose by Hypothalamic Pyruvate Metabolism. *Science* **309**, 943–947 (2005).
228. Chari, M. *et al.* Glucose Transporter-1 in the Hypothalamic Glial Cells Mediates Glucose Sensing to Regulate Glucose Production In Vivo. *Diabetes* **60**, 1901–1906 (2011).
229. Lam, C. K. L., Chari, M., Rutter, G. A. & Lam, T. K. T. Hypothalamic Nutrient Sensing Activates a Forebrain-Hindbrain Neuronal Circuit to Regulate Glucose Production In Vivo. *Diabetes* **60**, 107–113 (2010).
230. Hu, Z., Cha, S. H., Chohnan, S. & Lane, M. D. Hypothalamic malonyl-CoA as a mediator of feeding behavior. *Proc. Natl. Acad. Sci.* **100**, 12624–12629 (2003).
231. He, W., Lam, T. K. T., Obici, S. & Rossetti, L. Molecular disruption of hypothalamic nutrient sensing induces obesity. *Nat. Neurosci.* **9**, 227–233 (2006).
232. Hu, Z., Dai, Y., Prentki, M., Chohnan, S. & Lane, M. D. A Role for Hypothalamic Malonyl-CoA in the Control of Food Intake. *J. Biol. Chem.* **280**, 39681–39683 (2005).
233. Blouet, C., Jo, Y.-H., Li, X. & Schwartz, G. J. Mediobasal Hypothalamic Leucine Sensing Regulates Food Intake through Activation of a Hypothalamus-Brainstem Circuit. *J. Neurosci.* **29**, 8302–8311 (2009).
234. Su, Y. *et al.* Hypothalamic Leucine Metabolism Regulates Liver Glucose Production. *Diabetes* **61**, 85–93 (2012).
235. Buettner, C. & Camacho, R. C. Hypothalamic Control of Hepatic Glucose Production and Its Potential Role in Insulin Resistance. *Endocrinol. Metab. Clin. North Am.* **37**, 825–840 (2008).
236. Sefton, C. *et al.* Elevated Hypothalamic Glucocorticoid Levels Are Associated With Obesity and Hyperphagia in Male Mice. *Endocrinology* **157**, 4257–4265 (2016).

237. Zakrzewska, K. E. *et al.* Induction of obesity and hyperleptinemia by central glucocorticoid infusion in the rat. *Diabetes* **48**, 365–370 (1999).
238. Emilie Beaulieu-Bayne. Glucocorticoid Action in the Mediobasal Hypothalamus Regulates Glucose Production In Vivo. *MSc Thesis* (2019).
239. BEAULIEU-BAYNE, E., CARDOSO, M., KIM, H., YANG, S. & YUE, J. T. 104-OR: Glucoregulatory Effects of Hypothalamic Glucocorticoid Action In Vivo. *Diabetes* **68**, 104-OR (2019).
240. Miguel Cardoso. Hypothalamic Glucocorticoid Action Regulates Lipid Metabolism. *MSc Thesis* (2022).
241. Nicolaides, N. C., Kyratzi, E., Lamprokostopoulou, A., Chrousos, G. P. & Charmandari, E. Stress, the Stress System and the Role of Glucocorticoids. *Neuroimmunomodulation* **22**, 6–19 (2015).
242. McCall, J. G. *et al.* CRH Engagement of the Locus Coeruleus Noradrenergic System Mediates Stress-Induced Anxiety. *Neuron* **87**, 605–620 (2015).
243. Yi, C.-X. *et al.* Glucocorticoid Signaling in the Arcuate Nucleus Modulates Hepatic Insulin Sensitivity. *Diabetes* **61**, 339–345 (2012).
244. Ponsalle, P., Srivastava, L. S., Uht, R. M. & White, J. D. Glucocorticoids are Required for Food Deprivation-Induced Increases in Hypothalamic Neuropeptide Y Expression. *J. Neuroendocrinol.* **4**, 585–591 (1992).
245. Chen, H. L. & Romsos, D. R. Dexamethasone rapidly increases hypothalamic neuropeptide Y secretion in adrenalectomized ob/ob mice. *Am. J. Physiol.-Endocrinol. Metab.* **271**, E151–E158 (1996).
246. Zakrzewska, K. E. *et al.* Selective Dependence of Intracerebroventricular Neuropeptide Y-Elicited Effects on Central Glucocorticoids*. *Endocrinology* **140**, 3183–3187 (1999).
247. Bernard, C. *Leçons de physiologie expérimentale appliquée à la médecine*. (J.-B. Baillière, 1855).
248. Ludwig, M. Q. *et al.* A genetic map of the mouse dorsal vagal complex and its role in obesity. *Nat. Metab.* **3**, 530–545 (2021).
249. Li, R. J. W. *et al.* Nutrient infusion in the dorsal vagal complex controls hepatic lipid and glucose metabolism in rats. *iScience* **24**, (2021).

250. Filippi, B. M., Yang, C. S., Tang, C. & Lam, T. K. T. Insulin Activates Erk1/2 Signaling in the Dorsal Vagal Complex to Inhibit Glucose Production. *Cell Metab.* **16**, 500–510 (2012).
251. Obici, S., Zhang, B. B., Karkanias, G. & Rossetti, L. Hypothalamic insulin signaling is required for inhibition of glucose production. *Nat. Med.* **8**, 1376–1382 (2002).
252. Glucagon signalling in the dorsal vagal complex is sufficient and necessary for high-protein feeding to regulate glucose homeostasis in vivo. https://www.embopress.org/doi/epdf/10.15252/embr.201540492 doi:10.15252/embr.201540492.
253. Mantash Grewal. Glucagon Action in the Nucleus of Solitary Tract Regulates Hepatic Triglyceride Secretion. *MSc Thesis* (2023).
254. Yue, J. T. Y. *et al.* Inhibition of glycine transporter-1 in the dorsal vagal complex improves metabolic homeostasis in diabetes and obesity. *Nat. Commun.* **7**, 13501 (2016).
255. Lam, C. K. L. *et al.* Activation of N-Methyl-d-aspartate (NMDA) Receptors in the Dorsal Vagal Complex Lowers Glucose Production *. *J. Biol. Chem.* **285**, 21913–21921 (2010).
256. Yue, J. T. Y., Mighiu, P. I., Naples, M., Adeli, K. & Lam, T. K. T. Glycine Normalizes Hepatic Triglyceride-Rich VLDL Secretion by Triggering the CNS in High-Fat Fed Rats. *Circ. Res.* **110**, 1345–1354 (2012).
257. Fong, H. & Kurrasch, D. M. Developmental and functional relationships between hypothalamic tanycytes and embryonic radial glia. *Front. Neurosci.* **16**, (2023).
258. Freeman, M. Z., Cannizzaro, D. N., Naughton, L. F. & Bove, C. Fluoroquinolones-Associated Disability: It Is Not All in Your Head. *NeuroSci* **2**, 235–253 (2021).
259. Morimoto, M., Morita, N., Ozawa, H., Yokoyama, K. & Kawata, M. Distribution of glucocorticoid receptor immunoreactivity and mRNA in the rat brain: an immunohistochemical and in situ hybridization study. *Neurosci. Res.* **26**, 235–269 (1996).
260. Jiang, Z. *et al.* Acute Stress Desensitizes Hypothalamic CRH Neurons to Norepinephrine and Physiological Stress. Preprint at https://doi.org/10.1101/2019.12.31.891408 (2020).

261. Hu, W., Zhang, M., Czéh, B., Flügge, G. & Zhang, W. Stress Impairs GABAergic Network Function in the Hippocampus by Activating Nongenomic Glucocorticoid Receptors and Affecting the Integrity of the Parvalbumin-Expressing Neuronal Network. *Neuropsychopharmacology* **35**, 1693–1707 (2010).
262. Wu, N. & Tasker, J. G. Nongenomic Glucocorticoid Suppression of a Postsynaptic Potassium Current via Emergent Autocrine Endocannabinoid Signaling in Hypothalamic Neuroendocrine Cells following Chronic Dehydration. *eneuro* **4**, ENEURO.0216-17.2017 (2017).
263. Strehl, C. *et al.* Origin and functional activity of the membrane-bound glucocorticoid receptor. *Arthritis Rheum.* **63**, 3779–3788 (2011).
264. Jordi Folch, M. Lees, & G. H. Sloane Stanley. A SIMPLE METHOD FOR THE ISOLATION AND PURIFICATION OF TOTAL LIPIDES FROM ANIMAL TISSUES. *J Biol Chem* **226**, 497–509 (1957).
265. Puthanveetil, P. *et al.* The Increase in Cardiac Pyruvate Dehydrogenase Kinase-4 after Short-Term Dexamethasone Is Controlled by an Akt-p38-Forkhead Box Other Factor-1 Signaling Axis. *Endocrinology* **151**, 2306–2318 (2010).
266. Ritter, H. D. & Mueller, C. R. Expression microarray identifies the unliganded glucocorticoid receptor as a regulator of gene expression in mammary epithelial cells. (2014).
267. Ritter, H. D., Antonova, L. & Mueller, C. R. The Unliganded Glucocorticoid Receptor Positively Regulates the Tumor Suppressor Gene BRCA1 through GABP Beta. *Mol. Cancer Res.*
268. Farr, S. *et al.* Central Nervous System Regulation of Intestinal Lipoprotein Metabolism by Glucagon-Like Peptide-1 via a Brain–Gut Axis. *Arterioscler. Thromb. Vasc. Biol.* **35**, 1092–1100 (2015).
269. Hoffman, S., Alvares, D. & Adeli, K. GLP-1 attenuates intestinal fat absorption and chylomicron production via vagal afferent nerves originating in the portal vein. *Mol. Metab.* **65**, 101590 (2022).
270. Sandoval, D. A., Bagnol, D., Woods, S. C., D'Alessio, D. A. & Seeley, R. J. Arcuate Glucagon-Like Peptide 1 Receptors Regulate Glucose Homeostasis but Not Food Intake. *Diabetes* **57**, 2046–2054 (2008).

271. Fortin, S. M., Chen, J. & Hayes, M. R. Hindbrain melanocortin 3/4 receptors modulate the food intake and body weight suppressive effects of the GLP-1 receptor agonist, liraglutide. *Physiol. Behav.* **220**, 112870 (2020).
272. Corpa, E. S., McQuade, J., Krasnicki, S. & Conze, D. B. Feeding after fourth ventricular administration of neuropeptide Y receptor agonists in rats. *Peptides* **22**, 493–499 (2001).
273. Taher, J., Farr, S. & Adeli, K. Central nervous system regulation of hepatic lipid and lipoprotein metabolism. *Curr. Opin. Lipidol.* **28**, 32–38 (2017).
274. Yue, J. T. Y. & Lam, T. K. T. Lipid Sensing and Insulin Resistance in the Brain. *Cell Metab.* **15**, 646–655 (2012).
275. Bali, U., Phillips, T., Hunt, H. & Unitt, J. FKBP5 mRNA Expression Is a Biomarker for GR Antagonism. *J. Clin. Endocrinol. Metab.* **101**, 4305–4312 (2016).
276. Paakinaho, V., Makkonen, H., Jääskeläinen, T. & Palvimo, J. J. Glucocorticoid Receptor Activates Poised FKBP51 Locus through Long-Distance Interactions. *Mol. Endocrinol.* **24**, 511–525 (2010).
277. Viho, E. M. *et al.* Peripheral glucocorticoid receptor antagonism by relacorilant with modest HPA axis disinhibition. *J. Endocrinol.* JOE-22-0263 (2022) doi:10.1530/JOE-22-0263.
278. Sánchez, M. M., Young, L. J., Plotsky, P. M. & Insel, T. R. Distribution of Corticosteroid Receptors in the Rhesus Brain: Relative Absence of Glucocorticoid Receptors in the Hippocampal Formation. *J. Neurosci.* **20**, 4657–4668 (2000).
279. ANDERS HARFSTRAND. Glucocorticoid receptor immunoreactivity in monoaminergic neurons of rat brain. *Proc Nati Acad Sci USA Vol 83 Pp 9779-9783 Dec. 1986 Neurobiol.* **83**, 9779–9783 (1986).
280. Bailey, T. W., Appleyard, S. M., Jin, Y.-H. & Andresen, M. C. Organization and Properties of GABAergic Neurons in Solitary Tract Nucleus (NTS). *J. Neurophysiol.* **99**, 1712–1722 (2008).
281. Núñez, C. *et al.* Elevated Glucocorticoid Levels Are Responsible for Induction of Tyrosine Hydroxylase mRNA Expression, Phosphorylation, and Enzyme Activity in the Nucleus of the Solitary Tract during Morphine Withdrawal. *Endocrinology* **150**, 3118–3127 (2009).

282. Navarro-Zaragoza, J., Hidalgo, J. M., Laorden, M. L. & Milanés, M. V. Glucocorticoid receptors participate in the opiate withdrawal-induced stimulation of rats NTS noradrenergic activity and in the somatic signs of morphine withdrawal. *Br. J. Pharmacol.* **166**, 2136–2147 (2012).
283. Roozendaal, B., Williams, C. L. & McGaugh, J. L. Glucocorticoid receptor activation in the rat nucleus of the solitary tract facilitates memory consolidation: involvement of the basolateral amygdala. *Eur. J. Neurosci.* **11**, 1317–1323 (1999).
284. Huo, L., Maeng, L., Bjørbæk, C. & Grill, H. J. Leptin and the Control of Food Intake: Neurons in the Nucleus of the Solitary Tract Are Activated by Both Gastric Distension and Leptin. *Endocrinology* **148**, 2189–2197 (2007).
285. Qiu, W. *et al.* Multiple NTS neuron populations cumulatively suppress food intake. *eLife* **12**, e85640 (2023).
286. Chen, J. *et al.* A Vagal-NTS Neural Pathway that Stimulates Feeding. *Curr. Biol.* **30**, 3986-3998.e5 (2020).
287. Aklan, I. *et al.* NTS Catecholamine Neurons Mediate Hypoglycemic Hunger via Medial Hypothalamic Feeding Pathways. *Cell Metab.* **31**, 313-326.e5 (2020).
288. Ragozzino, F. J. *et al.* Corticosterone inhibits vagal afferent glutamate release in the nucleus of the solitary tract via retrograde endocannabinoid signaling. *Am. J. Physiol.-Cell Physiol.* **319**, C1097–C1106 (2020).
289. Bartness, T. J., Liu, Y., Shrestha, Y. B. & Ryu, V. Neural innervation of white adipose tissue and the control of lipolysis. *Front. Neuroendocrinol.* **35**, 473–493 (2014).
290. Lafontan, M. & Langin, D. Lipolysis and lipid mobilization in human adipose tissue. *Prog. Lipid Res.* **48**, 275–297 (2009).
291. Shigematsu, H. *et al.* Endogenous angiotensin II in the NTS contributes to sympathetic activation in rats with aortocaval shunt. *Am. J. Physiol.-Regul. Integr. Comp. Physiol.* **280**, R1665–R1673 (2001).
292. Schwarz, L. A. & Luo, L. Organization of the Locus Coeruleus-Norepinephrine System. *Curr. Biol.* **25**, R1051–R1056 (2015).
293. Shen, H., Fuchino, Y., Miyamoto, D., Nomura, H. & Matsuki, N. Vagus nerve stimulation enhances perforant path-CA3 synaptic transmission via the activation of

β-adrenergic receptors and the locus coeruleus. *Int. J. Neuropsychopharmacol.* **15**, 523–530 (2012).

294. Van Bockstaele, E. J., Peoples, J. & Telegan, P. Efferent projections of the nucleus of the solitary tract to peri-locus coeruleus dendrites in rat brain: Evidence for a monosynaptic pathway. *J. Comp. Neurol.* **412**, 410–428 (1999).
295. Miyazaki, M., Kim, Y.-C., Gray-Keller, M. P., Attie, A. D. & Ntambi, J. M. The Biosynthesis of Hepatic Cholesterol Esters and Triglycerides Is Impaired in Mice with a Disruption of the Gene for Stearoyl-CoA Desaturase 1. *J. Biol. Chem.* **275**, 30132–30138 (2000).
296. Lam, T. K. T. *et al.* Brain glucose metabolism controls the hepatic secretion of triglyceride-rich lipoproteins. *Nat. Med.* **13**, 171–180 (2007).
297. Julius, U. Influence of plasma free fatty acids on lipoprotein synthesis and diabetic dyslipidemia. *Exp. Clin. Endocrinol. Diabetes Off. J. Ger. Soc. Endocrinol. Ger. Diabetes Assoc.* **111**, 246–250 (2003).
298. Koonen, D. P. Y. *et al.* Increased Hepatic CD36 Expression Contributes to Dyslipidemia Associated With Diet-Induced Obesity. *Diabetes* **56**, 2863–2871 (2007).
299. Wilson, C. G. *et al.* Hepatocyte-Specific Disruption of CD36 Attenuates Fatty Liver and Improves Insulin Sensitivity in HFD-Fed Mice. *Endocrinology* **157**, 570–585 (2016).
300. Newberry, E. P. *et al.* Decreased Hepatic Triglyceride Accumulation and Altered Fatty Acid Uptake in Mice with Deletion of the Liver Fatty Acid-binding Protein Gene *. *J. Biol. Chem.* **278**, 51664–51672 (2003).
301. Golovko, M. Y. & Murphy, E. J. An improved method for tissue long-chain acyl-CoA extraction and analysis. *J. Lipid Res.* **45**, 1777–1782 (2004).
302. Deutsch, J., Grange, E., Rapoport, S. I. & Purdon, A. D. Isolation and Quantitation of Long-Chain Acyl-Coenzyme A Esters in Brain Tissue by Solid-Phase Extraction. *Anal. Biochem.* **220**, 321–323 (1994).
303. Wiesner, P., Leidl, K., Boettcher, A., Schmitz, G. & Liebisch, G. Lipid profiling of FPLC-separated lipoprotein fractions by electrospray ionization tandem mass spectrometry. *J. Lipid Res.* **50**, 574–585 (2009).

304. Tang, V. T. *et al.* Hepatic inactivation of murine Surf4 results in marked reduction in plasma cholesterol. *eLife* **11**, e82269 (2022).
305. Lee, H. Y. *et al.* Bax Inhibitor-1 regulates hepatic lipid accumulation via ApoB secretion. *Sci. Rep.* **6**, 27799 (2016).
306. Ginsberg, H. N. LIPOPROTEIN PHYSIOLOGY. *Endocrinol. Metab. Clin.* **27**, 503–519 (1998).
307. Freedman, D. S., Bowman, B. A., Otvos, J. D., Srinivasan, S. R. & Berenson, G. S. Levels and correlates of LDL and VLDL particle sizes among children: the Bogalusa heart study. *Atherosclerosis* **152**, 441–449 (2000).
308. Mallol, R. *et al.* Particle size measurement of lipoprotein fractions using diffusion-ordered NMR spectroscopy. *Anal. Bioanal. Chem.* **402**, 2407–2415 (2012).
309. Otvos, J. Measurement of triglyceride-rich lipoproteins by nuclear magnetic resonance spectroscopy. *Clin. Cardiol.* **22**, II-21-II–27 (1999).
310. Jackson, S. E. Hsp90: structure and function. *Top. Curr. Chem.* **328**, 155–240 (2013).
311. Kaplan, K. B. & Li, R. A prescription for ‘stress’ – the role of Hsp90 in genome stability and cellular adaptation. *Trends Cell Biol.* **22**, 576–583 (2012).
312. Salminen, A., Paimela, T., Suuronen, T. & Kaarniranta, K. Innate immunity meets with cellular stress at the IKK complex: Regulation of the IKK complex by HSP70 and HSP90. *Immunol. Lett.* **117**, 9–15 (2008).
313. Lee, J.-H. *et al.* Heat shock protein 90 (HSP90) inhibitors activate the heat shock factor 1 (HSF1) stress response pathway and improve glucose regulation in diabetic mice. *Biochem. Biophys. Res. Commun.* **430**, 1109–1113 (2013).
314. Jing, E. *et al.* Hsp90β knockdown in DIO mice reverses insulin resistance and improves glucose tolerance. *Nutr. Metab.* **15**, 11 (2018).
315. Yang, X. *et al.* Potential role of Hsp90 in rat islet function under the condition of high glucose. *Acta Diabetol.* **53**, 621–628 (2016).
316. Zheng, Z.-G. *et al.* Inhibition of HSP90β Improves Lipid Disorders by Promoting Mature SREBPs Degradation via the Ubiquitin-proteasome System. *Theranostics* **9**, 5769–5783 (2019).

317. Desarzens, S., Liao, W.-H., Mammi, C., Caprio, M. & Faresse, N. Hsp90 Blockers Inhibit Adipocyte Differentiation and Fat Mass Accumulation. *PLOS ONE* **9**, e94127 (2014).
318. Hartmann, J. *et al.* The involvement of FK506-binding protein 51 (FKBP5) in the behavioral and neuroendocrine effects of chronic social defeat stress. *Neuropharmacology* **62**, 332–339 (2012).
319. Hoeijmakers, L. *et al.* Depletion of FKBP51 in Female Mice Shapes HPA Axis Activity. *PLoS ONE* **9**, e95796 (2014).
320. Smedlund, K. B., Sanchez, E. R. & Hinds, T. D. FKBP51 and the molecular chaperoning of metabolism. *Trends Endocrinol. Metab.* **32**, 862–874 (2021).
321. Stechschulte, L. A. *et al.* FKBP51 Controls Cellular Adipogenesis through p38 Kinase-Mediated Phosphorylation of GRα and PPARγ. *Mol. Endocrinol.* **28**, 1265–1275 (2014).
322. Soukas, A., Cohen, P., Socci, N. D. & Friedman, J. M. Leptin-specific patterns of gene expression in white adipose tissue. *Genes Dev.* **14**, 963–980 (2000).
323. Stechschulte, L. A. *et al.* FKBP51 Null Mice Are Resistant to Diet-Induced Obesity and the PPARγ Agonist Rosiglitazone. *Endocrinology* **157**, 3888–3900 (2016).
324. Sidibeh, C. O. *et al.* FKBP5 expression in human adipose tissue: potential role in glucose and lipid metabolism, adipogenesis and type 2 diabetes. *Endocrine* **62**, 116–128 (2018).
325. Balsevich, G. *et al.* Stress-responsive FKBP51 regulates AKT2-AS160 signaling and metabolic function. *Nat. Commun.* **8**, 1725 (2017).
326. Ising, M. *et al.* FKBP5 Gene Expression Predicts Antidepressant Treatment Outcome in Depression. *Int. J. Mol. Sci.* **20**, 485 (2019).
327. Iii, J. C. O. *et al.* A New Anti-Depressive Strategy for the Elderly: Ablation of FKBP5/FKBP51. *PLOS ONE* **6**, e24840 (2011).
328. Pereira, M. J. *et al.* FKBP5 expression in human adipose tissue increases following dexamethasone exposure and is associated with insulin resistance. *Metabolism* **63**, 1198–1208 (2014).

329. Yang, L. *et al.* Hypothalamic Fkbp51 is induced by fasting, and elevated hypothalamic expression promotes obese phenotypes. *Am. J. Physiol.-Endocrinol. Metab.* **302**, E987–E991 (2012).
330. Balsevich, G. *et al.* Interplay between diet-induced obesity and chronic stress in mice: potential role of FKBP51. *J. Endocrinol.* **222**, 15–26 (2014).
331. Brix, L. M. *et al.* Contribution of the co-chaperone FKBP51 in the ventromedial hypothalamus to metabolic homeostasis in male and female mice. *Mol. Metab.* **65**, 101579 (2022).
332. Häusl, A. S. *et al.* Mediobasal hypothalamic FKBP51 acts as a molecular switch linking autophagy to whole-body metabolism. *Sci. Adv.* **8**, eabi4797 (2022).
333. Deng, Q. *et al.* Rapid Glucocorticoid Feedback Inhibition of ACTH Secretion Involves Ligand-Dependent Membrane Association of Glucocorticoid Receptors. *Endocrinology* **156**, 3215–3227 (2015).
334. Weiss, G. L., Rainville, J. R., Zhao, Q. & Tasker, J. G. Purity and stability of the membrane-limited glucocorticoid receptor agonist dexamethasone-BSA. *Steroids* **142**, 2–5 (2019).
335. Nahar, J., Rainville, J. R., Dohanich, G. P. & Tasker, J. G. Further evidence for a membrane receptor that binds glucocorticoids in the rodent hypothalamus. *Steroids* **114**, 33–40 (2016).
336. Deng, M.-Y. *et al.* Dexamethasone attenuates neuropathic pain through spinal microglial expression of dynorphin A via the cAMP/PKA/p38 MAPK/CREB signaling pathway. *Brain. Behav. Immun.* **119**, 36–50 (2024).
337. Steiner, A., Vogt, E., Locher, R. & Vetter, W. Stimulation of the phosphoinositide signalling system as a possible mechanism for glucocorticoid action in blood pressure control. *J. Hypertens.* **6**, S366 (1988).
338. Yamamoto, T., Matsuzaki, H., Kamada, S., Ono, Y. & Kikkawa, U. Biochemical assays for multiple activation states of protein kinase C. *Nat. Protoc.* **1**, 2791–2795 (2006).
339. Liu, J.-Y., Lin, S.-J. & Lin, J.-K. Inhibitory effects of curcumin on protein kinase C activity induced by 12-O-tetradecanoyl-phorbol-13-acetate in NIH 3T3 cells. *Carcinogenesis* **14**, 857–861 (1993).

340. Tusa, I. *et al.* Targeting the Extracellular Signal-Regulated Kinase 5 Pathway to Suppress Human Chronic Myeloid Leukemia Stem Cells. *Stem Cell Rep.* **11**, 929–943 (2018).
341. Bartholome, B. *et al.* Membrane glucocorticoid receptors (mGCR) are expressed in normal human peripheral blood mononuclear cells and up-regulated after in vitro stimulation and in patients with rheumatoid arthritis. *FASEB J.* **18**, 70–80 (2004).
342. Towle, A. C. & Sze, P. Y. Steroid binding to synaptic plasma membrane: differential binding of glucocorticoids and gonadal steroids. *J. Steroid Biochem.* **18**, 135–143 (1983).
343. Hua, S.-Y. & Chen, Y.-Z. Membrane Receptor-Mediated Electrophysiological Effects of Glucocorticoid on Mammalian Neurons. *Endocrinology* **124**, 687–691 (1989).
344. Mirdamadi, M. *et al.* Non-genomic uterorelaxant actions of corticosteroid hormones in rats: An in vitro and in vivo study. *Eur. J. Pharmacol.* **935**, 175346 (2022).
345. Espinoza, M. B. *et al.* Cortisol Induces Reactive Oxygen Species Through a Membrane Glucocorticoid Receptor in Rainbow Trout Myotubes. *J. Cell. Biochem.* **118**, 718–725 (2017).
346. Evanson, N. K., Tasker, J. G., Hill, M. N., Hillard, C. J. & Herman, J. P. Fast Feedback Inhibition of the HPA Axis by Glucocorticoids Is Mediated by Endocannabinoid Signaling. *Endocrinology* **151**, 4811–4819 (2010).
347. He, L.-M., Zhang, C.-G., Zhou, Z. & Xu, T. Rapid inhibitory effects of corticosterone on calcium influx in rat dorsal root ganglion neurons. *Neuroscience* **116**, 325–333 (2003).
348. Seger, R. & Krebs, E. G. The MAPK signaling cascade. *FASEB J.* **9**, 726–735 (1995).
349. Gutièrrez-Mecinas, M. *et al.* Long-lasting behavioral responses to stress involve a direct interaction of glucocorticoid receptors with ERK1/2–MSK1–Elk-1 signaling. *Proc. Natl. Acad. Sci.* **108**, 13806–13811 (2011).
350. Jubaidi, F. F. *et al.* The Role of PKC-MAPK Signalling Pathways in the Development of Hyperglycemia-Induced Cardiovascular Complications. *Int. J. Mol. Sci.* **23**, 8582 (2022).

351. Kang, J.-H. Protein Kinase C (PKC) Isozymes and Cancer. *New J. Sci.* **2014**, 231418 (2014).
352. Bahar, M. E., Kim, H. J. & Kim, D. R. Targeting the RAS/RAF/MAPK pathway for cancer therapy: from mechanism to clinical studies. *Signal Transduct. Target. Ther.* **8**, 1–38 (2023).
353. Kolch, W. *et al.* Protein kinase Cα activates RAF-1 by direct phosphorylation. *Nature* **364**, 249–252 (1993).
354. Corbit, K. C. *et al.* Activation of Raf-1 Signaling by Protein Kinase C through a Mechanism Involving Raf Kinase Inhibitory Protein *. *J. Biol. Chem.* **278**, 13061–13068 (2003).
355. Madamanchi, A. β-Adrenergic receptor signaling in cardiac function and heart failure. *McGill J. Med. MJM* **10**, 99–104 (2007).
356. Bylund, D. B. Subtypes of α1- and α2-adrenergic receptors. *FASEB J.* **6**, 832–839 (1992).
357. Shah, A., Rader, D. J. & Millar, J. S. The effect of PPAR-α agonism on apolipoprotein metabolism in humans. *Atherosclerosis* **210**, 35–40 (2010).
358. Hogue, J.-C. *et al.* Differential effect of fenofibrate and atorvastatin on in vivo kinetics of apolipoproteins B-100 and B-48 in subjects with type 2 diabetes mellitus with marked hypertriglyceridemia. *Metabolism* **57**, 246–254 (2008).
359. Bilz, S. *et al.* Effects of atorvastatin versus fenofibrate on apoB-100 and apoA-I kinetics in mixed hyperlipidemia. *J. Lipid Res.* **45**, 174–185 (2004).
360. Lucero, D. *et al.* Overproduction of altered VLDL in an insulin-resistance rat model: Influence of SREBP-1c and PPAR-α. *Clínica E Investig. En Arterioscler.* **27**, 167–174 (2015).
361. Stec, D. E. *et al.* Loss of hepatic PPARα promotes inflammation and serum hyperlipidemia in diet-induced obesity. *Am. J. Physiol.-Regul. Integr. Comp. Physiol.* **317**, R733–R745 (2019).
362. Knebel, B. *et al.* Liver-Specific Expression of Transcriptionally Active SREBP-1c Is Associated with Fatty Liver and Increased Visceral Fat Mass. *PLOS ONE* **7**, e31812 (2012).

363. Takanashi, M. *et al.* Critical Role of SREBP-1c Large-VLDL Pathway in Environment-Induced Hypertriglyceridemia of Apo AV Deficiency. *Arterioscler. Thromb. Vasc. Biol.* **39**, 373–386 (2019).
364. Karasawa, T. *et al.* Sterol Regulatory Element–Binding Protein-1 Determines Plasma Remnant Lipoproteins and Accelerates Atherosclerosis in Low-Density Lipoprotein Receptor–Deficient Mice. *Arterioscler. Thromb. Vasc. Biol.* **31**, 1788–1795 (2011).
365. Okazaki, H., Goldstein, J. L., Brown, M. S. & Liang, G. LXR-SREBP-1c-Phospholipid Transfer Protein Axis Controls Very Low Density Lipoprotein (VLDL) Particle Size *. *J. Biol. Chem.* **285**, 6801–6810 (2010).
366. D'arci Sutton. Mediators of Glucocorticoid Receptor Activation in the Dorsal Vagal Complex to Regulate Hepatic Glucose Production. (2024).
367. Dindia, L. *et al.* Novel Nongenomic Signaling by Glucocorticoid May Involve Changes to Liver Membrane Order in Rainbow Trout. *PLOS ONE* **7**, e46859 (2012).
368. Long, F. *et al.* Rapid nongenomic inhibitory effects of glucocorticoids on phagocytosis and superoxide anion production by macrophages. *Steroids* **70**, 55–61 (2005).
369. Patel, H. H. & Insel, P. A. Lipid Rafts and Caveolae and Their Role in Compartmentation of Redox Signaling. *Antioxid. Redox Signal.* **11**, 1357–1372 (2009).
370. Lu, Q. *et al.* Striatin assembles a membrane signaling complex necessary for rapid, nongenomic activation of endothelial NO synthase by estrogen receptor α. *Proc. Natl. Acad. Sci.* **101**, 17126–17131 (2004).
371. Pedram, A. *et al.* A Conserved Mechanism for Steroid Receptor Translocation to the Plasma Membrane. *J. Biol. Chem.* **282**, 22278–22288 (2007).
372. Acconcia, F. *et al.* Palmitoylation-dependent Estrogen Receptor α Membrane Localization: Regulation by 17β-Estradiol. *Mol. Biol. Cell* **16**, 231–237 (2005).
373. Chen, Q., Amaral, J., Biancani, P. & Behar, J. Excess membrane cholesterol alters human gallbladder muscle contractility and membrane fluidity. *Gastroenterology* **116**, 678–685 (1999).

374. Cooper, R. A. Influence of increased membrane cholesterol on membrane fluidity and cell function in human red blood cells. *J. Supramol. Struct.* **8**, 413–430 (1978).
375. Gametchu, B. & Watson, C. S. Correlation of membrane glucocorticoid receptor levels with glucocorticoid-induced apoptotic competence using mutant leukemic and lymphoma cells lines. *J. Cell. Biochem.* **87**, 133–146 (2002).
376. Chinnasamy, P. *et al.* Increased adipose catecholamine levels and protection from obesity with loss of Allograft Inflammatory Factor-1. *Nat. Commun.* **14**, 38 (2023).
377. Haidari, M. *et al.* Fasting and Postprandial Overproduction of Intestinally Derived Lipoproteins in an Animal Model of Insulin Resistance: EVIDENCE THAT CHRONIC FRUCTOSE FEEDING IN THE HAMSTER IS ACCOMPANIED BY ENHANCED INTESTINAL DE NOVO LIPOGENESIS AND ApoB48-CONTAINING LIPOPROTEIN OVERPRODUCTION *. *J. Biol. Chem.* **277**, 31646–31655 (2002).
378. Lewis, G. F. *et al.* Intestinal Lipoprotein Production Is Stimulated by an Acute Elevation of Plasma Free Fatty Acids in the Fasting State: Studies in Insulin-Resistant and Insulin-Sensitized Syrian Golden Hamsters. *Endocrinology* **145**, 5006–5012 (2004).
379. Puchalska, P. & Crawford, P. A. Metabolic and Signaling Roles of Ketone Bodies in Health and Disease. *Annu. Rev. Nutr.* **41**, 49–77 (2021).
380. Ho, S. W. *et al.* Effects of 17-allylamino-17-demethoxygeldanamycin (17-AAG) in transgenic mouse models of frontotemporal lobar degeneration and Alzheimer's disease. *Transl. Neurodegener.* **2**, 24 (2013).
381. Hanna, R., Abdallah, J. & Abou-Antoun, T. A Novel Mechanism of 17-AAG Therapeutic Efficacy on HSP90 Inhibition in MYCN-Amplified Neuroblastoma Cells. *Front. Oncol.* **10**, 624560 (2021).
382. Wagatsuma, A. *et al.* Pharmacological targeting of HSP90 with 17-AAG induces apoptosis of myogenic cells through activation of the intrinsic pathway. *Mol. Cell. Biochem.* **445**, 45–58 (2018).
383. Schopf, F. H., Biebl, M. M. & Buchner, J. The HSP90 chaperone machinery. *Nat. Rev. Mol. Cell Biol.* **18**, 345–360 (2017).

384. Dickey, C. A. *et al.* The high-affinity HSP90-CHIP complex recognizes and selectively degrades phosphorylated tau client proteins. *J. Clin. Invest.* **117**, 648–658 (2007).
385. Evans, C. G., Wisén, S. & Gestwicki, J. E. Heat Shock Proteins 70 and 90 Inhibit Early Stages of Amyloid β-(1–42) Aggregation in Vitro. *J. Biol. Chem.* **281**, 33182–33191 (2006).
386. Allen, M., Millett, P., Dawes, E. & Rushton, N. Lactate dehydrogenase activity as a rapid and sensitive test for the quantification of cell numbers *in vitro*. *Clin. Mater.* **16**, 189–194 (1994).
387. Palmisano, B. T., Zhu, L., Eckel, R. H. & Stafford, J. M. Sex differences in lipid and lipoprotein metabolism. *Mol. Metab.* **15**, 45–55 (2018).
388. Varlamov, O., Bethea, C. L. & Roberts, C. T. Sex-Specific Differences in Lipid and Glucose Metabolism. *Front. Endocrinol.* **5**, (2015).
389. Xu, Y. & López, M. Central regulation of energy metabolism by estrogens. *Mol. Metab.* **15**, 104–115 (2018).
390. Xu, Y. *et al.* Distinct Hypothalamic Neurons Mediate Estrogenic Effects on Energy Homeostasis and Reproduction. *Cell Metab.* **14**, 453–465 (2011).
391. Thammacharoen, S., Lutz, T. A., Geary, N. & Asarian, L. Hindbrain Administration of Estradiol Inhibits Feeding and Activates Estrogen Receptor-α-Expressing Cells in the Nucleus Tractus Solitarius of Ovariectomized Rats. *Endocrinology* **149**, 1609–1617 (2008).
392. Itani, S. I., Pories, W. J., MacDonald, K. G. & Dohm, G. L. Increased protein kinase C theta in skeletal muscle of diabetic patients. *Metab. - Clin. Exp.* **50**, 553–557 (2001).
393. Griffin, M. E. *et al.* Free fatty acid-induced insulin resistance is associated with activation of protein kinase C theta and alterations in the insulin signaling cascade. *Diabetes* **48**, 1270–1274 (1999).
394. Schmitz-Peiffer, C. Targeting protein kinase C epsilon or theta as a therapeutic strategy for insulin resistance. *Drug Discov. Today Ther. Strateg.* **2**, 105–110 (2005).

395. Kim, J. K. *et al.* PKC-θ knockout mice are protected from fat-induced insulin resistance. *J. Clin. Invest.* **114**, 823–827 (2004).
396. Benoit, S. C. *et al.* Palmitic acid mediates hypothalamic insulin resistance by altering PKC-θ subcellular localization in rodents. *J. Clin. Invest.* **119**, 2577–2589 (2009).
397. Estradiol-17β-BSA stimulates Ca2+ uptake through nongenomic pathways in primary rabbit kidney proximal tubule cells: Involvement of cAMP and PKC. https://onlinelibrary.wiley.com/doi/epdf/10.1002/%28SICI%291097-4652%28200004%29183%3A1%3C37%3A%3AAID-JCP5%3E3.0.CO%3B2-N.